Mechanistic Studies on the Cerium Catalyzed Belousov-Zhabotinsky Reaction

DISSERTATION
zur
Erlangung des Doktorgrades
der Naturwissenschaften
(Dr. rer. nat.)

dem
Fachbereich Chemie
der Philipps-Universität Marburg
vorgelegt von

Shuhua Yan
aus Changchun/China

Marburg/Lahn 2001

Vom Fachbereich Physikalische Chemie der Philipps-Universität Marburg als Dissertation angenommen am ?
Tag der mündlichen Prüfung: ?
Erstgutachter: Prof. Dr. H.-D. Försterling
Zweitgutachter: Prof. Dr. Armin Schweig

Contents

Foreword

This thesis presents my work at the Department of Chemistry, the Philipps University of Marburg, Germany. The study has been carried out in the period from August 1998 to May 2001 under the instruction of Professor Dr. Horst-Dieter Försterling. I would like to thank Prof. Försterling for his continuous guidance, support and encouragement during this whole period of time, and for his invaluable effort in correcting this thesis.

Thanks to Mr. D. Mrotzek for his helpful assistance in the laboratory.

My deepest appreciation for my husband, my daughter, my parents-in-law and my parents for their love, support and encouragement.

Shuhua Yan

Marburg, Germany, 8 May 2001.

Chapter 1

Introduction

The study of oscillating chemical reactions is a new field of chemistry that began accidentally in the 1950s when B. P. Belousov observed time periodic oscillations in a homogeneous solution of bromate, citric acid, and ceric ions, and chemical waves in an unstirred sample[1~2]. A. M. Zhabotinsky continued Belousov's work, and the class of oscillatory, metal-ion-catalyzed oxidations of organic compounds by bromate ion is now referred to as the Belousov-Zhabotinsky (BZ) reaction. This reaction at first seemed to violate the second law of thermodynamics. However, in 1968, Lefever and Prigogine[3] showed that the observed oscillatory phenomena could be explained by nonlinearities resulting from the autocatalytic nature of the reaction, and that there was no violation of the laws of thermodynamics. In 1972 Field, Körös and Noyes[4] established the first chemical model leading to oscillations in the BZ reaction, which is usually referred to as the FKN model. Thus, the foundations were laid for a field that has grown enormously, particularly because of its profound implications for the dynamics of biological and social systems. A large number of variants of the classic BZ reaction have been discovered since this early work.

Despite much experimental and theoretical effort, there remain difficulties in understanding the detailed mechanism of the oscillatory reaction.

According to the FKN theory[4] there are two states (reduced and oxidized) available to the BZ reaction depending on the bromide concentration. When the bromide level is high the reduced state is dominant where the catalyst ion is in or approaches its reduced state, Ce^{3+}, and the overall chemistry is the bromination of malonic acid (MA) with simultaneous removal of Br^-. The reduced state becomes unstable when $[Br^-]$ becomes sufficiently low allowing the autocatalytic BrO_3^- - $HBrO_2$ reaction to take over and oxidize Ce^{3+} to Ce^{4+}. The resulting oxidized state is characterized by high

concentrations of $HBrO_2$, Ce^{4+} and organic radicals. In this state the regeneration of bromide by Ce^{4+} oxidation of brominated organic compounds, mainly bromomalonic acid, grows up. Then [Br^-] jumps to a high level and the cycle start again. The FKN mechanism is thus referred to as bromide controlled. This theory supplies a basic form of the chemistry for understanding and modeling the oscillatory phenomena. Its simplified version, the Oregonator[5] was applied successfully to model oscillations and other nonlinear phenomena in the BZ reaction. It turned out, however, that the organic radicals play a more important role than it was originally suspected[6]. On the other hand, no success was achieved in reproducing the experimental oscillations using a realistic FKN model without making any simplifications[7~9].

The most difficult bromate-driven oscillators to rationalize within the FKN framework are those that show oscillations in color and/or redox potential but not in [Br^-]. Noszticzius[10] added Ag^+ to an oscillating BZ reagent and found that high-frequency oscillations persist even under conditions when [Br^-] is too low to control the oscillations. He referred to these oscillations as "non-bromide-controlled". A controversy concerning the existence of another control intermediate started. Brusa et al.[11] suggested that malonyl radicals ($MA^\bullet$) could replace bromide if they were able to react either with $HBrO_2$ or $BrO_2^\bullet$ radicals. In 1989 Försterling and Noszticzius[12] proved that malonyl radicals react with $BrO_2^\bullet$ at a diffusion controlled rate. Thus an additional negative feedback loop was discovered in the BZ reaction. The failure of a new mechanistic model, the Radicalator, in which malonyl radical is the only control intermediate, indicates that bromide control cannot be completely replaced by $MA^\bullet$ control.

A detailed mechanism including 26 dynamic variables and 80 elementary reactions was developed by Györgyi, Turányi, and Field[13] (referred as GTF model) in 1990 for the system with cerium as a catalyst and malonic acid as an organic substrate. In the GTF model, 66 reactions are devoted to reactions involving radical species as products or as reactants. However, disproportionation rather than recombination was assumed for organic radicals when they react with each other as no direct experimental evidence was available at that time. Another basic assumption in their model is radical transfer like

$$MA^{\bullet} + BrMA \rightarrow BrMA^{\bullet} + MA \qquad GTF_{61}$$

This reaction was regarded to be important as it strengthens the negative feedback loop via bromide. However, it was proved by ESR and bromide stoichiometry experiments that reaction GTF_{61} does not contribute to the chemistry of the BZ reaction[14~16]. Without this reaction, the GTF model fails to predict oscillations at all. Moreover, the GTF model fails to predict any oscillation in the cerium catalyzed BZ system with bromomalonic acid (BrMA) as an organic substrate.

Recently, Gao and Försterling presented a model involving 18 elementary reactions for the BZ system with BrMA as an organic substrate[24] (referred as GF model). In the GF model two different negative feedback loops are involved: 1) the bromide generated from the organic process removes $HBrO_2$ to inhibit the autocatalytic reaction; 2) the bromomalonyl radicals formed in the organic subset capture $BrO_2^{\bullet}$ radicals to inhibit the autocatalytic process. With this model they successfully explained the observations in a $[Ru(bipy)_3]^{2+}$/bromomalonic acid/bromate system. An open problem in the chemical mechanism of the GF model is the decomposition route of the bromomalonyl bromite ($MABrO_2$), a recombination product formed in the control reaction between bromomalonyl radical ($BrMA^{\bullet}$) and $BrO_2^{\bullet}$. Two routes were assumed: 1) hydrolysis leading to bromotartronic acid (BrTTA) and bromous acid ($HBrO_2$); 2) a route leading to an unknown product P and Br^-.

$$BrMABrO_2 \rightarrow Br^- + P \qquad GF_{17}$$

$$BrMABrO_2 \rightarrow HBrO_2 + BrTTA \qquad GF_{18}$$

To shed more light on the mechanism of the BZ reaction we performed experiments with the classical catalyst, cerium, in this work. After collecting all the available experimental data for the Ce^{4+} catalyzed system, we suggest a new model including both negative feedback loops. A good qualitative agreement between experimental data and model calculations is obtained for a large range of initial conditions.

Chapter 2

Experimental

2.1 Instruments

A diode array spectrophotometer (8452A, Hewlett Packard) equipped with an IBM compatible AT computer was used either to take absorption spectra or to follow kinetics. A deuterium lamp was used in the spectrophotometer to illuminate the samples in a wavelength range from 190 to 820 nm. Using this instrument we were able to follow absorbances at different wavelengths (up to 6) or to take complete spectra (scan time 0.1 s) as a function of time.

A self-made dual wavelength fiber optics spectrophotometer[25] equipped with different cell holders for different reaction cells (16 mL cell with an optical path length of 1.9 cm; 25 mL cell with an optical path length of 2.5 cm; 140 mL cell with an optical path length of 10.8 cm) was used for most of the kinetic measurements. The light absorption was monitored using the single beam or the dual wavelength mode. With this apparatus we were able to follow absorbance changes at two different wavelengths simultaneously.

To follow the concentration change of bromide or hypobromous acid in the reaction system, a commercial AgBr electrode (Radiometer, Kopenhagen, Type F1022Br) was inserted into the cell; a 1 M KCl-silver chloride electrode was used as a reference which was connected to the solution by a salt bridge with sintered glass diaphragms on both ends of the tubing filled with 1 M sulfuric acid (double junction). The potential change of the electrode was measured with a WTW DIGI 610 pH meter.

The temperature of the system was electronically controlled at 20.0 ± 0.1 °C and the solution was stirred with a magnetic stirrer. To exclude oxygen from the system, a stream of nitrogen was applied through the solution 15 min before starting the reaction and constantly during the reaction (in the case of 16 mL cell). The solution was bubbled

with nitrogen 15 min before the transfer into the cell; the system was closed, and a nitrogen stream was applied above the surface of the solution to provide an inert gas blanket during the reaction.

The HPLC experiments were performed with a Shimadzu instrument (LC-10AS pump, CTO-10A column oven, SPD-10A dual wavelength UV detector working at 220 nm) equipped with an ion exchange column (Merck, Polyspher OA KC with a length of 30 cm and diameter of 9.5 mm) at 45 °C. The eluent is 0.01 M H_2SO_4, flow rate 0.40 mL / min. Vacuum was applied to degas the eluent.

The output signals from the detector were collected in two channels which are connected to two Keithley 155 microvoltmeters. Using different input ranges the microvoltmeters can be set to different sensitivities: high sensitivity detects the minor components and low sensitivity shows the major components. The output of the micro-voltmeters are fed into the multiplexer input of an analog-digital converter (AD) connected to an IBM PC.

The numerical integration of the kinetic differential equations was performed with the program DIFFGL which is based on Gear's method.

2.2 Chemicals

H_2SO_4 (96%), NaBr, $NaClO_4$, $Ce(SO_4)_2 \cdot 4H_2O$, $Ce_2(SO_4)_3$ (all Fluka pa.) were used without further purification.

Bromomalonic acid was prepared according to the method reported by Försterling and Stuk et al.[14] The purity of bromomalonic acid was checked with HPLC and by measuring the rate constant of the Ce^{4+}/BrMA reaction. Tartronic acid (TA, Heraeus, puriss.) was purified by treating the solid with an excess of acetic acid ethylester.

$NaBrO_3$ (Fluka pa.) was recrystallized twice from water. $NaBrO_2$ and HOBr were prepared according to the method reported by Noszticzius et. al[17,18]

All solutions were prepared from doubly distilled water. The measurements were carried out at 20 °C in 1 M H_2SO_4.

Chapter 3

Results and Discussion

3.1 The Inorganic Subset

3.1.1 Current model

One essential part of the Belousov–Zhabotinsky system is the autocatalytic oxidation of Ce^{3+} by acidic bromate. The basic form of this chemistry was presented by Field, Körös, and Noyes (FKN)[4] in 1972, which is given by reactions R_1~R_6. Försterling et al. modified this model by splitting R_4 into two elementary reactions (R_{4a} and R_{4b}) and including the decomposition of acidic bromate R_7 following direct experiments[19, 20]. Thus, the current model consists of 9 elementary reactions (Table 3-1). Most of them are reversible. Gao[22] confirmed the kinetics and mechanism of this model by studying the ruthenium catalyzed BZ system (catalyst Ce^{3+} replaced by $[Ru(bipy)_3]^{2+}$).

To examine this model, we performed experiments in the absence of oxygen, which was achieved by bubbling nitrogen through the reaction mixture for 15 minutes before starting the reaction. The reactions were carried out in 1 M sulfuric acid at 20 °C with an optical cell of 10.8 cm path length (140 mL volume). A homemade spectrophotometer was used to monitor Ce^{4+} (432 nm single beam technique) and $BrO_2^{\bullet}$ (550/670 nm dual-wavelength method).

The concentrations of Ce^{4+} and $BrO_2^{\bullet}$ were calculated from the measured absorbances A_{432} and A_{550} in the following way:

$$A_{432} = d(\varepsilon_{Ce^{4+}}^{432}[Ce^{4+}] + \varepsilon_{BrO_2^{\bullet}}^{432}[BrO_2^{\bullet}]) \tag{3.1}$$

Table 3-1: Mechanistic model of the autocatalytic reaction (oxidation of Ce^{3+} by acidic bromate).

Nr.	Reactions			Rate constants $k_+/(M^{-1}s^{-1})$	$k_-/(M^{-1}s^{-1})$	Ref.
R_1	$Br^- + HOBr + H^+$	$\rightleftharpoons$	$Br_2 + H_2O$	$8\times10^9\ M^{-1}$	110 M	[21]
R_2	$Br^- + HBrO_2 + H^+$	$\rightleftharpoons$	$2\ HOBr$	$2.5\times10^6\ M^{-1}$	2×10^{-5}	[23]
R_3	$Br^- + BrO_3^- + 2\ H^+$	$\rightleftharpoons$	$HOBr + HBrO_2$	$1.2\ M^{-2}$	3.2	[24]
R_{4a}	$HBrO_2 + H^+$	$\rightleftharpoons$	$H_2BrO_2^+$	2.0×10^6	1.0×10^8	[19]
R_{4b}	$HBrO_2 + H_2BrO_2^+$	$\rightleftharpoons$	$HOBr + BrO_3^- + 2\ H^+$	1.7×10^5	0	[19]
R_{5a}	$HBrO_2 + BrO_3^- + H^+$	$\rightleftharpoons$	$Br_2O_4 + H_2O$	$48\ M^{-1}$	3200 M	[24]
R_{5b}	Br_2O_4	$\rightleftharpoons$	$2\ BrO_2^\bullet$	7.5×10^4 M	1.4×10^9	[21]
R_6	$Ce^{3+} + BrO_2^\bullet + H^+$	$\rightleftharpoons$	$Ce^{4+} + HBrO_2$	$6.0\times10^4\ M^{-1}$	1.2×10^4	[25]
R_7	$2\ BrO_3^- + 2\ H^+$	$\rightarrow$	$2\ HBrO_2 + 2\ O_2$	$6.0\times10^{-10}\ M^{-2}$	0	[20]

$$A_{550} = d(\varepsilon^{550}_{Ce^{4+}}[Ce^{4+}] + \varepsilon^{550}_{BrO_2^\bullet}[BrO_2^\bullet]) \tag{3.2}$$

Solving these equations for the Ce^{4+} and $BrO_2^\bullet$ concentrations we obtain:

$$[Ce^{4+}] = \frac{1}{d}\times\frac{A_{550}/\varepsilon^{550}_{BrO_2^\bullet} - A_{432}/\varepsilon^{432}_{BrO_2^\bullet}}{\varepsilon^{550}_{Ce^{4+}}/\varepsilon^{550}_{BrO_2^\bullet} - \varepsilon^{432}_{Ce^{4+}}/\varepsilon^{432}_{BrO_2^\bullet}} \tag{3.3}$$

$$[BrO_2^\bullet] = \frac{1}{d}\times\frac{A_{550}/\varepsilon^{550}_{Ce^{4+}} - A_{432}/\varepsilon^{432}_{Ce^{4+}}}{\varepsilon^{550}_{BrO_2^\bullet}/\varepsilon^{550}_{Ce^{4+}} - \varepsilon^{432}_{BrO_2^\bullet}/\varepsilon^{432}_{Ce^{4+}}} \tag{3.4}$$

where A_{432} and A_{550} are the absorbance at 432 nm and 550 nm, $\varepsilon^{432}_{Ce^{4+}}$, $\varepsilon^{432}_{BrO_2^\bullet}$, $\varepsilon^{550}_{Ce^{4+}}$ and $\varepsilon^{550}_{BrO_2^\bullet}$ are molar extinction coefficients of Ce^{4+} and $BrO_2^\bullet$ at the individual wavelengths, d is the optical path length, $[Ce^{4+}]$ and $[BrO_2^\bullet]$ are concentrations. By introducing the measured values d = 10.8 cm, $\varepsilon^{432}_{Ce^{4+}}$ = 190 $cm^{-1}\ M^{-1}$, $\varepsilon^{432}_{BrO_2^\bullet}$ = 806 $cm^{-1}\ M^{-1}$, $\varepsilon^{550}_{Ce^{4+}}$ = 0.5

cm^{-1} M^{-1} and $\varepsilon_{BrO_2^{\bullet}}^{550}$ = 337 $cm^{-1}M^{-1}$ into Equations (3.3) and (3.4), we obtained typical concentration curves for Ce^{4+} and $BrO_2^{\bullet}$ in the reaction of 3.0×10^{-4} M Ce^{3+} with 0.02 M and 0.1 M bromate (see Figure 3-1 solid lines). Each curve is composed of two parts: (a) A fast reaction period follows immediately after the injection. During this time both concentrations increase rapidly. (b)Then a slow reaction period ensues. During this time, the Ce^{4+} concentration approaches very slowly its final value, and the $BrO_2^{\bullet}$ concentration decreases after reaching a maximum.

We performed the simulation on the basis of the model in Table 3-1. The calculated results (dashed lines and circles in Figure 3-1) prove that both features of the curves of Ce^{4+} and $BrO_2^{\bullet}$ formation can be well described by the current model.

Next, the inhibition effect of bromide was checked by adding 3×10^{-4} M bromide into 0.02 M bromate when 3×10^{-4} M Ce^{3+} was injected. From the result displayed in Figure 3-2, we can see that a 160 seconds induction period appears before the start of the autocatalytic reaction. The simulation of the bromide inhibition effect was performed with the same model as for Figure 3-1. Unfortunately, the calculated induction time (dashed line and circles) is only one third of that observed in the experiment, implicating that the inhibition effect is underestimated in the model. The major reason for this underestimation may be the assignment of the rate constants because the chemistry is accepted.

The source of each rate constant involved in the model is given in Table 3-1 . The values of k_1 and k_{-1} reported by Eigen and Kustin[26] have been adjusted to 1M H_2SO_4 by FKN[4] and by Försterling et al.[23], and do not seem to require modification.

The disproportionation of $HBrO_2$ (R_4) was investigated by Försterling and Varga[19] in sulfuric acid medium at different acidities. The rate of this reaction was found to increase from 0.3 M H_2SO_4 to 3.0 M H_2SO_4 by a factor of 9. To account for this dependency, R_4 ($2\ HBrO_2 \rightleftharpoons HOBr + BrO_3^- + H^+$) was splitted into two elementary reactions (R_{4a}, R_{4b}) accordingly. For fast equilibrium R_{4a}, k_4 can be approximated by $k_4 = [H^+]k_{4b}\frac{k_{4a}}{k_{-4a}}$. For 1 M sulfuric acid, $[H^+]$ = 1.29 M was calculated according to

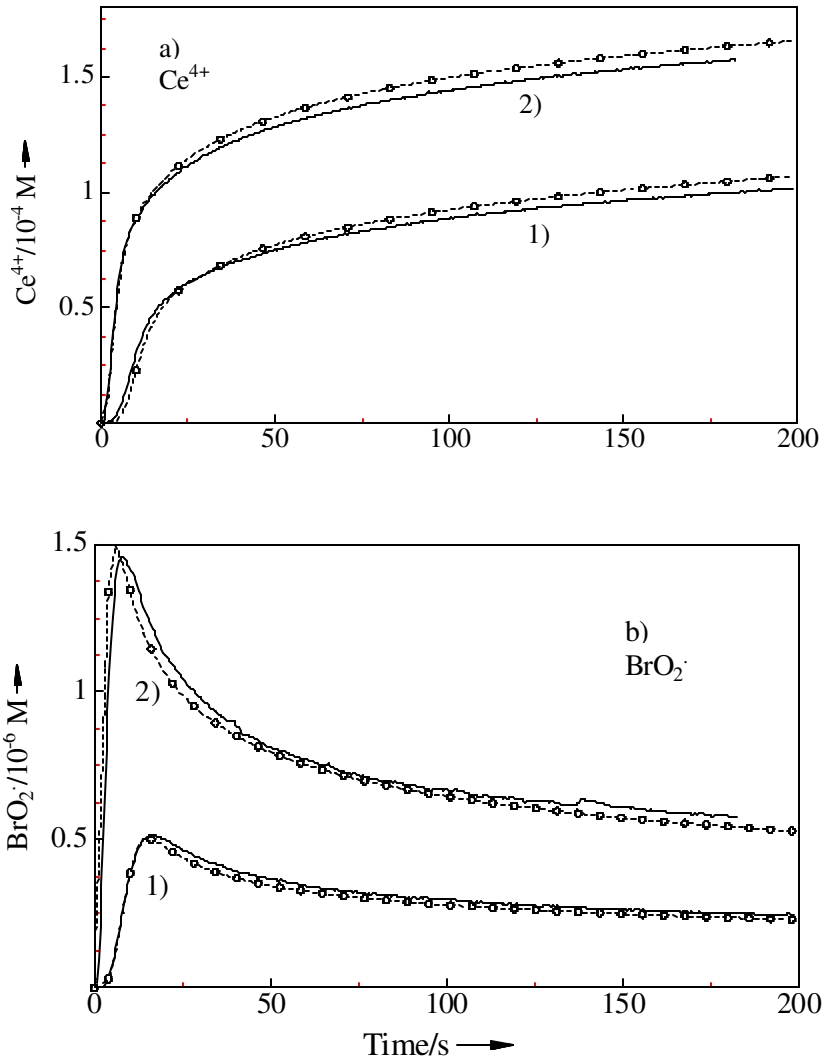

Figure 3-1: Autocatalytic formation of Ce^{4+} and $BrO_2^{\bullet}$ when 3.0×10^{-4} M Ce^{3+} was injected into 0.02 M and 0.1 M bromate in 1M H_2SO_4.

The experiments (solid lines) were carried out at 20°C in an optical cell with a path length of 10.8 cm and a volume of 140 mL. The kinetics was measured by following the absorbance at 432 nm for Ce^{4+} and at 550 nm for $BrO_2^{\bullet}$. $[Ce^{3+}]_0 = 3.0\times10^{-4}$ M ; $[BrO_3^-]_0 = 0.02$M (curve 1), 0.1M (curve 2)

The calculated curves (dashed lines and circles) are obtained by using the reaction scheme ($R_1 \sim R_7$) and the rate constants in Table 3-1.

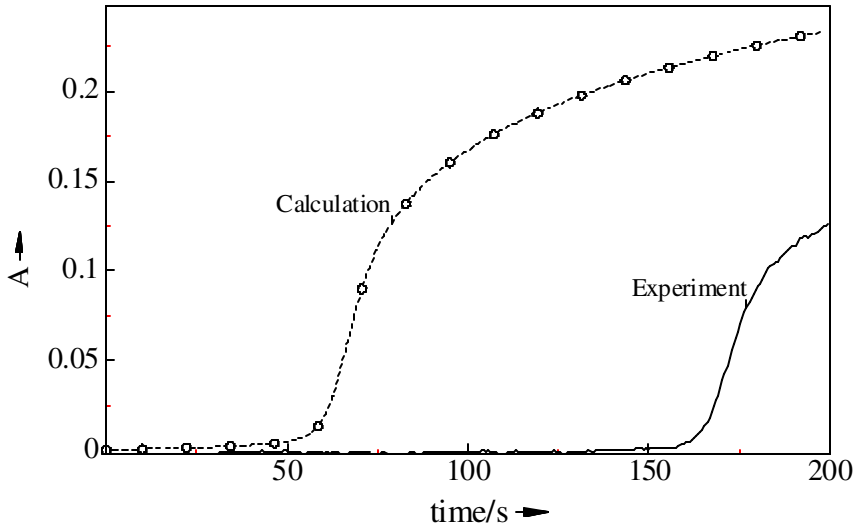

Figure 3-2: The change of absorbance A in the autocatalytic reaction inhibited by bromide.

The experimental conditions and the calculation are the same as in Figure 3-1. $[BrO_3^-]_0$ = 0.02 M; $[Ce^{3+}]_0 = 3.0\times 10^{-4}$ M ; $[Br^-]_0 = 3 \times 10^{-4}$ M, T = 20°C, H_2SO_4 = 1 M. Solid line: experiment, dashed line and circles: calculation.

Robertson et al.'s result[27] and we obtain $k_4 = 4500\ M^{-1}s^{-1}$.

R_2 has been well investigated [18, 21]. The latest value $k_2 = 2.5\times10^6\ M^{-2}s^{-1}$ was determined by Försterling et al[23] from the reaction of $HBrO_2$ with Br_2 in 1 M H_2SO_4. However, a too small rate constant for the disproportionation of $HBrO_2$, $k_4 = 3000\ M^1s^{-1}$, was used in the evaluation of their data. Replacing this value by $k_4 = 4500\ M^{-1}s^{-1}$ in the simulation, k_2 is modified to $2.9\times10^6\ M^{-2}s^{-1}$ here .

Lamberz[28] investigated reaction R_3 with bromate in excess ($[BrO_3^-]$ = 0.1 M) in a concentration range of sulfuric acid from 0.1 M to 0.7 M. Gad[22] extended these experiments to initial concentrations of sulfuric acid of 0.9 and 1.0 M by using lower concentrations of bromide and bromate, and concluded that k_3 is 1.2 M^3s^{-1}. However, Kshirsagar and Field[29] found 2.5 $M^{-3}\ s^{-1}$ under similar conditions but with bromide in

excess. In view of the critical effect of R_3 to the first feedback loop (inhibition by bromide) and the uncertainty of rate constant k_3, more work needs to be done here.

Kuhnert et al.[30] obtained a value k_{5a} = 30 $M^{-2}s^{-1}$ from the investigation of the ferroin catalyzed autocatalytic reaction in 0.613 M H_2SO_4 at 25 °C, but the interpretation leading to this result ignored the effect of R_4. Field and Försterling[21] found a higher value k_{5a} = 42 $M^{-2}s^{-1}$ in the cerium catalyzed system at 20 °C. Gao and Försterling[24] redetermined k_{5a} at 20 °C using Kuhnert's method with the ruthenium trisbipyridyl complex as a catalyst; using numerical simulations including all side reactions, the experimental curve was well modeled with k_{5a} = 48 $M^{-2}s^{-1}$. From the equilibrum constant K_{5a} =0.015 M^{-2} [21], the rate constant of the backward reaction was recalculated. These values are accepted here.

k_{5b}, k_{-5b} and k_6 shown in Table 3-1 are well established values. With regard to k_{-6}, Försterling and Varga[19] found a strong dependence on acidity as well as on ionic strength. More work is needed to establish a relationship with ionic strength in 1 M H_2SO_4. The decomposition of acidic bromate was addressed recently[20].

3.1.2 Kinetics of the $BrO_2^\bullet$ Decomposition

Bromine dioxide ($BrO_2^\bullet$) was found to be an intermediate in the oscillating system[31, 32] as well as in the set of inorganic reactions[33,34]. Although $BrO_2^\bullet$ is thought to be kinetically unstable (decomposing instantly into $Br^\bullet$ + O_2 with an estimated Br-OO bond energy of about 1 kcal/mol[35]), there is another path for $BrO_2^\bullet$ decay within the reaction scheme proposed for the BZ reaction: the recombination via reaction R_{-5} (2 $BrO_2^\bullet$ + $H_2O \rightarrow HBrO_2 + HBrO_3$).

Pacios and Gómez[36] theoretically studied $BrO_2^\bullet$ by means of *ab initio* correlated calculations, also predicted a small barrier between 1.2 and 1.7 kcal/mol for the dioxide dissociation. Nevertheless, the experimental characterization of $BrO_2^\bullet$ is far from complete, and kinetic studies dealing with this species are scarce. To get more

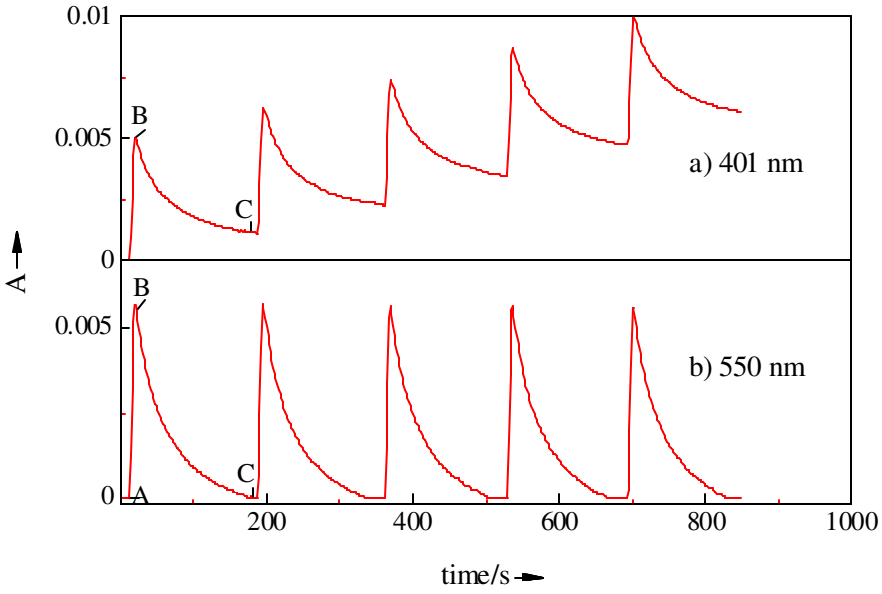

Figure 3-3: The absorbance change A in a flash light experiment.

The experiment was performed with a 1 M solution of BrO_3^- in 1M H_2SO_4 at 20°C. Elimination of O_2 by applying a stream of N_2. The optical path length is 10.3 cm; wavelength 401 nm *(a)* and 550 nm *(b)*. Each peak corresponds to one flush pulse.

information about the stability of this dioxide, we carried out a flash-light experiment, in which $BrO_2^\bullet$ is formed in situ by photolysis of a bromate solution[37]:

$$BrO_3^-{}^\bullet H_2O \xrightarrow{h\gamma} (BrO_3^-{}^\bullet H_2O)^* \rightarrow BrO_2^\bullet + {}^\bullet OH + OH^- \qquad Z_1$$

The flash photolysis setup consists of a xenon arc flash lamp, 10 parallel connected capacitors supplying 400 µF capacitance to the lamp and a high-voltage pulse generator. The dual-wavelength method at 401 and 550 nm was used to detect the transient $BrO_2^\bullet$ and to follow its concentration with time.

A 1 M solution of bromate in 1 M sulfuric acid was bubbled with N_2 for 15 min. to remove oxygen before being poured into a quartz cell with 10.3 cm optical path length. In Figure 3-3 the absorbance change after the flash pulse is displayed (each peak corresponding to firing the flash once). We found that immediately after the flash pulse

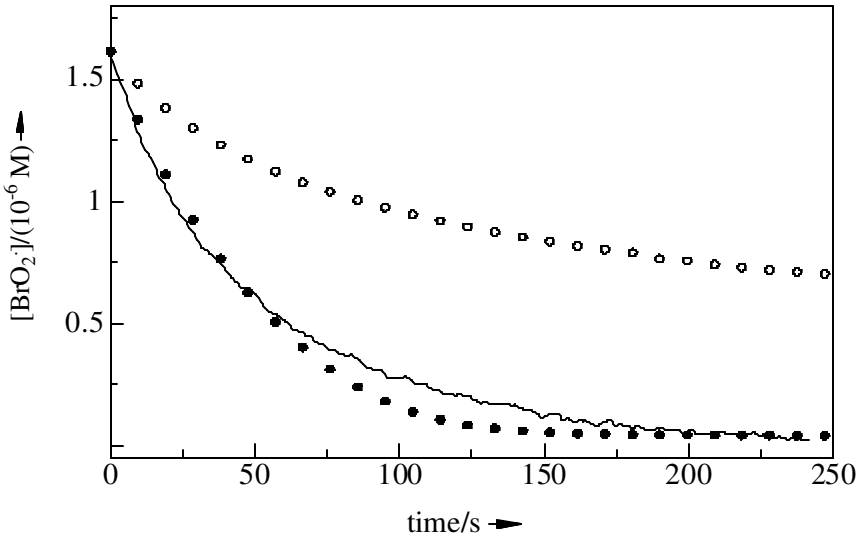

Figure 3-4: The decay of the $BrO_2^{\bullet}$ concentration as a function of time.

The same experiment as Figure 3-3. The concentration of $BrO_2^{\bullet}$ is obtained from A_{550} with the optical path length d = 10.3 cm and the extinction coefficient ε_{550} = 337 $cm^{-1}M^{-1}$. Solid line: experiment (corresponding to the part BC in Figure 3-3b).

The calculated curves are obtained from the model in Table 3-1. Circles: calculated with reactions R_{4a}, R_{4b}, R_{5a}, R_{5b} and R_7. Dots: calculated by including the $BrO_2^{\bullet}$ decomposition reaction R_{17} ($k_{17} = 0.06\ s^{-1}$).

the absorption signals at 401 and 550 nm sharply and synchroneously rise to a maximum indicating a fast rise of $BrO_2^{\bullet}$ to about 1.5×10^{-6} M (the extinction coefficients of $BrO_2^{\bullet}$ at these two wavelengths are ε_{401} = 360 $cm^{-1}M^{-1}$ and ε_{550} = 337 $cm^{-1}M^{-1}$). After that a slow decay followed due to the decay of $BrO_2^{\bullet}$ (part B-C of the curves). It is interesting to see that the decay of the signals in the two channels is not syncheronous: when the absorbance at 550 nm approaches zero implicating that all the generated $BrO_2^{\bullet}$ has disappeared, the absorbance at 401 nm approaches a limiting value. We assume that besides the recombination reaction, $BrO_2^{\bullet}$ also decomposes to a species absorbing light at 401 nm.

Transforming the absorbance – time curve into the form of the concentration – time curve with the relation $A_{550} = \varepsilon_{550} \times d \times [BrO_2^{\bullet}]$, we obtained the decay of $BrO_2^{\bullet}$ as a function of time (Figure 3-4 solid line).

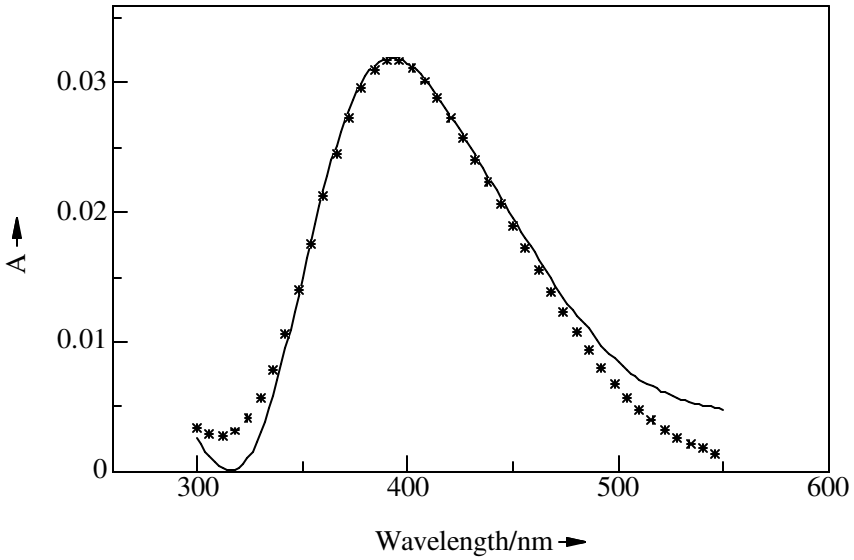

Figure 3-5: The absorption spectrum of the solution (25 flash pulses applied).

The experimental conditions are the same as Figure 3-3. Solid line: the absorption spectrum of a solution taken after 25 flash pulses. Asterisks: the spectrum of a solution of bromine.

To see the decay of $BrO_2^\bullet$ in the model, the reactions R_1~R_5 and R_7 were used together with the corresponding rate constants in Table 3-1. The calculated result shows that only one half of the $BrO_2^\bullet$ should disappear within 250 seconds (circles in Figure 3-4). Apparently, the model simulation supports our assumption that besides the reaction R_{-5} there is another path consuming $BrO_2^\bullet$.

Now we focus our attention on the product found at the end of $BrO_2^\bullet$ decay. A second flash pulse was applied on the same system when all $BrO_2^\bullet$ generated in the last pulse disappeared (signal at 550 nm approaches zero). Similar kinetics were observed after each flash pulse, and the absorbance at 401 nm reaches A = 0.006 after five flash pulses due to the accumulation of the product in the solution (see Figure 3-3).

The absorption spectrum of a solution with the accumulated product is displayed in Figure 3-5. We find that the spectrum is in the range between 350 and 550 nm, and its maximum is at the same place as that of bromine (asterisks). Hence, we assume that $BrO_2^\bullet$ decomposes into bromine. This assumption is supported by Pacios and Gómez's

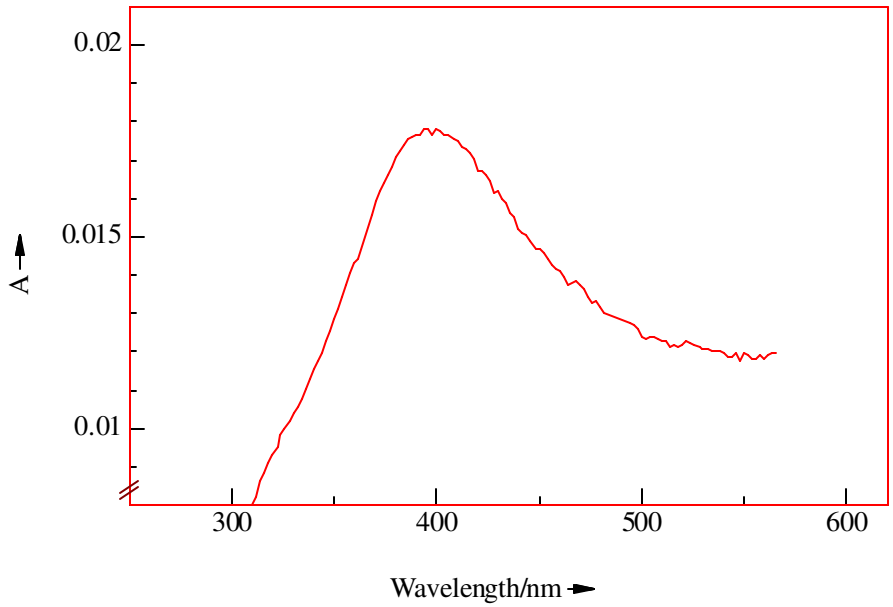

Figure 3-6: Flash light experiment - the absorption difference as a function of wavelength after bubbling.

The experimental conditions are the same as given in Figure 3-3. 15 flash pulses were applied to the solution, and the spectrum difference is caused by bubbling N_2 for 15 min. (see text).

prediction that $BrO_2^{\bullet}$ dissociates into $Br^{\bullet}$ + O_2 with a small energy barrier, because $Br^{\bullet}$ radicals are very easy to recombine leading to Br_2.

In addition, if the product is really bromine, the spectrum should change after a treatment of bubbling because bromine is easy to be removed from the solution by bubbling with gas. The following treatments were performed: first 15 flash pulses were applied to a 1 M solution of bromate in 1 M H_2SO_4, and a UV spectrum of the flashed solution was taken, called spectrum 1; then, bubble this solution with N_2 for 15 minutes and take a second spectrum, this is spectrum 2; finally, calculate the difference of spectra 1 and 2 and display the result in Figure 3-6 (solid line). It can be clearly seen that the spectrum difference caused by bubbling (in another word, the species removed

by bubbling) has the same UV-spectrum as the product (Figure 3-5), and coincides with the absorption spectrum of bromine (Figure 3-5 asterisks).

Now we are convinced that, besides the recombination and disproportionation via R_{-5} $BrO_2^\bullet$ dissociates into bromine via $Br^\bullet$ radical. The mechanism is:

$BrOO^\bullet$	$\rightarrow$	$Br^\bullet + O_2$	R_{17a}
$Br^\bullet + Br^\bullet$	$\rightarrow$	Br_2	R_{17b}
$Br^\bullet + BrOO^\bullet$	$\rightarrow$	$Br_2 + O_2$	R_{17c}
$BrO_2^\bullet$	$\rightarrow$	$\frac{1}{2} Br_2 + O_2$	R_{17}

We add the overall step R_{17} into the mechanism of the BZ reaction. As for the rate constant k_{17}, the system is too complicate to evaluate it directly from the experimental curves. Fortunately, the oxybromine chemistry is quite clear and the rate constants for all those reactions are derived from direct measurements, so we can draw a conclusion for k_{17} from simulation. On the basis of R_1~R_5, R_7 and R_{17} and the corresponding rate constants in Table 3-1, we performed the simulation by setting k_{17} as a parameter. A good fit to the experimental curves is achieved with $k_{17} = 0.06$ s^{-1} and $k_{-17} = 0$ (dots in Figure 3-4). Apparently, the dissociation reaction is too slow to be important for the kinetic of the oscillatory reaction. But this discovery verified the result of a quantum mechanical calculation that $BrOO^\bullet$ is more stable than $OBrO^\bullet$; this may be significant for an understanding of the decomposition path of organic radical-$BrO_2^\bullet$ recombination products.

3.1.3 $HBrO_2$ / Ce^{4+} and $BrO_2^\bullet$ / Ce^{3+} Reactions

The reaction of bromous acid with Ce^{4+} (reaction R_{-6}) is responsible for the slowing down of the autocatalytic oxidation of Ce^{3+} by bromate in the BZ reaction. The rate constant of this reaction was determined by Försterling and Varga[19] with a spectroscopic method. It was found that the rate constant depends on the ionic strength of the reaction mixture: k_{-6} decreases from 4×10^4 $M^{-1}s^{-1}$ in 0.3 M H_2SO_4 to 1×10^3 $M^{-1}s^{-1}$ in 3 M H_2SO_4. This dependence was attributed to the effect of ionic strength on the

equilibrium constants for the formation of sulfato complexes. However, few data are available in the range of ionic strength from 1.5 M to 2.5 M, which is the usual range for the BZ reaction.

To measure k_{-6} Försterling and Varga[19] designed an experiment with Ce^{4+} in excess over $HBrO_2$ and they followed the small decay of the Ce^{4+} absorbance. Because of the consumption of Ce^{4+} and the disproportionation of $HBrO_2$, the rate constant k_{-6} had to be evaluated from the slopes of the initial part of the Ce^{4+} curves, $\upsilon = \left(\frac{d\Delta Ce^{4+}}{dt} \right)_0$, where the concentrations of both cerium and bromous acid were taken as initial values. It must be mentioned that this reaction proceeds very fast and both concentrations (Ce^{4+} and $BrO_2^{\bullet}$) decrease seriously with time. Thus, errors can be caused if the measured range is not the early phase of the reaction. To confirm their result and obtain more data for evaluating the relationship between ionic strength and k_{-6}, we repeat the measurement using a different method.

Försterling et al.[25] have successfully obtained the rate constant k_6 (Ce^{3+} reacting with $BrO_2^{\bullet}$) by using the reaction of methanol with bromate. We consider this reaction here for determining the backward rate constant k_{-6} as well as the forward k_6. The first step of the methanol-bromate reaction is:

$$CH_3OH + 2\ HBrO_3 \rightarrow HCOOH + 2\ HBrO_2 + H_2O \qquad Z_2$$

This reaction is followed by the steps R_{5a} - R_{5b}, and $BrO_2^{\bullet}$ is formed as an intermediate. The advantage of this experimental setup is that the concentration of $BrO_2^{\bullet}$ can be kept almost constant[25], and its reaction with Ce^{3+} is quasi first-order kinetics.

In these experiments the actual operation is: a required amount of CH_3OH in 1 M sulfuric acid was injected into acidic bromate solution of different concentration to generate a certain concentration of $BrO_2^{\bullet}$, the formation of $BrO_2^{\bullet}$ was followed by the dual wavelength method at 550 nm; as soon as the $BrO_2^{\bullet}$ signal was constant, $Ce_2(SO_4)_3$ in 1 M sulfuric acid was injected, and the formation of Ce^{4+} was monitored at 401 nm (Figure 3-7).

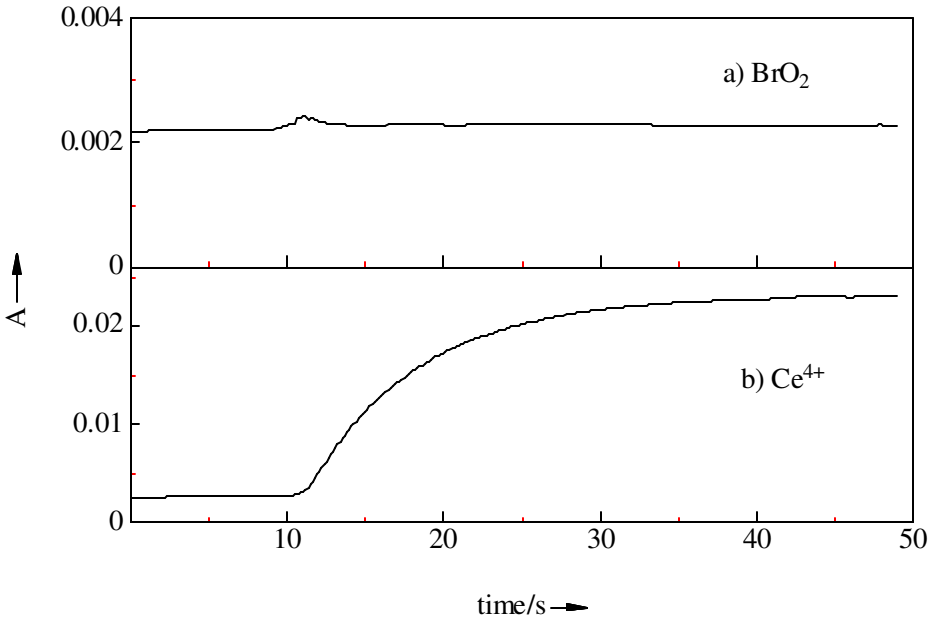

Figure 3-7: Generation of $BrO_2^{\bullet}$ by the injection of methanol into acidic bromate.

The experiment was performed with a cell of 10.8 cm optical path length (140 mL volume) at 20 °C in 1 M H_2SO_4. 1 mL of a 2.96 M solution of methanol was injected into 0.05 M bromate solution. As soon as the absorbance of $BrO_2^{\bullet}$ was constant, 0.25 mL of 2.2×10^{-3} M $Ce_2(SO_4)_3$ solution were injected. Wavelength λ = 550 nm a), λ = 401 nm b).

To confirm that the effect on the rate constant is really due to the ionic strength, more experiments were performed by adding $NaClO_4$ to change the ionic strength while the bromate concentration was kept constant.

We consider the reaction:

$$Ce^{3+} + BrO_2^{\bullet} + H^+ \rightleftharpoons Ce^{4+} + HBrO_2 \qquad R_6$$

According to equation R_6, the rate of Ce^{4+} formation is:

$$\frac{d[Ce^{4+}]}{dt} = k_6'[Ce^{3+}] - k_{-6}'[Ce^{4+}] = k_6'(c_0 - [Ce^{4+}]) - k_{-6}'[Ce^{4+}] \qquad (3.5)$$

where c_0 is the initial concentration of Ce^{3+}, $k_6^{'} = k_6[H^+][BrO_2^{\bullet}]_0$ and $k_{-6}^{'} = k_{-6}[HBrO_2]_0$; $[BrO_2^{\bullet}]_0$ and $[HBrO_2]_0$ are steady state concentrations.

Using the relation for the absorbance of Ce^{4+}

$$A = d\varepsilon[Ce^{4+}] \tag{3.6}$$

we obtain by integration

$$\ln \frac{A_\infty - A}{A_\infty} = -(k_6^{'} + k_{-6}^{'})t \tag{3.7}$$

(A_∞ is the absorbance of Ce^{4+} at the end of the reaction)

For each experiment discussed above, the left hand side of Equation (3.7) is plotted as a function of time, two example plots are displayed in Figure 3-8. The plots demonstrate that the reaction can indeed be treated as first order kinetics. The slope of the straight line is the sum of the rate constants for the forward and backward reactions:

$$\text{Slope} = -(k_6^{'} + k_{-6}^{'}) \tag{3.8}$$

To evaluate k_6 and k_{-6} from the experimental curves, we consider the equilibrium condition:

$$\frac{[Ce^{4+}]_\infty}{[Ce^{3+}]_\infty} = \frac{[Ce^{4+}]_\infty}{(c_0 - [Ce^{4+}]_\infty)} = \frac{k_6^{'}}{k_{-6}^{'}} \tag{3.9}$$

$[Ce^{4+}]_\infty$ is the concentration of Ce^{4+} at the end of the reaction. Solving Equations (3.8) and (3.9) we obtain expressions for $k_6^{'}$ and $k_{-6}^{'}$ and for k_6 and k_{-6}, respectively:

$$k_6^{'} = -\frac{slope \times [Ce^{4+}]_\infty}{c_0} \tag{3.10}$$

$$k_{-6}^{'} = -\frac{slope \times (c_0 - [Ce^{4+}]_\infty)}{c_0} \tag{3.11}$$

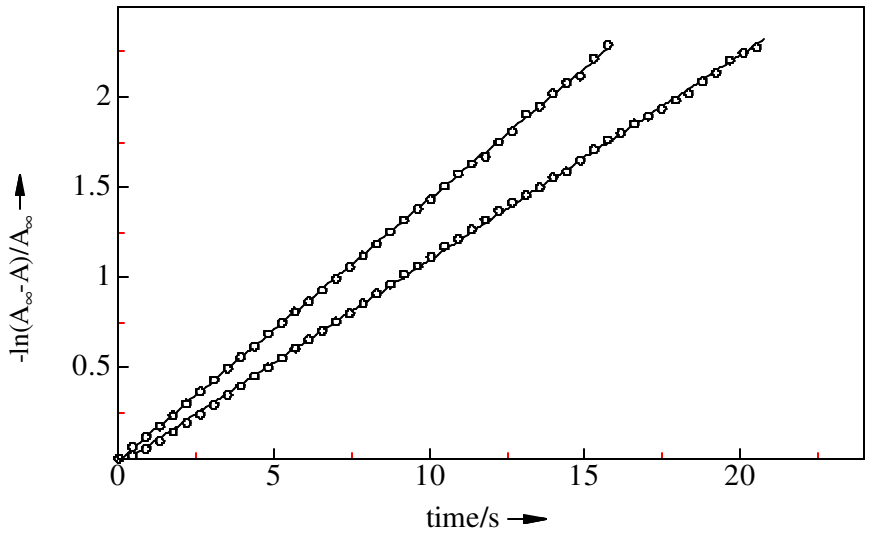

Figure 3-8: $Ce^{3+}/BrO_2^{\bullet}$ – reaction. Evaluation of the first order rate constant from Equation (3.7). The time is measured from the injection of Ce^{3+}.

$$k_6 = \frac{slope[Ce^{4+}]_\infty}{[H^+][BrO_2^\bullet]c_0} \tag{3.12}$$

$$k_{-6} = \frac{slope(c_0 - [Ce^{4+}]_\infty)}{[HBrO_2]c_0} \tag{3.13}$$

At constant $BrO_2^{\bullet}$ the concentration of $HBrO_2$ is constant as well, and can be calculated from the equilibrium constants K_{5a}, K_{5b}.

$$[HBrO_2] = \frac{[BrO_2^\bullet]^2}{K_{5a}K_{5b}[BrO_3^-][H^+]} \tag{3.14}$$

Table 3-2 shows the experimental details and the results for k_{-6} and k_6 (columns 9 and 10). It turns out that the forward rate constant k_6 does not depend on the ionic strength, and the mean value 5.7×10^4 $M^{-1}s^{-1}$ is consistent with the result reported by Försterling et al.[25] (6.0×10^4 $M^{-1}s^{-1}$). On the other hand, k_{-6} decreases with increasing ionic strength just as discovered by Försterling and Varga[19]. The values of k_{-6} displayed in Table 3-2 are plotted as a function of ionic strength in Figure 3-9. The triangles represent data

Table 3-2: Second-order rate constants k_{-6} and k_6 obtained in systems with different ionic strength.

1~10: the results in this work. Temperature 20 °C, sulfuric acid 1 M ([H^+] = 1.29 M), the formation of Ce^{4+} was measured at 401 nm with a 140 mL volume cell (optical path length 10.8cm). 11~14: the results from Försterling and Varga[19].

No.	$c_0/10^{-6}$ M	$[BrO_3^-]_0$ /M	$[NaClO_4]$ /M	-Slope $/s^{-1}$	$[BrO_2^\bullet]$ $/10^{-6}$ M	$[Ce^{4+}]_\infty$ $/10^{-6}$ M	Ionic strength /M	$k_{-6}/10^4$ $M^{-1}s^{-1}$	$k_6/10^4$ $M^{-2}s^{-1}$
1.	7.10	0.05	0	0.146	0.623	2.26	1.62	1.33	5.78
2.	3.88	0.10	0	0.174	1.08	1.28	1.67	1.03	4.13
3.	7.12	0.05	0.11	0.142	0.619	2.45	1.73	1.25	6.11
4.	7.12	0.05	0.20	0.137	0.646	2.55	1.82	1.09	5.89
5.	7.12	0.05	0.40	0.133	0.673	2.91	2.02	0.90	6.27
6.	3.14	0.50	0	0.281	2.67	1.71	2.07	0.93	4.44
7.	7.12	0.05	0.60	0.130	0.70	3.11	2.22	0.77	6.26
8.	7.12	0.05	0.80	0.122	0.673	3.44	2.42	0.72	6.78
9.	1.57	1.00	0	0.310	3.88	1.06	2.57	0.69	4.18
10.	7.12	0.05	1.0	0.125	0.754	3.73	2.62	0.54	6.74
11.							0.80	2.40	
12.							1.60	1.20	
13.							2.40	0.70	
14.							2.60	0.60	

obtained with different initial concentration of bromate; the asterisks are obtained in the systems with the same bromate concentration but adding different amount of NaClO4 for changing the ionic strength; the dots are taken from Försterling and Varga[19] work. We found that the values resulting from the different methods are completely consistent with each other, and the dependence of k_{-6} on ionic strength can be represented by a power series:

$$k_{-6} = a_0 + a_1 \times \mu + a_2 \times \mu^2 + a_3 \times \mu^3$$

where μ is the ionic strength of the reaction mixture; a_0 = -1.74743 $M^{-1}s^{-1}$, a_1 = 6.75949 M^{-2} s^{-1}, a_2 = - 4.30066 $M^{-3}s^{-1}$, a_3 = 0.797993 $M^{-4}s^{-1}$.

Figure 3-10 displays the experimental results in the range of ionic strength from 1.5 M to 2.5 M, the usual range for the BZ reaction.

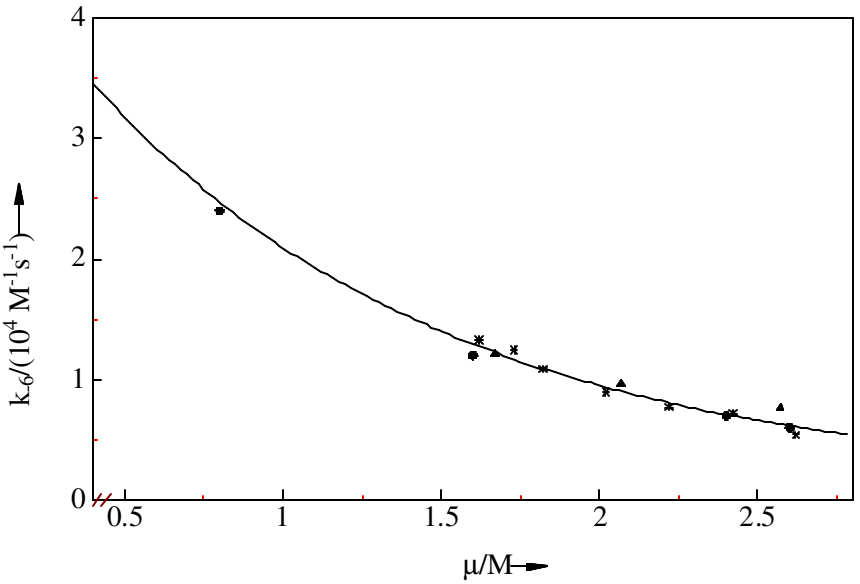

Figure 3-9: Second order rate constants k_{-6} as a function of the ionic strength of the solution.

The data are taken from Table 3-2 and reference 19 (for 4 points). Different ionic strength was achieved by changing the concentration of bromate (triangles) and adding $NaClO_4$ (asterisks). Dots: taken from Försterling and Varga's work.

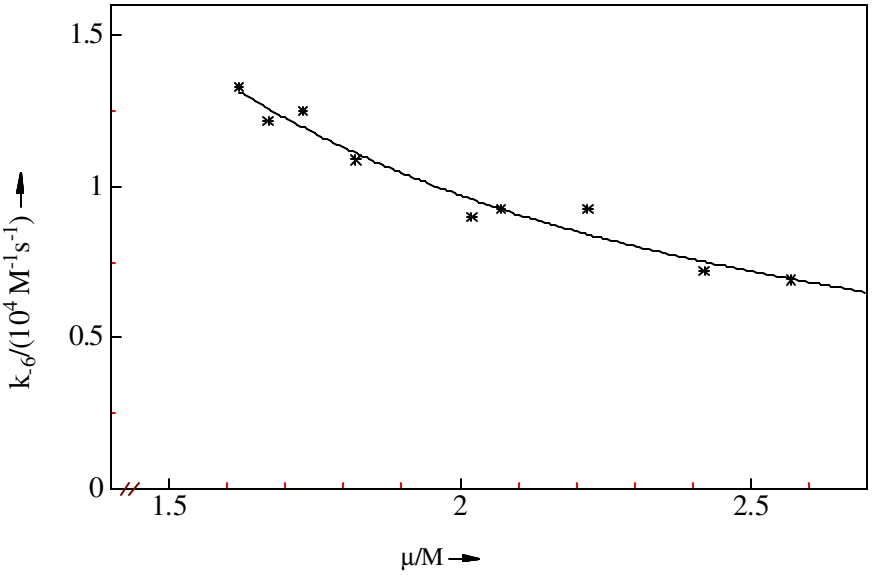

Figure 3-10: Dependence of k_{-6} on ionic strength μ in the range μ = 1.5 ~ 2.6 M.

The asterisks: experimental data taken from Table 3-2. Solid line: calculated with the power series: $k_{-6} = a_0 + a_1 \times \mu + a_2 \times \mu^2 + a_3 \times \mu^3$, for the coefficients see text.

3.1.4 Kinetics of Reaction R_3

$$Br^- + BrO_3^- + 2H^+ \rightleftharpoons HOBr + HBrO_2$$

R_3 is one of the component steps of the reaction Z_3,

$$5\,Br^- + BrO_3^- + 6\,H^+ \rightarrow 3\,Br_2 + 3\,HO_2 \qquad Z_3$$

It initiates the overall process and determines the reaction rate, since the rate of Z_3 was proved in kinetics studies[38, 39] to be proportional to $[Br^-]\times[BrO_3^-]\times[H^+]^2$.

Lamberz[40] investigated this reaction in the case of bromate in excess with $[BrO_3^-]_0$ = 0.1 M in a concentration range of sulfuric acid from 0.1 M to 0.7 M. The rate constant k_3 = 1.2 $M^{-3}s^{-1}$ in 1 M sulfuric acid was extrapolated from an acidity dependence plot. Gao[22] extended these experiments to 0.9 and 1.0 M sulfuric acid by using lower concentrations of bromide and bromate, and found the same result as Lamberz.

Kshirsagar and Field[29] verified this result by simulating the experimental absorbance when essentially stoichiometric amounts of Br^- and BrO_3^- react, and a value k_3 = 2.5 M^{-3} s^{-1} was obtained. This value is larger by a factor of 2 than that obtained by Lamberz and Gao. On the other hand, to fit their experimental data for the bromine hydrolysis in bromate solution they had to change the equilibrium constant for reaction R_1 (Br^- + HOBr + H^+ $\rightleftharpoons$ Br_2 + HO_2), $K_1 = \dfrac{[Br_2]}{[Br^-][HOBr][H^+]}$, from 7.1×10^7 M^{-2}[21] to 1.5×10^9 M^{-2}. Otherwise the calculated rate of HOBr formation was much higher than observed. It seems strange that K_1 may be wrong by a factor of 20.

In order to understand Kshirsagar-Field's problem, Försterling and Murányi[23] reexamined the bromine-bromate reaction by using lower initial concentrations of bromine and by using a more sensitive method of detection. As in the Kshirsagar – Field experiment, the rate of bromine disappearance turned out to be smaller by a factor of about 3 compared to the calculations.

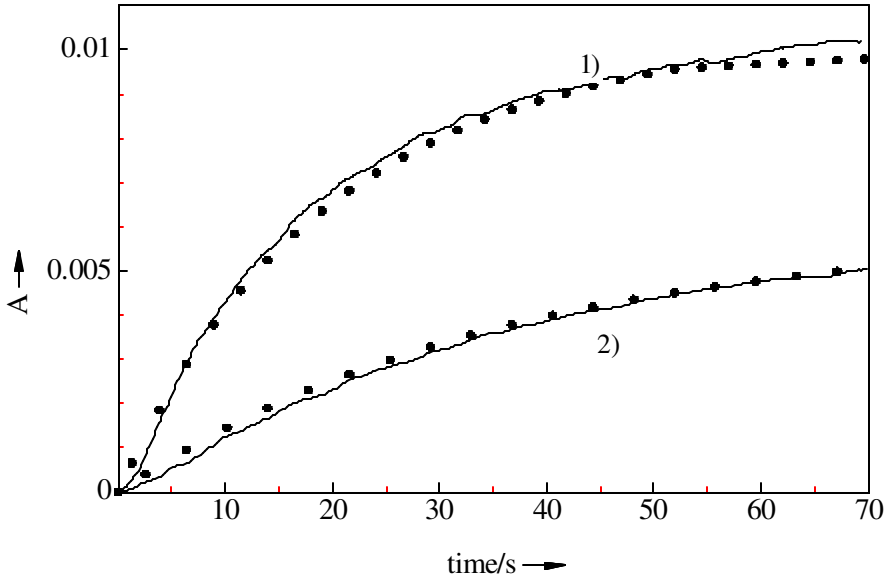

Figure 3-11: Change of absorbance A as a function of time after the injection of bromide into excess bromate (1) and of bromate into excess bromide (2).

The experiments (solid lines) were carried out with a cell of 10.2 cm path length (23 mL volume) in 1 M sulfuric acid at 20 °C. Dual-wavelength method was used to follow the kinetics (401 nm). Curve 1: $[Br^-]_0 = 1\times10^{-5}$ M, $[BrO_3^-]_0 =$ 0.01 M. Curve 2: $[Br^-]_0 =$ 0.01 M, $[BrO_3^-]_0 = 1\times10^{-6}$ M. The dots are calculated with reactions R_1~R_5 and R_7, the rate constants k_1, k_2, k_4, k_5 and k_7 are those listed in Table 3-1; k_3 see text.

One possibility for the difficulty in explaining the Kshirsagar-Field and Försterling-Murányi experiments may be the uncertainty of k_3. Bromide generated during the hydrolysis of bromine in these experiments reacts directly with bromate. The hydrolysis of bromine R_1 is very fast, thus the rate of the bromine-bromate reaction is controlled by the reaction of bromide with bromate, R_3. If k_3 used in the simulation is higher than the actual value, the calculated overall rate of HOBr formation and bromine disappearance must be higher too.

Because of all these facts, we reexamined the bromide-bromate reaction R_3.

Two sets of experiments were carried out. 1) The concentration of bromide is in excess over bromate in analogy with Kshirsagar-Field's work; 2) the bromate concentration is in large excess over bromide as in Lamberz and Gao's measurements. All these experiments were performed with an optical cell of 10.2 cm path length (23 mL volume) at 20 °C. The stock solutions were used without any bubbling treatment as oxygen has no significant effect. The kinetics of Br_2 formation was followed spectroscopically by single beam (401 nm) or dual-wavelength fiber optics measurement (signal wavelength 401 nm, reference 670 nm). Figure 3-11 shows the typical curves measured in each of the two sets experiments.

Results for Bromide in Excess

The first set of experiments was done in the case of excess bromide. The reaction medium is 1 M sulfuric acid. Different initial concentrations of bromate (1.0×10^{-6} M ~ 6.8×10^{-6} M) as well as bromide (0.005 M ~ 0.04 M) were applied.

For the evaluation, we consider the mechanism of the overall reaction Z_3:

$$3\ Br^- + 3\ HOBr + 3\ H^+ \rightleftharpoons 3\ Br_2 + 3\ H_2O \qquad R_1$$

$$Br^- + HBrO_2 + H^+ \rightleftharpoons 2\ HOBr \qquad R_2$$

$$Br^- + BrO_3^- + 2\ H^+ \rightleftharpoons HOBr + HBrO_2 \qquad R_3$$

$$5\ Br^- + BrO_3^- + 6\ H^+ \rightarrow 3\ Br_2 + 3\ H_2O \qquad Z_3$$

The rate for bromine formation is:

$$\frac{d[Br_2]}{dt} = k_1[Br^-][HOBr][H^+] \tag{3.15}$$

According to the stationary-state method, the rate for the intermediates can be set to zero, namely,

$$\frac{d[HOBr]}{dt} = -k_1[Br^-][HOBr]_{ss}[H^+] + 2k_2[Br^-][HBrO_2]_{ss}[H^+] + k_3[Br^-][BrO_3^-][H^+]^2 = 0$$

$$\frac{d[HBrO_2]}{dt} = -k_2[Br^-][HBrO_2]_{ss}[H^+] + k_3[Br^-][BrO_3^-][H^+]^2 = 0$$

The steady-state concentrations of $HBrO_2$ and HOBr are obtained,

$$[HBrO_2]_{ss} = \frac{k_3[H^+][BrO_3^-]}{k_2} \quad \text{and} \quad [HOBr]_{ss} = \frac{3k_3[H^+][BrO_3^-]}{k_1}$$

Then the rate equation (3.15) becomes (3.16) by substitution.

$$\frac{d[Br_2]}{dt} = 3k_3[Br^-][BrO_3^-][H^+]^2 \tag{3.16}$$

When bromide is in large excess over bromate,

$$[Br^-] = [Br^-]_0 \tag{3.17}$$

the concentration of bromate is calculated from it's initial concentration c_0 according to the stoichiometry.

$$[BrO_3^-] = c_0 - \frac{1}{3}[Br_2] \tag{3.18}$$

(c_0 represents the initial concentration of bromate)

Substituting (3.17) and (3.18) for [Br^-] and [BrO_3^-] in the rate equation (3.16), respectively, we obtain

$$\frac{d[Br_2]}{dt} = 3k_3[Br^-]_0[H^+]^2(c_0 - \frac{1}{3}[Br_2]) \tag{3.19}$$

Using the initial conditions

$$t = 0, \quad [Br_2]_0 = 0; \quad [BrO_3^-]_0 = c_0 = \frac{1}{3}[Br_2]_\infty$$

and the relation

$$A = d\varepsilon \cdot [Br_2]$$

for the absorbance of bromine (ε = extinction coefficient of bromine; d = optical path length) we obtain Equation (3.20) by integration.

$$\ln\frac{A_\infty - A}{A_\infty} = -k_{obs}t \tag{3.20}$$

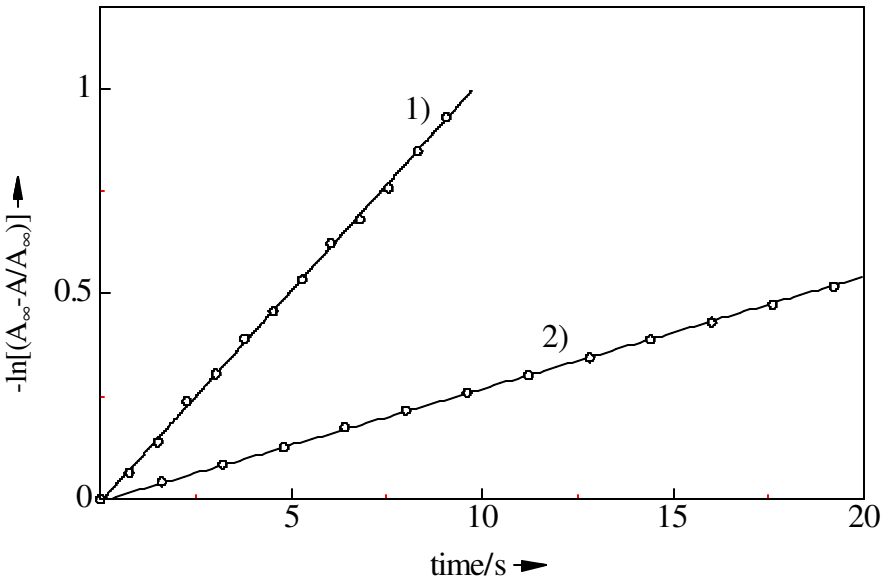

Figure 3-12: Evaluation of first order rate constants k_{obs} with Equation (3.20) for the experiments with different initial concentrations of bromide.

The experimental conditions are the same as in Figure 3-11. The concentrations are 1) $[Br^-]_0$ = 0.04 M, $[BrO_3^-]_0 = 4.3\times10^{-6}$ M; and 2) $[Br^-]_0$ = 0.01 M, $[BrO_3^-]_0 = 6.8\times10^{-6}$ M. Circles: experimental data. Solid lines: regression curves.

$$k_{obs} = k_3[Br^-]_0[H^+]^2 \qquad (3.21)$$

($A_\infty = 3\cdot c_0\cdot d\cdot\varepsilon$, absorbance at the end of reaction).

For all experiments mentioned above, we obtained excellent straight logarithmic plots by plotting the left hand side of Equation (3.20) as a function of time, two of them are displayed in Figure 3-12. From the slopes of the straight lines the first-order rate constants (k_{obs}) were evaluated, the values are shown in Table 3-3. Plotting k_{obs} as a function of $[Br^-]_0$ in Figure 3-13 yields a straight line, just as expected from Equation (3.21). From the slope 2.57 $M^{-1}s^{-1}$ of this straight line and the acidity $[H^+]$ = 1.29 M we calculate k_3 = 1.54 $M^{-3}s^{-1}$. This value is smaller by a factor of 1.6 than Kshirsagar – Field's result which was obtained under similar conditions. This discrepancy may result from the model leading to k_3 = 2.5 $M^{-3}s^{-1}$. As mentioned above, Kshirsagar and Field

obtained k_3 by simulating the experimental curves. In their simulations 1.5×10^9 M^{-2} was used for equilibrium constant K_1, which was later proved to be higher by a factor of 15 than the experimental result[4].

Table 3-3: The first order rate constants k_{obs} with different $[Br^-]_0$.

The experimental conditions are the same as in Figure 3-11. k_{obs} is evaluated from the slopes of the logarithmic plots.

No.	$[Br^-]_0/(10^{-2}M)$	$[BrO_3^-]_0/(10^{-6}M)$	k_{obs} / $(10^{-2}s^{-1})$
1	0.4	4.3	1.1
2	1.0	6.8	2.7
3	2.0	1.0	5.6
4	3.0	4.3	8.0
5	4.0	4.3	10.3

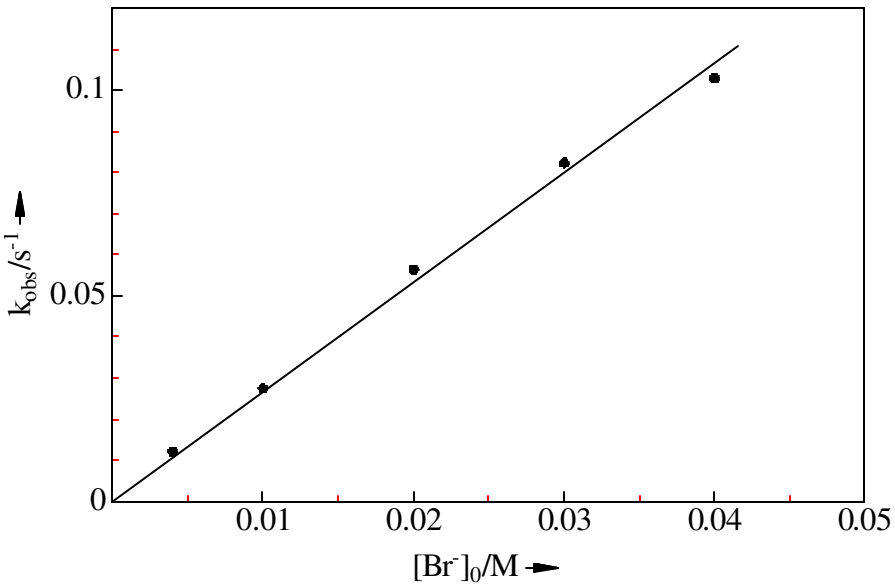

Figure 3-13: The first order rate constants k_{obs} as a function of the initial concentrations of bromide.

The data are taken from Table 3-3. k_3 = 1.54 $M^{-3}s^{-1}$ is calculated from the slope 2.57 $M^{-1}s^{-1}$ of the straight line and $[H^+]$ = 1.29 M for $[H_2SO_4]$ = 1 M.

Results for Bromate in Excess

The second set of experiments was done in the case of excess bromate. A similar derivation is performed as for excess bromide.

Here, $[BrO_3^-] = [BrO_3^-]_0$

and $[Br^-] = c_0 - \frac{5}{3}[Br_2]$

(c_0 represents the initial concentration of bromide).

Then, the rate equation (3.16) becomes:

$$\frac{d[Br_2]}{dt} = 3k_3[BrO_3^-]_0[H^+]^2(c_0 - \frac{5}{3}[Br_2])$$

Using the initial conditions

$$t = 0, \quad [Br_2]_0 = 0; \; [Br^-]_0 = c_0 = \frac{5}{3}[Br_2]_\infty$$

and the relation

$$A = d\varepsilon[Br_2]$$

the following equations are obtained:

$$\ln\frac{A_\infty - A}{A_\infty} = -k_{obs}t \tag{3.22}$$

$$k_{obs} = 5k_3[BrO_3^-]_0[H^+]^2 \tag{3.23}$$

($A_\infty = \frac{3}{5}\cdot c_0 \cdot d\varepsilon$, absorbance at the end of reaction)

In analogy with the case of excess bromide, the first-order rate constant k_{obs} was evaluated from the slopes of the logarithmic plots, leading to k_3 according to Equation (3.23). However, some problems appear in this case.

First, the logarithmic plots are not as straight as in the case of excess bromide if 90% of the reaction is chosen for the evaluation (circles in Figure 3-14a), and the average slope deviates a lot from the initial part of the reaction (solid line in Figure 3-14a). To get a straight logarithmic plot and facilitate the comparison between individual measurements, we consistently selected the experimental curves within the first half life

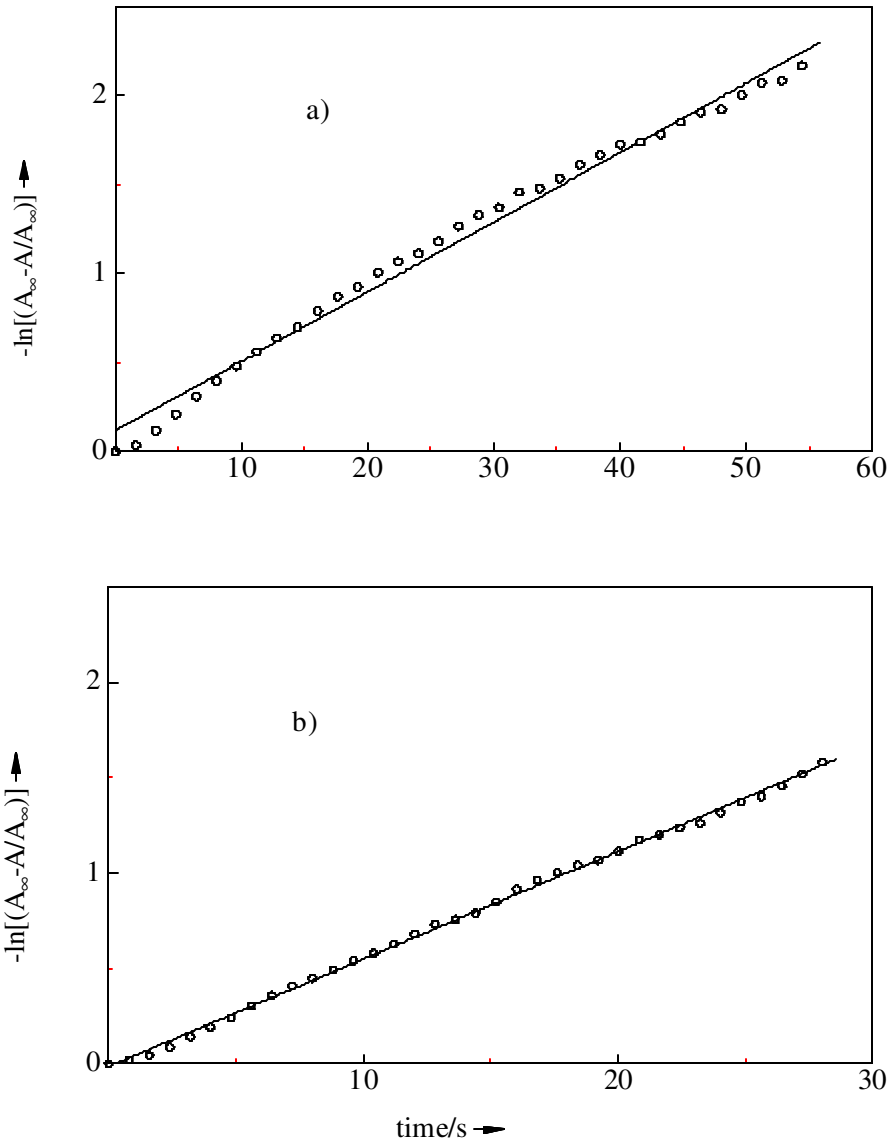

Figure 3-14: Evaluation of first order rate constants k_{obs} with Equation (3.22).

The experimental conditions are the same as in Figure 3-11. The initial concentrations are $[Br^-]_0 = 1\times 10^{-5}$ M, $[BrO_3^-]_0 = 0.01$ M. Circles: the logarithmic plots. Solid lines: regression curves. a): 90% of the reaction was selected for the evaluation. b): only the first half life of the reaction was selected.

of the reaction for evaluation, then, each logarithmic plot is as straight as in Figure 3-14b. k_{obs} is evaluated from its slope.

Table 3-4: Determination of k_3 with different recrystallized bromate samples.

The experimental conditions are the same as in Figure 3-11. $[BrO_3^-]_0$ = 0.01 M; $[Br^-]_0 = 1\times 10^{-5}$ M. k_{obs} was evaluated from the initial slope of the logarithmic plot. Each sample of bromate was recrystallized from hot water two times.

Sample	$k_{obs}/(10^{-2}s^{-1})$	$k_3/ M^{-3} s^{-1}$
1	5.1	0.61
2	7.0	0.84
3	6.7	0.80
4	6.8	0.77
5	5.2	0.62
6	5.5	0.64
7	5.9	0.71
Mean value		0.71 ± 0.1

Table 3-5: Successive – injection experiment.

$[BrO_3^-]_0$ = 0.03M, H_2SO_4 = 1 M, T = 20 °C

Number.of injections	$[Br^-]_0$ (M)	k_{obs}/s^{-1}
1	4.3×10^{-6}	0.136
2	4.3×10^{-6}	0.209
3	4.3×10^{-6}	0.215
4	4.3×10^{-6}	0.268

The second problem is concerned with the bromate samples. We found that it is difficult to reproduce the results if different preparations of bromate are used. Table 3-4 shows the results measured with different bromate samples. We can see that the values of k_{obs} are slightly different although all experimental conditions are the same. Our interpretation is that bromate recrystallized from hot water may still contain some HOBr impurity, so the first-order rate constants obtained from the logarithmic plots include contributions from step R_1 additionally to R_3. Separate preparations may contain slightly different impurities and consequently give us different values of k_{obs}. This assumption is supported by a successive-injection experiment, in which a second injection of equal amount of bromide into the same acidic bromate system was conducted after the first reaction was finished. We can see from Table 3-5 that the first-

order rate constant increases with the number of the injections. That is because more and more bromine has been accumulated, and the HOBr is also getting higher in the reaction system (because of the back reaction R_{-1}). When bromide is injected, it reacts directly with HOBr existing beforehand (not from the start step R_3) making the formation of bromine faster than expected from R_3.

To avoid the interference from the impurity, we selected bromate samples according to the results of pre-measurements. Only those giving lowest k_3 in the first injection and showing increasing first order rate constant in the successive – injection experiment can be used for the measurement of rate constant k_3.

Additionally, we found in the pre-measurements that k_3 (see Table 3-4) is much smaller than that obtained in the case of excess bromide (k_3 = 1.54 $M^{-3}s^{-1}$, see the caption of Figure 3-13). In order to understand this striking fact, we performed additional experiments by varying the initial concentrations of bromide and bromate.

Constant bromate. The concentration of bromide was varied from 1.74×10^{-6} M to 3×10^{-4} M while 0.01 M bromate and 1 M H_2SO_4 were always kept constant. Unfortunately, the initial concentration of bromide cannot be reduced below 1.7×10^{-6} M because of the sensitivity of detection (this initial concentration corresponds to an absorbance change of 2×10^{-3} at 400 nm). k_{obs} was evaluated from the initial slopes of the logarithmic plots as described before. k_3 is calculated according to Equation (3.23) with $[BrO_3^-]_0$ = 0.01 M and $[H^+]$ = 1.29 M. Both results are displayed in Table 3-6. We are surprised to see that the values of k_{obs} and k_3 are not constant at constant $[BrO_3^-]_0$ but depend on the initial concentration of bromide: k_3 increases from 0.48 $M^{-3}s^{-1}$ (for 1.74×10^{-6} M $[Br^-]_0$) to 1.56 $M^{-3}s^{-1}$ (for 3×10^{-4} M $[Br^-]_0$). We repeated these measurements with the same initial conditions but in 0.5 M H_2SO_4 medium (Table 3-7). As in 1 M H_2SO_4 system the values of k_3 as well as k_{obs} strongly depend on $[Br^-]_0$. In Figure 3-15 k_3 is plotted as a function of $[Br^-]_0$ for each acidity. We find that the increasing trend is serious when $[Br^-]_0$ is comparatively low. The experimental curves can be described by a power series (solid lines):

$$k_3 = b_0 + b_1\times[Br^-]_0 + b_2\times[Br^-]_0^2 + b_3\times[Br^-]_0^3$$

Table 3-6: Dependence of k_3 on the initial concentration of bromide at 1 M H_2SO_4.

The experiments were performed as in Figure 3-11. $[H_2SO_4]$ = 1 M, $[BrO_3^-]_0$ = 0.01 M. k_{obs} was evaluated from the initial slope of the logarithmic plot, k_3 was calculated from k_{obs} according to Equation (3.23) with $[H^+]$ =1.29 M.

No.	$[Br^-]_0/(10^{-6}$ M)	$k_{obs}/(10^{-2}s^{-1})$	$k_3/(M^{-3}s^{-1})$
1	1.74	4.00	0.48
2	3.04	4.24	0.51
3	4.30	4.56	0.55
4	6.52	4.68	0.56
5	8.60	4.91	0.59
6	10.0	5.12	0.62
7	13.9	6.15	0.73
8	21.7	7.13	0.84
9	54.8	9.69	1.15
10	79.1	10.6	1.25
11	100	10.6	1.25
12	139	12.0	1.42
13	183	12.0	1.42
14	217	13.0	1.54
15	261	12.8	1.51
16	300	13.2	1.56

Table 3-7: Dependence of k_3 on the initial concentration of bromide at 0.5 M H_2SO_4.

The experimental conditions and the evaluation of data are the same as in Table 3-6 but at 0.5 M H_2SO_4.

No.	$[Br^-]_0/(10^{-6}$M)	$k_{obs}/(10^{-2}s^{-1})$	$k_3/(M^{-3}s^{-1})$
1	2.9	0.903	0.44
2	4.3	0.751	0.37
3	6.47	0.904	0.44
4	8.43	0.992	0.49
5	10.0	1.01	0.50
6	20.1	1.26	0.62
7	49.7	1.77	0.87
8	82.6	1.91	0.94
9	138	2.41	1.18
10	186	2.40	1.18
11	213	2.49	1.22
12	268	2.55	1.25

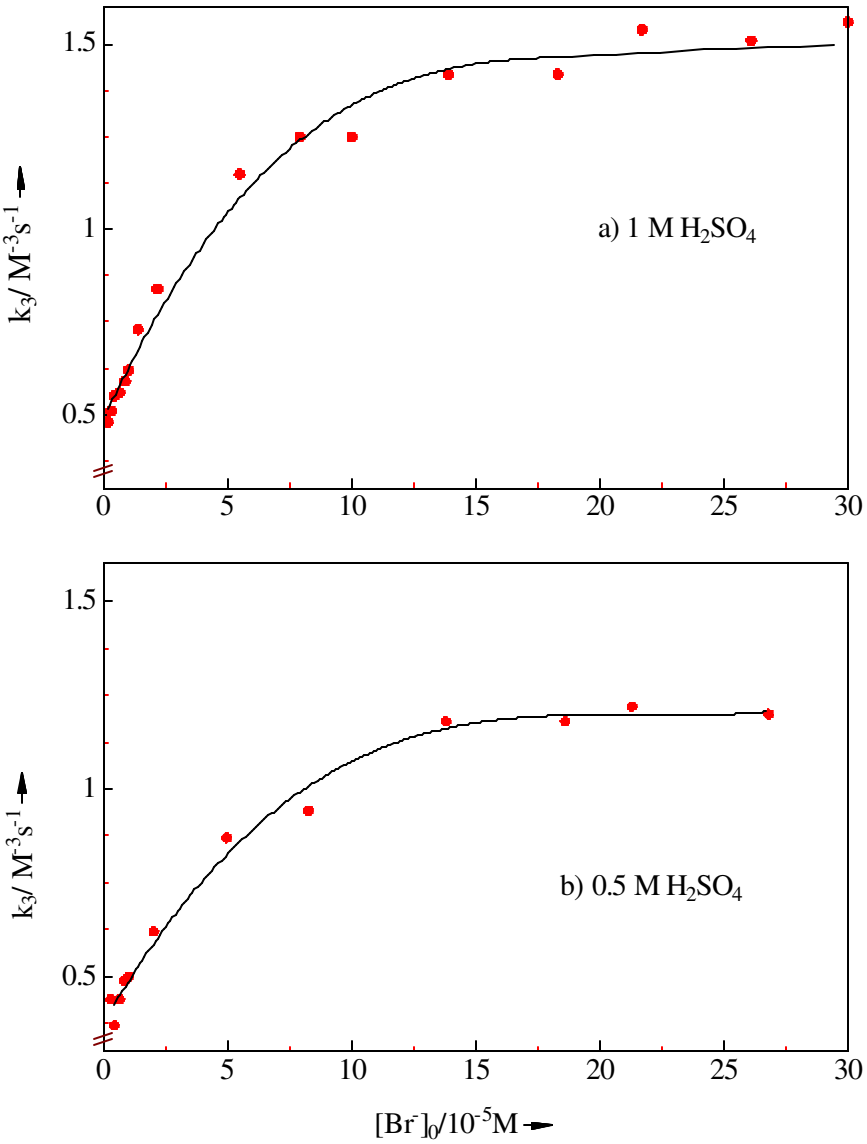

Figure 3-15: Fourth order rate constant k_3 (bromate in excess) versus the initial concentration of bromide ($[BrO_3^-]_0$ = 0.01 M).

Dots : the experimental data taken from Table 3-6 (a) and Table 3-7 (b). Solid line: calculated by a power series:

$$k_3 = b_0 + b_1 \times [Br^-]_0 + b_2 \times [Br^-]_0^2 + b_3 \times [Br^-]_0^3$$

for the coefficients see text. H_2SO_4 = 1 M (a), 0.5 M (b).

The coefficients b_0, b_1, b_2, and b_3 are :

for 1 M sulfuric acid: $b_0 = 0.48789\ M^{-3}s^{-1}$, $b_1 = 0.143911\times10^{5}\ M^{-4}s^{-1}$,
$b_2 = -\ 0.707958\times10^{8}\ M^{-5}s^{-1}$, $b_3 = 0.116631\times10^{12}\ M^{-6}s^{-1}$.

for 0.5 M sulfuric acid: $b_0 = 0.376896 M^{-3}s^{-1}$, $b_1 = 0.114617\times10^{5}\ M^{-4}s^{-1}$,
$b_2 = -\ -\ 0.531409\times10^{8}\ M^{-5}s^{-1}$, $b_3 = 0.818152\times10^{11}\ M^{-6}s^{-1}$.

Constant bromide. We turn to investigate the effect of the bromate concentration by performing the experiments with a fixed value of the bromide concentration (4.3×10^{-6} M). 1 M H_2SO_4 was always used, the initial concentration of bromate was varied from 0.01 M to 0.2 M. Higher concentrations of bromate cannot be used, because the reaction will proceed too fast to be followed. The results are displayed in Table 3-8. Plotting k_{obs} as a function of $[BrO_3^-]_0$ in Figure 3-16, we obtain the experimental dependence of k_{obs} on $[BrO_3^-]_0$. Equation (3.23) indicates that k_{obs} should increase linearly with $[BrO_3^-]_0$. However, the experimental curve shows a different behavior. When bromate is rather low (less than 0.05 M), k_{obs} increases linearly with $[BrO_3^-]_0$ as expected, above 0.05 M bromate, k_{obs} deviates more and more from the expectation of Equation (3.23) and tends to become constant. Apparently, it is not reasonable to calculate k_3 from the slope of the linear part of the curve in Fig.3-16.

A possible reaction path explaining the dependence of the rate constant k_{obs} on the initial concentration of bromate may be the formation of a complex [HBr-$HBrO_3$] as an intermediate:

$$Br^- + BrO_3^- + 2\,H^+ \underset{k_{-31}}{\overset{k_{31}}{\rightleftharpoons}} [HBr\text{-}HBrO_3] \xrightarrow{k_{32}} HOBr + HBrO_2$$

The formation of the complex is treated as a fast equilibrium (K_{31} = equilibrium constant). We deduce the rate law for the decay of the complex according to the stationary-state method.

Table 3-8: The first order rate constants k_{obs} with different bromate in 1 M H_2SO_4.

The experimental conditions and the evaluation of the data are the same as in Table 3-6. 4.3×10^{-6} M bromide was used in all cases.

No.	$[BrO_3^-]_0$/M	k_{obs} / s^{-1}	k_3/(M^{-3} s^{-1})
1	0.01	0.0455	0.55
2	0.02	0.0845	0.51
3	0.03	0.136	0.54
4	0.044	0.202	0.55
5	0.052	0.251	0.58
6	0.061	0.275	0.54
7	0.083	0.340	0.49
8	0.101	0.436	0.52
9	0.122	0.449	0.44
10	0.152	0.490	0.39
11	0.20	0.533	0.32

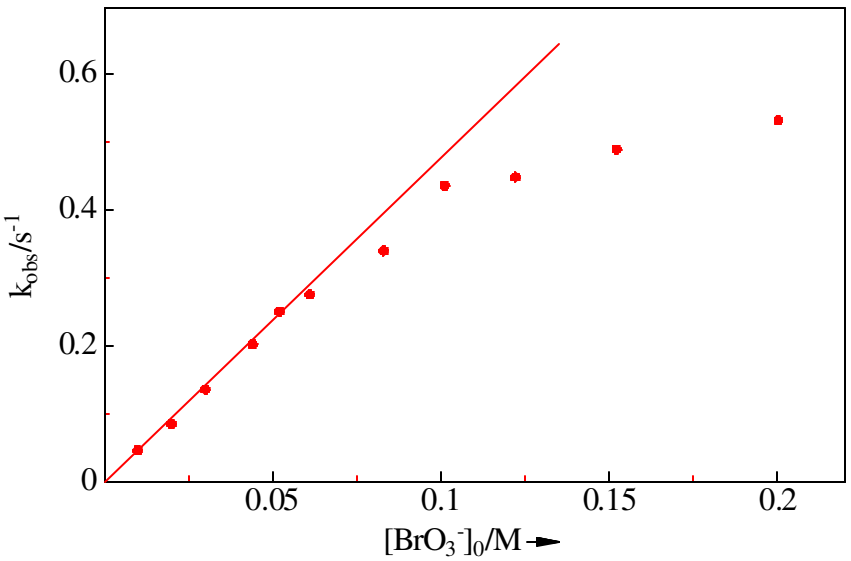

Figure 3-16: The first order rate constant k_{obs} (bromate in excess) versus the initial concentration of bromate ($[Br^-]_0 = 4.3\times10^{-6}$ M).

Dots : the experimental data taken from Table 3-8. Solid line: slope of the linear part of the complete curve.

$$K_{31} = \frac{[HBr - HBrO_3]}{[Br^-][BrO_3^-][H^+]^2} \tag{3.24}$$

$$\frac{d[HOBr]}{dt} = k_{32}[HBr - HBrO_3] \tag{3.25}$$

When bromate is in large excess over bromide,

$$[BrO_3^-] = [BrO_3^-]_0 \text{ and } [Br^-] + [HBr^- - HBrO_3^-] + [HOBr] = [Br^-]_0$$

then $$\frac{d[Br^-]}{dt} + \frac{d[HBr - HBrO_3]}{dt} + \frac{d[HOBr]}{dt} = 0 \tag{3.26}$$

according to Equations (3.24) and (3.25), (3.26) can be rewritten as

$$\frac{1}{K_{31}[BrO_3^-]_0[H^+]^2} \times \frac{d[HBr - HBrO_3]}{dt} + \frac{d[HBr - HBrO_3]}{dt} + k_{32}[HBr - HBrO_3] = 0$$

Thus,

$$\frac{d[HBr - HBrO_3]}{dt} = -k'[HBr - HBrO_3] \tag{3.27}$$

with the abbreviation

$$k' = \frac{k_{32}K_{31}[BrO_3^-]_0[H^+]^2}{1 + K_{31}[BrO_3^-]_0[H^+]^2} \tag{3.28}$$

From (3.24) the concentration of the complex is

$$[HBr - HBrO_3] = K_{31}[Br^-][BrO_3^-]_0[H^+]^2$$

then, $$\frac{d[HBr - HBrO_3]}{dt} = K_{31}[BrO_3^-]_0[H^+]^2 \frac{d[Br^-]}{dt} \tag{3.29}$$

we obtain: $$\frac{d[Br^-]}{dt} = -k'[Br^-]$$

In this reaction, 4 additional Br^- ions disappear in each cycle, thus the rate of Br^- consumption should be modified accordingly.

$$\frac{d[Br^-]}{dt} = -5k'[Br^-] \tag{3.30}$$

From the stoichiometry

$$\frac{d[Br_2]}{dt} = -\frac{3}{5}\frac{d[Br^-]}{dt}$$

$$[Br_2] = \frac{3}{5}([Br^-]_0 - [Br^-])$$

we obtain the rate law for the formation of bromine,

$$\frac{d[Br_2]}{dt} = 5k'(\frac{3}{5}[Br^-]_0 - [Br_2]) \tag{3.31}$$

In our experiments $5k'$ is represented by k_{obs}, then

$$k_{obs} = 5k' = \frac{5k_{32}K_{31}[BrO_3^-]_0[H^+]^2}{1 + K_{31}[BrO_3^-]_0[H^+]^2} \tag{3.32}$$

If the concentration of bromate is rather low, the second term of the denominator in Equation (3.32) can approximately be neglected; on the other hand, if the bromate concentration is very high, the first term is negligible:

$$k_{obs} = 5k_{32}K_{31}[BrO_3^-]_0[H^+]^2 \quad \text{for low bromate} \tag{3.33}$$

$$k_{obs} = 5k_{32} \quad \text{for high bromate} \tag{3.34}$$

Equations (3.33) and (3.34) indicate that, when the concentration of bromate is rather low k_{obs} increases linearly with $[BrO_3^-]_0$; when it is increased k_{obs} tends to become constant. That is just what we observe in the experiments. In other words, the formation of the complex [HBr-$HBrO_3$] as an intermediate might be a possible mechanism for the reaction of bromide with bromate.

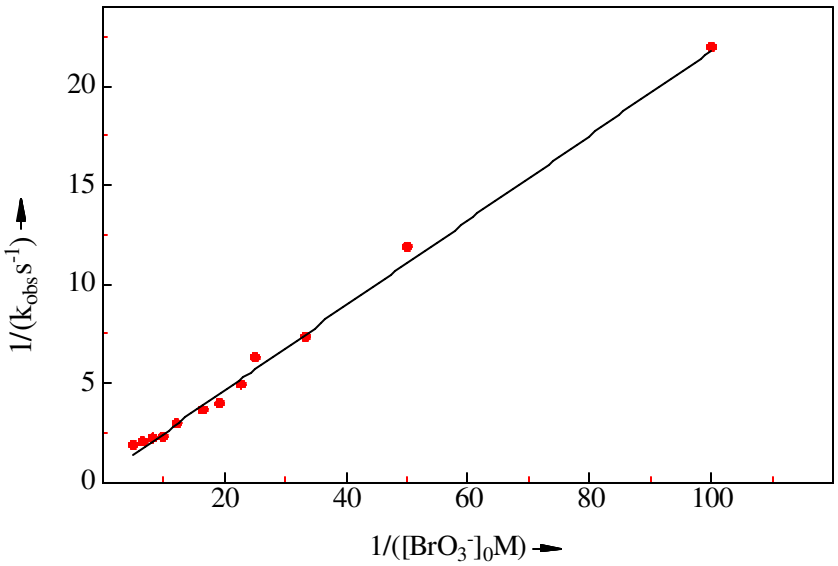

Figure 3-17: Reciprocal plot for experimental k_{obs} as a function of $\frac{1}{[BrO_3^-]_0}$.

Dots: the experimental data taken from Table 3-8. Solid line: the corresponding slope. From the slope 0.19 $M^{-1}s$ and the ordinate section 0.87 s of this straight line, K_{31} = 2.8 M^{-2}, k_{32} = 0.23 s^{-1} are obtained.

Inverting Equation (3.32) yields

$$\frac{1}{k_{obs}} = \frac{1}{5k_{32}} + \frac{1}{5k_{32}K_{31}[H^+]^2} \times \frac{1}{[BrO_3^-]_0} \tag{3.35}$$

Equation 3.35 means that the plot $\frac{1}{k_{obs}}$ versus $\frac{1}{[BrO_3^-]_0}$ should be a straight line with a slope of $\frac{1}{5k_{32}K_{31}[H^+]^2}$ and an ordinate section of $\frac{1}{5k_{32}}$. In Figure 3-17 we plot the reciprocal of the experimental k_{obs} (Table 3-8) as a function of $\frac{1}{[BrO_3^-]_0}$. It is indeed a straight line. From the slope 0.19 M^{-1} s and the ordinate section 0.87 s of that straight line we obtain K_{31} = 2.8 M^{-2} and k_{32} = 0.23 s^{-1}.

Vice versa, we are able now to calculate k_{obs} from Equation (3.32) using K_{31} = 2.8 M^2 and k_{32} = 0.23 s^{-1} and then k_3. In Figure 3-18a the values of k_{obs} calculated from (3.32)

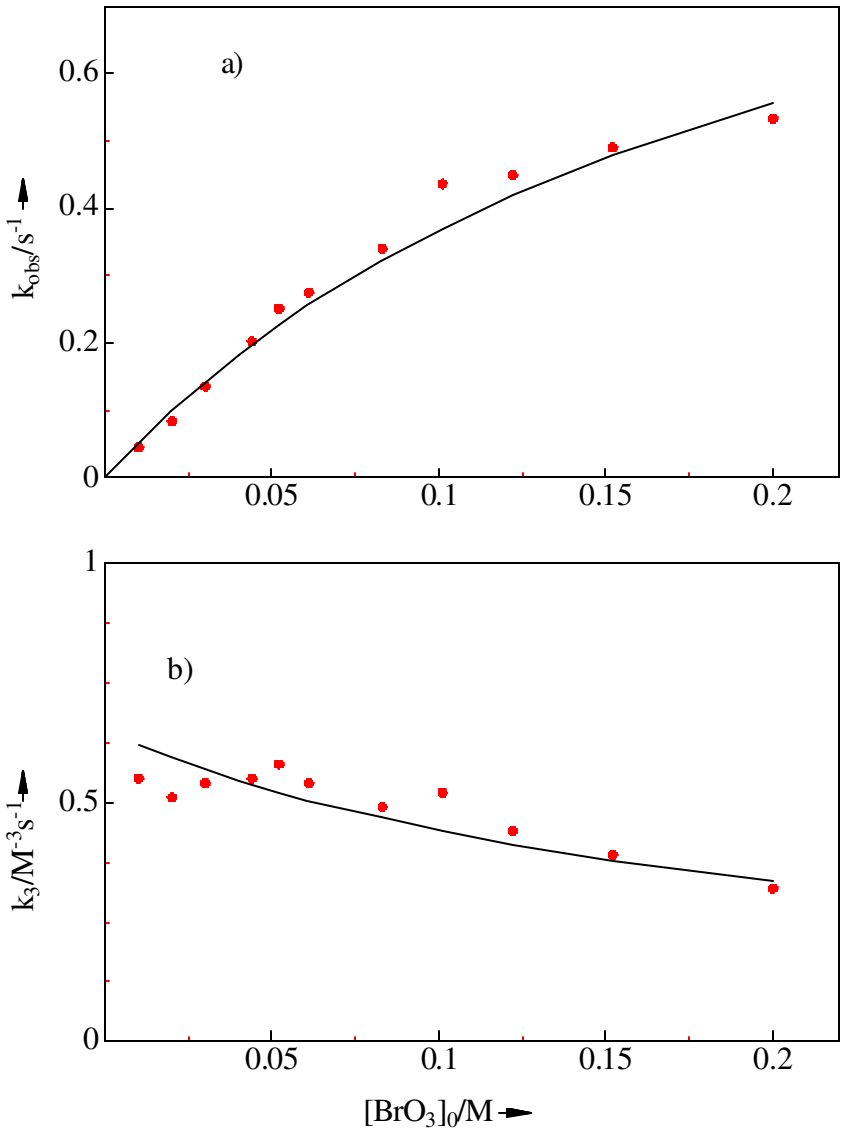

Figure 3-18: Theoretical and experimental rate constants as a function of $[BrO_3^-]_0$.

Dots: experimental data taken from Table 3-8. Solid lines: theoretical results. The theoretical k_{obs} are calculated from Equation (3.32). The theoretical k_3 are calculated from the theoretical k_{obs} according to Equation (3.23) and $[H^+] = 1.29$ M.

are plotted as a function of $[BrO_3^-]_0$ together with the experimental ones. Obviously, the theoretical results agree with the experiments very well. We can see from Figure 318b that the theoretical k_3 calculated from the theoretical k_{obs} are in good agreement with those calculated from experimental k_{obs} according to Equation (3.23). These two plots

convincingly prove that the fourth order rate constant k_3 decreases with increasing initial concentration of bromate.

Conclusion

Our investigation shows that the mechanism of the bromate-bromide reaction is much more complex than assumed so far.

1. In the case of excess bromide, $k_3 = 1.54\ M^{-3}s^{-1}$ is independent of the bromide initial concentration.
2. In the case of excess bromate, k_3 depends on the initial concentration of both bromide and bromate.
3. k_3 increases with the initial concentration of bromide, the dependence can be described by a power series: $k_3 = b_0 + b_1 \times [Br^-]_0 + b_2 \times [Br^-]_0^2 + b_3 \times [Br^-]_0^3$.
4. k_3 decreases with increasing bromate concentration. This dependence can be explained by a complex formation mechanism.

Based on these points we conclude that it is not reasonable in the system of excess bromate to use k_3 measured under excess bromide and vice versus; it is also not reasonable in the system of rather low bromide (bromate) to use k_3 measured under higher bromide (bromate) concentration though bromate is in large excess and vice versus.

Simulations

To check the reliability of our evaluation method, numerical simulations were performed. We first simulated the reaction of bromide with bromate. The full reaction scheme (R_1~R_5) and the corresponding rate constants but k_3 in Table 3-1 were used. As for k_3, the results obtained in this work were applied, namely, $k_3 = 1.54\ M^{-3}s^{-1}$ throughout the case of excess bromide; it is a power series related with $[Br^-]_0$ in the case of excess bromate. The results are shown in Figure 3-11 (dots, curve 1 is the case of

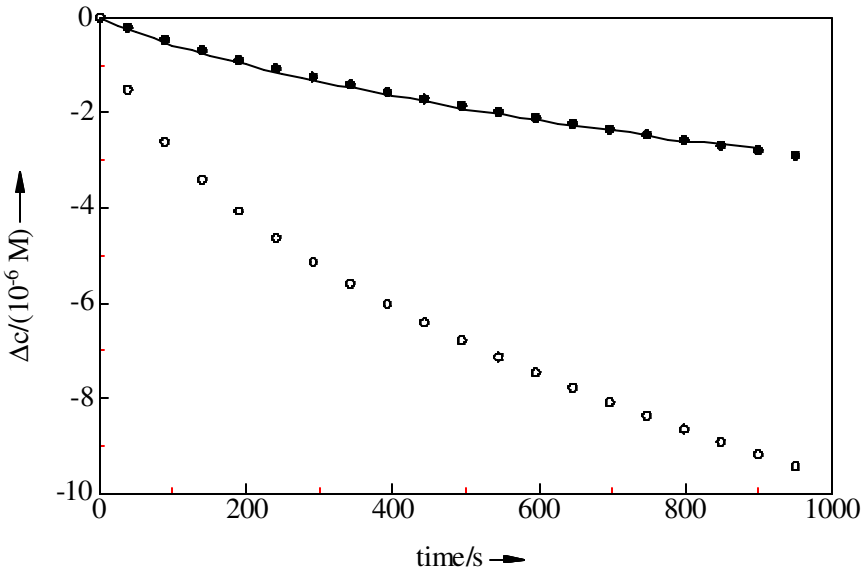

Figure 3-19: Decay of bromine in the reaction with bromate in 1M sulfuric acid.

Solid line: the experimental curve of Figure 7 in reference[23]. $[Br_2]_0 = 5\times10^{-5}$M, $[BrO_3^-]_0 = 0.1$ M, $H_2SO_4 = 1$ M, T = 20 °C.

The calculated curves are obtained on the basis of the full reaction scheme $R_1 \sim R_5$ and the corresponding rate constants in Table 3-1. Circles: calculated with $k_3 = 1.2$ $M^{-3}s^{-1}$ (Försterling and Murányi). Dots: calculated with the power series:

$$k_3 = 0.86\times (b_0 + b_1\times[Br^-]_0 + b_2\times[Br^-]_0^2 + b_3\times[Br^-]_0^3)$$

(for the coefficients see text).

excess bromate and curve 2 is that of excess bromide). Apparently, in both cases the calculations reproduce the experiments very well.

Moreover, we resume Försterling and Murányi's [23] work to simulate the reaction of 0.1 M bromate with 5×10^{-5}M bromine. The simulation was performed as in the bromide-bromate reaction. According to the dependence on the bromate concentration (Figure 3-18b), k_3 in 0.1 M bromate system should be lower than that in the 0.01 M system by 14%, the power series of k_3 obtained from 0.01 M bromate is multiplied by a factor of 0.86. Figure 3-19 demonstrates that the decay of bromine in the reaction with bromate can also be modeled successfully.

3.1.5 Potential Change of the AgBr Electrode

Ion-selective electrodes play an important role in monitoring chemical oscillations. The AgBr electrode is of importance in studying BZ oscilllating reactions, because bromide ions are essential components in the complex mechanism .

AgBr electrodes contain a silver bromide membrane. If the concentration of bromide ions in a solution is sufficiently large, the potential is a linear function of the bromide concentration just as anticipated from the Nernst equation. Corrosive agents determine the potential response when the bromide concentration is below it's solubility limit. According to the model of Nosztizius et al.[18, 41], oxidative agents, like hypobromous acid, attack the electrode membrane and remove bromide ions from the surface, as in the reaction:

$$AgBr \rightleftharpoons Ag^{+} + Br^{-} \qquad Z_4$$

$$Br^{-} + HOBr + H^{+} \rightleftharpoons Br_2 + H_2O \qquad Z_5$$

The relative excess of the Ag^{+} ions produced this way at the surface of the silver bromide membrane determines the potential response.

Bromate and $HBrO_2$ can affect the electrode potential in the same direction as HOBr due to the reactions R_2 and R_3:

$$Br^{-} + HBrO_2 + H^{+} \rightleftharpoons 2\,HOBr \qquad R_2$$

$$Br^{-} + BrO_3^{-} + 2\,H^{+} \rightleftharpoons HOBr + HBrO_2 \qquad R_3$$

In the BZ system, $HBrO_2$ is always present in concentrations too low to change the potential of the AgBr electrode. Nosztizius et al.[18] have investigated the reaction with bromate in detail in 1.5 M sulfuric acid. The potential change caused by acidic bromate is not significant at bromate concentrations lower than 0.01 M; larger effects were observed at higher concentrations but a longer time was needed to achieve a steady state potential. In our experiments, we add bromate first and start the reaction after the steady

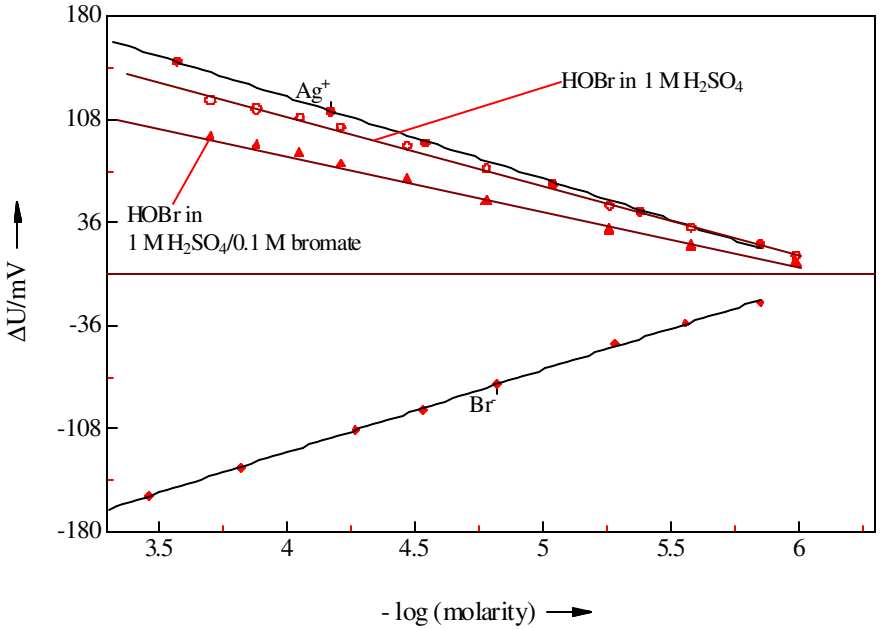

Figure 3-20: Response of the AgBr electrode versus the concentration of Br^-, Ag^+ and HOBr in 1M H_2SO_4.

The experiments were carried out by inserting a AgBr electrode into a well stirred reaction cell. The response of the electrode to the addition of Br^-(squares) and Ag^+ (dots) was measured in 1 M H_2SO_4 medium; the response to HOBr was measured in 1 M H_2SO_4 (circles) and 0.1 M bromate + 1 M H_2SO_4 (triangles). The solid lines correspond to linear fit.

state potential has been established. Therefore we can neglect the effect of bromate in the simulation of the electrode potential.

There are essentially two species left determining the potential of AgBr electrode in the systems investigated here, namely Br^- and HOBr. To simulate the experimental potential change, we first establish the potential response calibration of the electrode to Br^- and HOBr by successively adding small volumes of dilute samples containing known amounts of Ag^+, Br^- or HOBr into 140mL 1 M H_2SO_4. Ag^+ was used to check the reliability of the electrode.

Figure 3-20 shows the results of four measurements at 20°C with the same electrode. From the slope of the linear fit (solid line) for the bromide curve we obtain

$\frac{dU}{dpBr} = 57.4\,mV$. A similar treatment for Ag^+ ion results in $\frac{dU}{dpAg} = -57.3\ mV$. These values are in good agreement with the Nernst value (59.16 mV), and the electrode is equally sensitive to silver ions and to bromide ions.

The circles in Figure 3-20 represent potential changes caused by adding HOBr into 1M H_2SO_4. From the linear part (solid line) of the complete curve we obtain $\frac{dU}{dpHOBr} = -50.6\ mV$, this value is 15% lower than expected from the Nernst equation.

In an additional experiment, we investigated the potential response of the AgBr electrode to HOBr in the medium of 1 M H_2SO_4 plus bromate. The deviation of the potential response to HOBr from the ideal Nernst behavior increases with the concentration of bromate. The triangles in Figure 3-20 are obtained with 0.1 M BrO_3^- in 1 M H_2SO_4. The slope of the linear part indicates $\frac{dU}{dpHOBr} = -37.8\ mV$, 36% lower than Nernst value. Therefore, it is not reasonable to use Ag+ ions instead of HOBr in calibration measurements.

Based on these facts, the following equations are used to obtain the potential changes for different concentrations of Br^- and HOBr:

$$\Delta U_{Br^-} = \begin{cases} 0 & [Br^-] \le 5\times10^{-7}\,M \\ -57.4mV \times \log\frac{[Br^-]}{[Br^-]_0} & [Br^-] > 5\times10^{-7}\,M \end{cases}$$

$$\Delta U_{HOBr} = \begin{cases} 0 & [HOBr] \le 5\times10^{-7}M \\ a\times\log\frac{[HOBr]}{[HOBr]_0} & [HOBr] > 5\times10^{-7}M \end{cases}$$

$$\Delta U = \Delta U_{Br^-} + \Delta U_{HOBr}$$

where a represents the measured value of $\frac{-dU}{dpHOBr}$ in experiments with different concentrations of bromate (e.g. a = 37.8 mV for the system with 0.1 M bromate in 1 M sulfuric acid) ; $[Br^-]_0$ and $[HOBr]_0$ are the background concentrations before the start of the reaction:

$$[Br]_0 = [HOBr]_0 = 5\times10^{-7}\ M^{[24]}$$

3.1.6 The Overall Autocatalytic Reaction

In the proceeding chapters, we have discussed some reactions involved in the overall autocatalytic reaction, and we have modified the model accordingly. The new set of rate constants included in the scheme R_1~R_7 and R_{17} are shown in Table 3-9 .

Table 3-9: The new set rate constants for the cerium catalyzed autocatalytic reaction.

forward	reference	backward	reference
$k_1 = 8\times10^9\ M^{-2}s^{-1}$	[21]	$k_{-1} = 110\ s^{-1}$	[21]
$k_2 = 2.9\times10^6\ M^{-2}s^{-1}$	[23], a)	$k_{-2} = 2\times10^{-5}\ M^{-1}s^{-1}$	[23]
$k_3 = f(Br^-)\ M^{-3}\ s^{-1}$	a)	$k_{-3} = 3.2\ M^{-1}\ s^{-1}$	[24]
$k_{4a} = 2\times10^6\ M^{-1}s^{-1}$	[19]	$k_{-4a} = 1\times10^8 s^{-1}$	[19]
$k_{4b} = 1.7\times10^5\ M^{-1}s^{-1}$	[19]	$k_{-4b} = 0$	[19]
$k_{5a} = 48\ M^{-2}s^{-1}$	[24]	$k_{-5a} = 3200 s^{-1}$	[24]
$k_{5b} = 7.5\times10^4 s^{-1}$	[21]	$k_{-5b} = 1.4\times10^9\ M^{-1}s^{-1}$	[21]
$k_6 = 6.0\times10^4\ M^{-2}s^{-1}$	[25]	$k_{-6} = f(\mu)\ M^{-1}s^{-1}$	[19], a)
$k_7 = 6\times10^{-10}\ M^{-3}s^{-1}$	[20]	$k_{-7} = 0$	[20]
$k_{17} = 0.06\ s^{-1}$	a)	$k_{-17} = 0$	a)

a): This work.

$f(Br^-) = b_0 + b_1\times[Br^-]_0 + b_2\times[Br^-]_0^2 + b_3\times[Br^-]^3$; $b_0 = 0.48789\ M^{-3}s^{-1}$, $b_1 = 0.143911\times10^5\ M^{-4}s^{-1}$, $b_2 = -0.707958\times10^8\ M^{-5}s^{-1}$, $b_3 = 0.116310\times10^{12}\ M^{-6}s^{-1}$.

$f(\mu) = a_0 + a_1\times\mu + a_2\times\mu^2 + a_3\times\mu^3$; $a_0 = -1.74743\ M^{-1}s^{-1}$, $a_1 = 6.75949\ M^{-2}s^{-1}$, $a_2 = -4.30066\ M^{-3}s^{-1}$, $a_3 = 0.797993\ M^{-4}s^{-1}$

To confirm the mechanism and test the validity of the modification as well, we studied the autocatalytic reaction in three cases:

1) Standard case. In the range of bromate concentrations above 0.01M, the auto-catalytic reaction shows a very short or no induction period.

2) Lower concentration range of bromate (0.01-0.001 M). An induction period appears as the concentration of bromate decreases.

3) Add bromide. The effect of bromide on the induction period can be easily deduced by adding it to the solution just at the addition of the cerous ions (start of the raction).

The general experimental conditions in all cases are the same as described in Chapter 3.1.1. In the standard cases, a AgBr electrode was inserted in the reaction cell to obtain more information about HOBr. Figure 3-21 shows an example of three simultaneously measured signals after the injection of Ce^{3+} into acidic bromate: absorbance changes at 401 nm (Curve 1, left hand scale, range 0 – 0.4); 550 nm (curve 2, left hand scale, range 0 - 3×10^{-3}), and the potential change of the AgBr electrode (curve 3, right hand scale). The concentrations of Ce^{4+} and $BrO_2^{\bullet}$ were calculated from the measured absorbance *A* as introduced in Chapter 3.1.1.

The simulations of the autocatalytic reaction in each case were performed with the full scheme R_1~R_7, R_{17} and the corresponding rate constants in Table 3-9. The initial conditions for the simulation are set just as in the experiments. What must be mentioned is the setting of a background concentration $[BrO_2^{\bullet}]_0 = 3\times10^{-7}\times[BrO_3^-]_0$. Szalai et al.[20] measured the absorption spectra of 1 M $NaBrO_3$ in 1 M sulfuric acid at different times *t* after preparation, and found that after one hour $[BrO_2^{\bullet}] = 6\times10^{-7}$ M. In our experiments, the bromate stock solution was prepared in water in order to avoid the decomposition of bromate before the start of the reaction. However, half an hour is still needed to get everything ready for the measurement, so it is reasonable to set $[BrO_2^{\bullet}]_0 = 3\times10^{-7}\times[BrO_3^-]_0$.

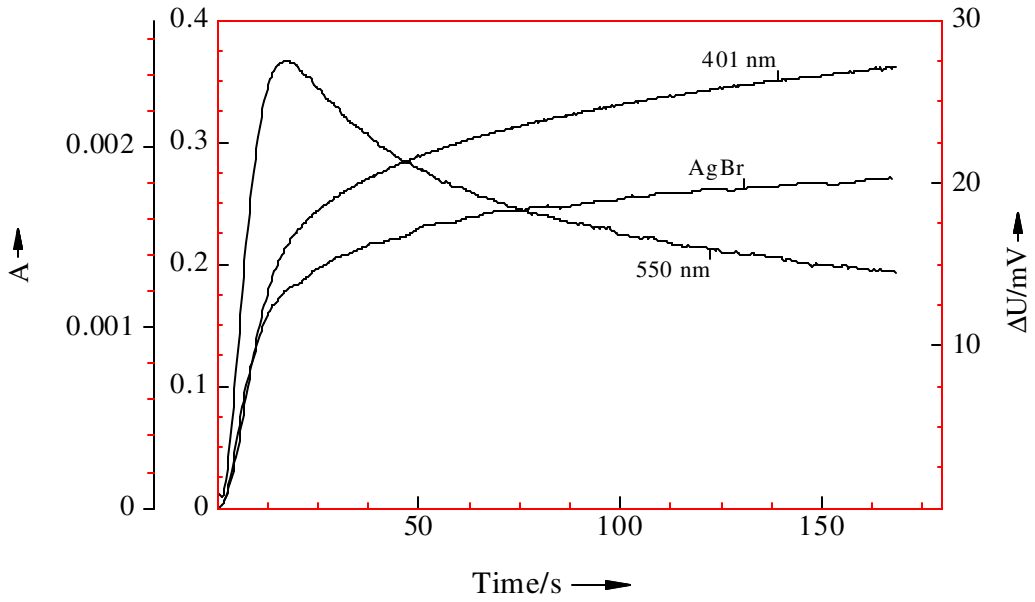

Figure 3-21: The autocatalytic reaction – three simultaneously measured signals.

The experiment was started with the injection of 1.07×10^{-4} M Ce^{3+} into 0.05 M bromate. H_2SO_4 = 1 M, T = 20 °C. Optical path length 10.8 cm. 1) 401 nm (left hand scale 0-0.4); 2) 550 nm(left hand scale 0-0.002); 3) AgBr electrode (right hand scale).

Standard cases

In the first set of experiments 3.0×10^{-4} M Ce^{3+} react with various concentrations of bromate (0.01, 0.02, 0.05 and 0.1 M). The concentration changes of Ce^{4+} and $BrO_2^{\bullet}$ after the injection of Ce^{3+} into bromate are displayed in Figure 3-22 (solid lines). We can see that, when $[BrO_3^-]_0$ = 0.01 M the reaction starts after about 10 seconds induction period; when $[BrO_3^-]_0 \geq 0.02$ M the reactions start immediately after the injection. The results of the corresponding numerical simulations (dots and dashes) show that all features of the experimental curves in this range are quantitatively modeled.

To test the model further, we repeated the experiments with the same bromate conditions, but using lower concentration of Ce^{3+} (1.07×10^{-4} M). The AgBr electrode was applied in these experiments to monitor the formation of HOBr. The formation of

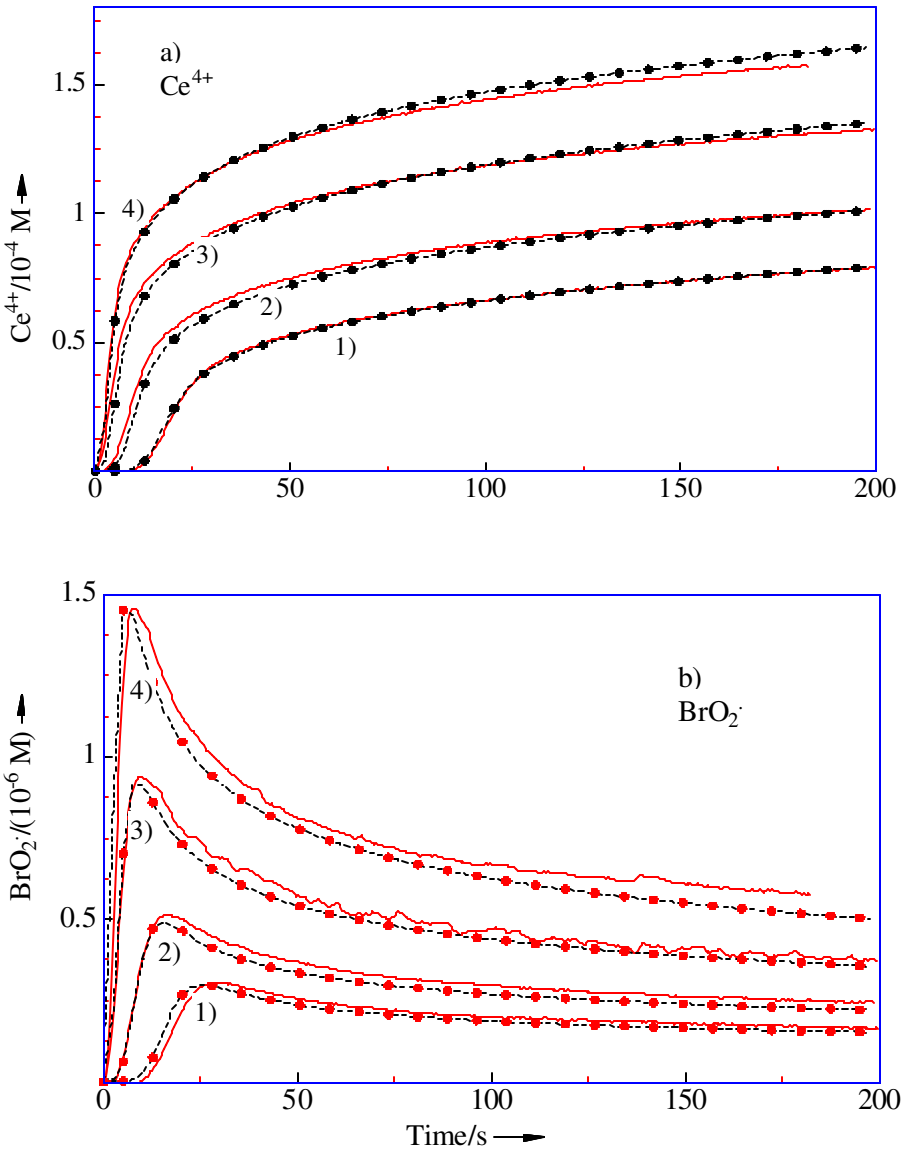

Figure 3-22: Autocatalytic reaction with 3.0×10^{-4} M Ce^{3+} and different concentrations of bromate in 1 M H_2SO_4.

The experimental conditions are the same as Figure 3-21 but Ce^{4+} was followed at 432 nm. The initial concentrations are $[Ce^{3+}]_0 = 3.0\times10^{-4}$ M, $[BrO_3^-]_0$ = 0.01 M (1); 0.02 M (2); 0.05 M (3); 0.1 M (curve 4). Solid lines: experiments. Dots and dashes: calculations. The calculated curves are obtained by using the full scheme (R_1~R_7, R_{17}) and the new set of rate constants in Table 3-9.

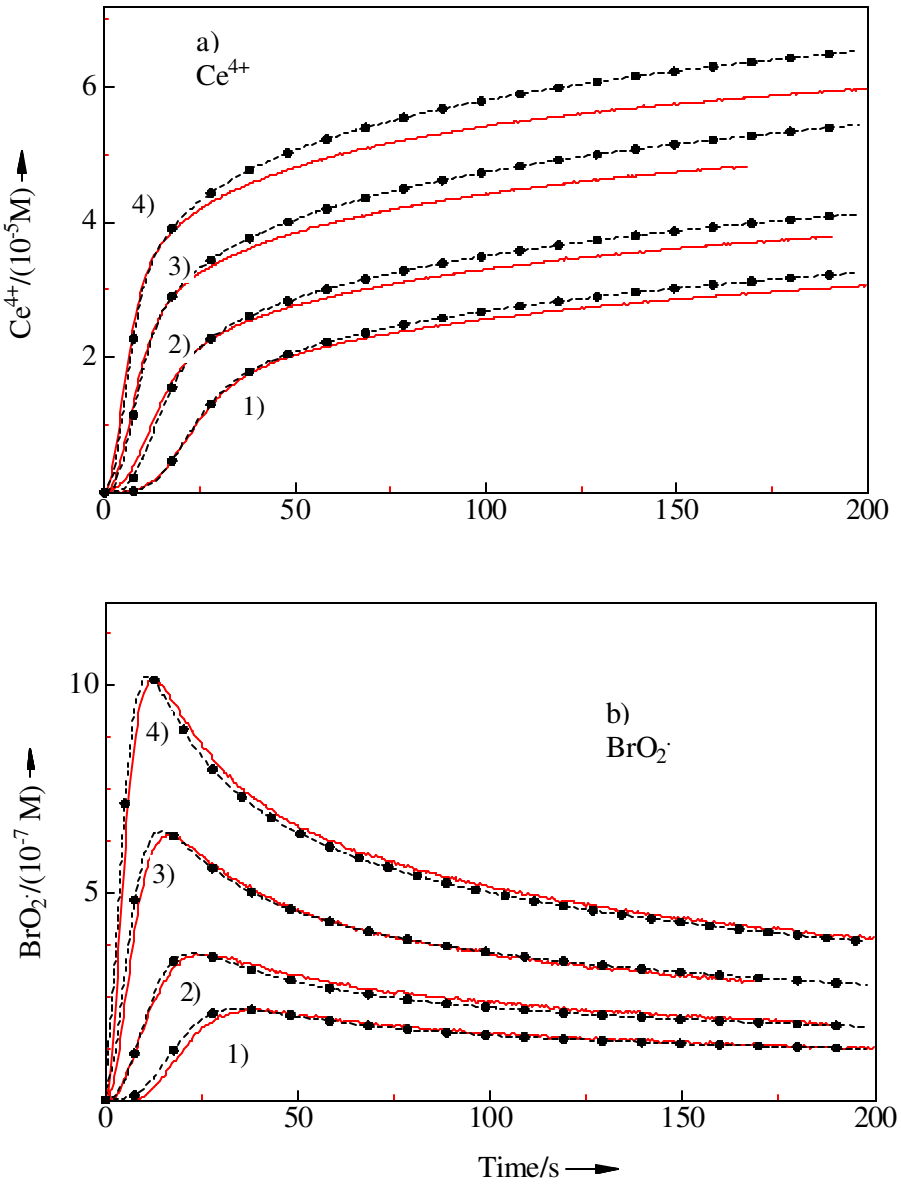

Figure 3-23: Autocatalytic reactions with 1.07×10^{-4} M Ce^{3+}.

The experimental conditions are the same as Fig. 321, the simulations are as in Fig. 3-22. The initial concentrations $[Ce^{3+}]_0$ = 1.07×10^{-4} M, $[BrO_3^-]_0$ = 0.01 M (1); 0.02 M (2); 0.05 M (3); 0.1 M (4). Solid lines: experiments. Dots and dashes: calculations.

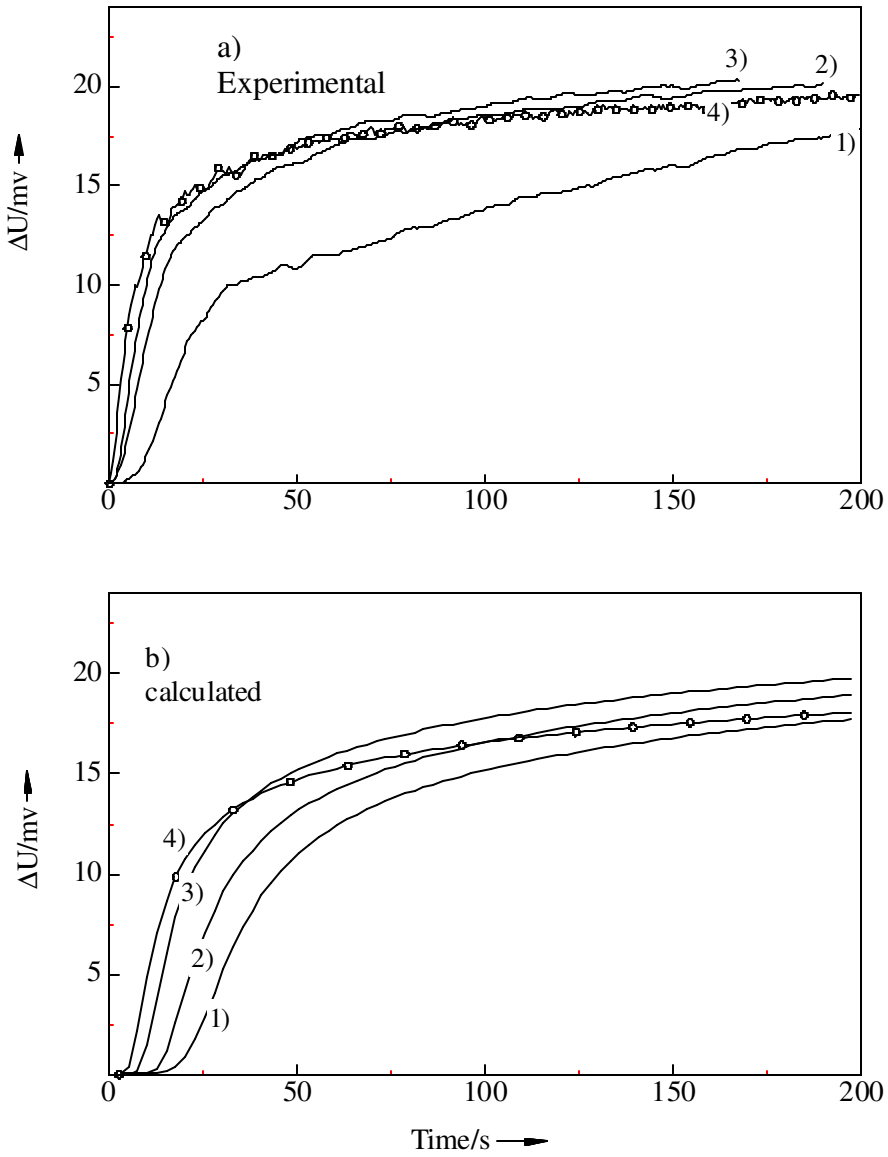

Figure 3-24: Autocatalytic reactions with 1.07×10^{-4} M Ce^{3+}- the change of AgBr electrode potential.

The same experiment as Fig. 3-23, a AgBr electrode was inserted into the reaction cell. The simulations are the same as in Fig. 3-22 but the equations for ΔU depending on the concentrations of Br^- and HOBr (Chapter 3.1.5) were used to calculate the potential change. (a): experiments. (b): calculations.

Ce^{4+} and $BrO_2^{\bullet}$ is shown in Figure 3-23 (a and b). There is no essential difference with those of 3.0×10^{-4} M Ce^{3+} cases except the absolute amount of Ce^{4+} and $BrO_2^{\bullet}$. The simulations were repeated for this lower Ce^{3+} cases, the calculated results are compared with the experiments in Figure 3-23 (dots and dashes). We found that the agreement between experiments and simulations is as good as for the higher Ce^{3+} cases although the calculated Ce^{4+} concentration is somehow higher than that of the experiments (indicating that the formation of Ce^{4+} might depend on the initial conditions).

Figure 3-24 shows that the calculated electrode potential changes are in good agreement with the experimental results too. Thus, we conclude that the modified model can quantitatively explain the observed behavior of the autocatalytic reaction.

Inhibition Effect of Bromide

The major problem of the old model is the underestimation of the inhibition effect which is reflected by the length of the induction time. So it is very important to check the modified model in this respect.

As the concentration of Ce^{3+} has no effect on the induction period, it is fixed at 3.0×10^{-4} M in all these experiments. Various initial concentrations of bromate (from 0.02 M to 0.1 M) and bromide (between 0.714×10^{-4} and 3.0×10^{-4} M) were used. To facilitate the comparison between experiments with different initial concentrations, the reagents were added into the reaction cell in the same order: 1 M sodium bromate aqueous solution was added into sulfuric acid solution (leading to a certain concentration of bromate and 1 M sulfuric acid) - bubbling N_2 for 15 min. - sodium bromide and Ce^{3+}(in 1 M H_2SO_4) were injected simultaneously. The induction times were measured from the injection. Figure 3-25 shows the absorbance change during the reaction ($[BrO_3^-]_0$ = 0.02 M (a); 0.05 M (b) and 0.1 M (c)) in the presence of Br^- (0.714×10^{-4} M (curve1), 1.43×10^{-4} M (curve 2) and 3×10^{-4} M (curve 3)). We can see that soon after the injections the signal increases due to the formation of bromine until a stationary value is reached. The length of the stationary state increases with the initial concentration of bromide and decreases with the bromate concentration. After that the autocatalytic reaction starts.

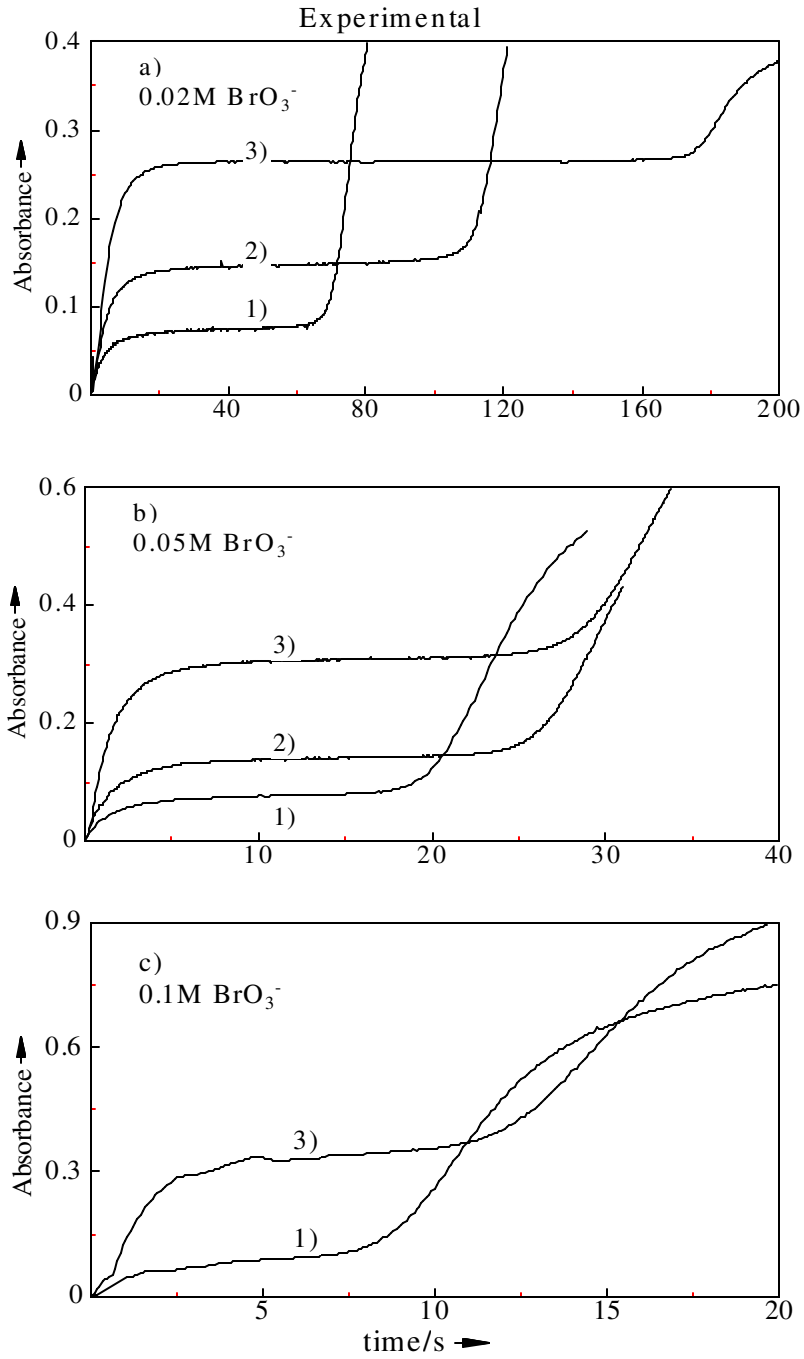

Figure 3-25: Delay of the start in the autocatalytic reaction with different concentrations of bromate in the presence of bromide. The absorbance at $\lambda = 432$ nm is measured.

The experimental conditions are the same as Fig. 3-22. The initial concentrations are $[Ce^{3+}]_0 = 3.0\times 10^{-4}$ M, $[BrO_3^-]_0 = 0.02$ M (a); 0.05 M (b); 0.1 M (c). $[Br^-]_0 = 0.714\times 10^{-4}$ M (curve1); 1.43×10^{-4} M (curve 2); 3.0×10^{-4} M (curve 3).

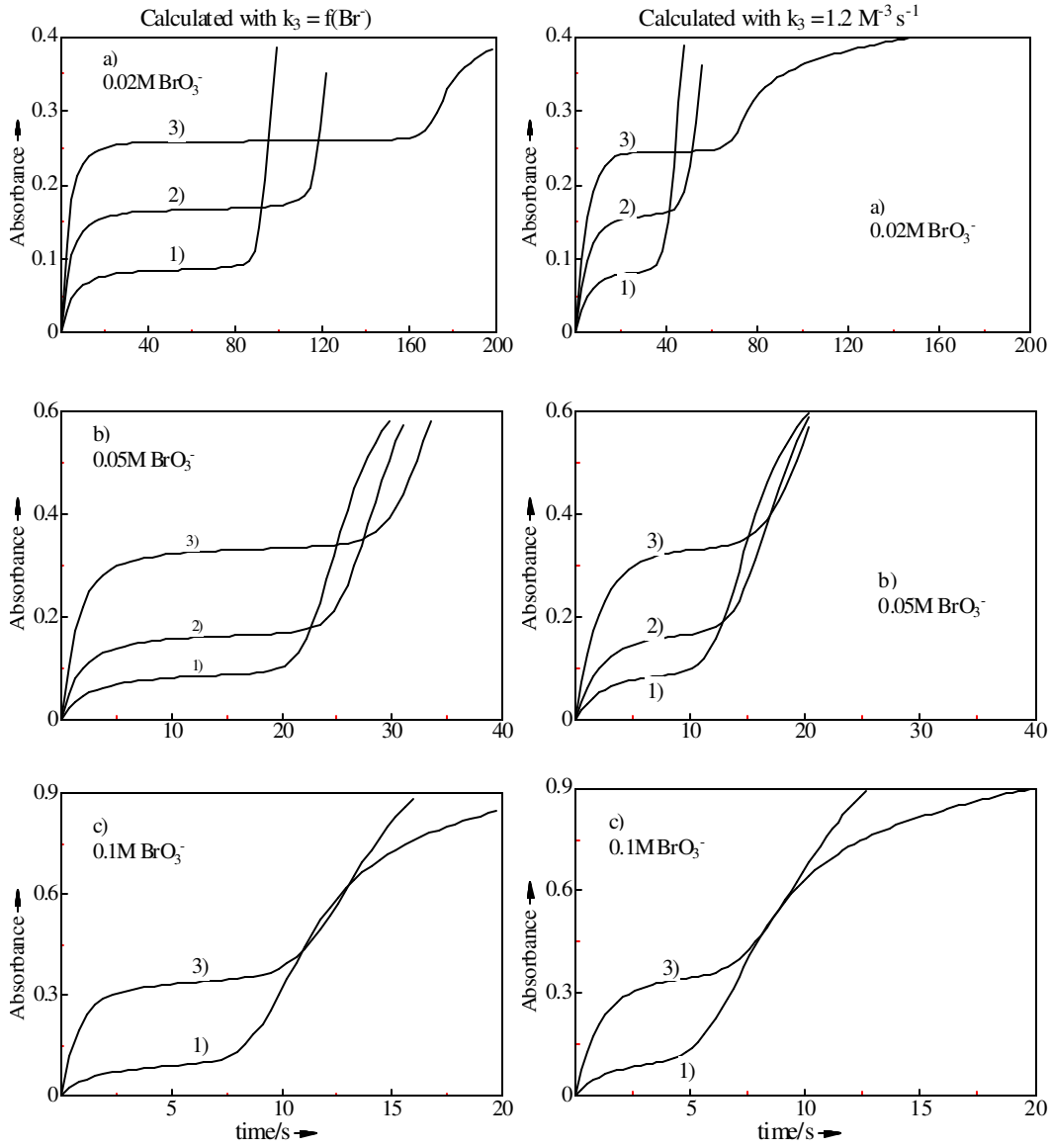

Figure 3-26: Simulations of the bromide inhibition effect by using different values of k_3

The simulations are performed for the systems shown in Figure 3-25 by using the modified model but with different values for k_3 : f(Br^-) (left hand side); 1.2 $M^{-3}s^{-1}$ throughout (right hand side).

The simulations of the inhibition effect were performed as in the standard cases with R_1~R_7 and R_{17}, in which a power series related to $[Br^-]_0$ was used. The calculated results are shown in Figure 3-26 (left hand side). It turns out that all of our observations, the

formation of bromine and the induction period for various initial conditions of both bromate and bromide, are explained very well by the modified model.

Within these modifications, the most important one is that for k_3. This argument is confirmed by the results of the following calculations. We repeated the simulation by using the old value of k_3, 1.2 $M^{-3}s^{-1}$ (right hand side of Figure 3-26). The results show that the prediction for two features becomes worse. First, in the cases of higher bromide concentration (e.g. 3.0×10^{-4} M) the calculated formation of bromine is not as fast as that observed in the experiments. That is because the rate constant of the control step, k_3, actually depends on the concentration of bromide. According to the relationship between $[Br^-]$ and k_3, k_3 = 1.6 $M^{-3}s^{-1}$ at $[Br^-] = 3.0\times10^{-4}$ M, and slows down with the consumption of bromide; when the bromide concentration decreases to 7×10^{-5} M k_3 just reaches 1.2 $M^{-3}s^{-1}$, therefore, using 1.2 $M^{-3}s^{-1}$ throughout in the calculation cannot precisely predict the rate of bromine formation. The second problem of this simulation lies in the length of the induction periods: the autocatalytic reaction under all the 8 conditions starts too early. In fact, the added bromide ions are transformed to bromine by the reaction with bromate, and this reaction is too fast with k_3 = 1.2 $M^{-3}s^{-1}$, considering the low bromide level near to the start of the autocatalysis.

Lower Bromate Concentration Case

In the system with low concentration of bromate ($[BrO_3^-]_0 < 0.01$ M), the autocatalytic reaction starts after an induction period. In literature there exist various, or even contradictive, conclusions about the length of this induction period. Some authors found that this period was irreproducible and could be seriously decreased by bubbling any gas including oxygen[48], while others believed that it was lengthened by bubbling oxygen[49].

The aim of this work is to clarify the effect of bubbling on the induction period. 0.001 M acidic bromate was used to oxidize 1×10^{-4} M Ce^{3+} using four different bubbling methods. Figure 3-27 displays the results, the starting points are the injections of Ce^{3+}.

(a) ***Without bubbling***. The air saturated solutions were used in this experiment without any bubbling treatment. The injection of Ce^{3+} was made as soon as the aqueous bromate was added into the sulfuric acid solution. About 42 minutes induction time is observed (curve a).

(b) ***Bubbling nitrogen separately***. Each one of the solutions, aqueous bromate, 1 M and 2 M sulfuric acid was bubbled with nitrogen for 15 minutes before the preparation of the reaction mixture. Ce^{3+} was injected immediately after the mixing of aqueous bromate with sulfuric acid as in (a). The resulting curve (b) shows very little difference from curve (a).

(c) ***Bubbling nitrogen***. In this case aqueous bromate and H_2SO_4 were mixed first. Then, the acidic bromate solution was bubbled with a stream of nitrogen for 15 minutes and introduced into the reaction cell. Finally, Ce^{3+} solution was injected to start the reaction (curve (c)). The induction time was decreased to about 21 min.

(d) ***Bubbling oxygen***. Repeat the experiment as in (c), but oxygen was used instead of nitrogen. The induction time was reduced to 12 minutes (curve (d)).

The results of (a), (c) and (d) seem to be consisting with Barkin et.al.'s conclusion [48] that the induction time decreased after bubbling of any of nitrogen and oxygen. However, this conclusion cannot explain the irreproducibility of the induction time. They claim that the bubbling removes bromine from the system and consequently shortens the induction time. In this system two bubblings of equal time (curves (c) and (d)) should show little difference on the length of induction time.

The experience acquired from the experiment of the bromide-bromate reaction tells us that trace amounts of bromide impurity (in bromate or sulfuric acid) is inevitable, it may inhibit the autocatalytic reaction by consuming $HBrO_2$ via reaction R_2 and cause the induction period. Bromate consumes Br^- in acidic media, the autocatalytic oxidization of Ce^{3+} by bromate occurs when this inhibitor is used up. That means the time when bromate stays in acidic medium determines the induction period. If we count the

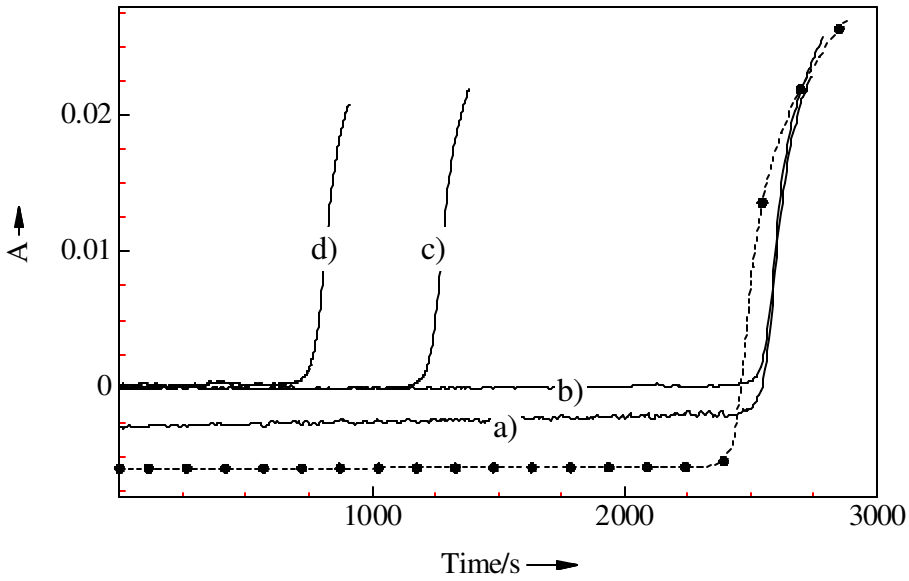

Figure 3-27: Induction periods of (0.001M BrO_3^- + 1×10^{-4} M Ce^{3+}) with different bubbling methods.

The experimental conditions are the same as in Figure 3-21 but the bubbling methods were changed. a): without bubbling; b): each stock solution was bubbled with N_2 for 15 minutes separately; c): bubbling N_2 through the reaction mixture 15 minutes after mixing the reagents; d): the same as c but replacing N_2 by O_2.

Dashes and dots: calculated as in Fig. 3-22 with $[Br^-]_0 = 5\times10^{-7}$ M. y-axes of curve a and calculation are shifted to avoid overlap.

induction period from the moment when aqueous bromate enters the sulfuric acid it should be reproducible.

In view of that argument, we repeated the experiments by counting the induction period from two starting points: 1) when aqueous bromate was added into sulfuric acid (expressed by $T(BrO_3^-)$); 2) when Ce^{3+} was injected into the reaction mixture (expressed by $T(Ce^{3+})$). The results are shown in Table 3-10. Just as expected, the values of $T(BrO_3^-)$ are comparable for all the cases (column 3) while the values of $T(Ce^{3+})$ are indeed irreproducible (column 4). To confirm this results, we repeated experiment (a)

with acidic bromate prepared some days ago: the reaction started immediately after the injection of Ce^{3+} (curve not shown). Hence, we conclude that the induction time of the autocatalytic reaction with low bromate concentrations is caused by bromide impurities, has nothing to do with the bubbling treatment. The reason why the induction time was shortened by bubbling of any gas is because the impurities are consumed during the bubbling. At much higher bromate concentrations the effect becomes too small to inhibit the autocatalytic reaction.

Finally, we performed simulations as in the preceding parts to estimate the amount of impurities by using $[Br^-]_0$ as a parameter. The best fit to the experimental induction time, $T(BrO_3^-)$, is $[Br^-]_0 = 5\times10^{-7}$ M (dashes and dots in Fig. 3-27).

Table 3-10: The induction time of 0.001 M bromate oxidizing 1×10^{-4} M Ce^{3+} with different bubbling methods.

$T(BrO_3^-)$: induction time measured from the addition of bromte ; $T(Ce^{3+})$: induction time measured from the addition of Ce^{3+}.

		$T(BrO_3^-)$	$T(Ce^{3+})$
No.	bubble gas	minutes	minutes
a	no bubbling	43	42
b	separate N_2	42	42
c	N_2 in mixture	42	12
d	O_2 in mixture	40	21

3.2 The organic subset

The organic chemistry of the BZ reaction mainly involves the reduction of the metal-ion catalyst by the organic substrate and the organic subprocesses. Despite the fact that the classical BZ reaction, the cerium ion catalysed oxidation and bromination of malonic acid by bromate, is the most studied system, there are still important processes in the negative feedback loops which are not well understood due to the complexity of the organic reaction subset. In this section we investigate reactions important for the negative feedback loops.

For a long time it was assumed that the bromomalonyl radical produced by the oxidation of bromomalonic acid disappears in a disproportionation path to give BrMA and BrTA[14]. However, later on it was found that the end products of the Ce^{4+}-BrMA reaction are bromoethenetricarboxylic acid (BrEETRA), bromide and carbon dioxide[43] indicating that the bromomalonyl radicals disappear in a radical-radical recombination path rather than by disproportionation.

3.2.1 Reaction of Ce^{4+} with Bromomalonic Acid

The oxidation of bromomalonic acid by Ce^{4+} is a key process in the cerium catalysed BZ reaction as it is involved in both feedback loops. Jwo and Noyes have spectrophotometrically investigated this reaction[44], and obtained a peculiar result that there were two different periods during which the reaction was first order in Ce^{4+}, and the transition between them is virtually discontinuous like a "break point". This phenomenon might be caused by the dissolved oxygen, because we have found that oxygen decreases the rate of Ce^{4+}-BrMA reaction by a factor of 2. If dissolved oxygen is not completely excluded from the system, the curve of Ce^{4+} must show a "break point", since the reaction proceeds slowly in the presence of oxygen and speeds up when the dissolved oxygen is consumed up.

To exclude oxygen we applied a stream of nitrogen through the solution 15 minutes before starting the reaction and constantly during the reaction. The experiments were performed with an optical cell of 1.9 cm path length (15 mL volume) in 1 M sulfuric acid at 20 °C. The solution of $Ce(SO_4)_2$ was also bubbled with nitrogen for 40 minutes before the injections. Using the dual wavelength method the absorbance change at 401 nm was followed.

Figure 3-28 displays the decay of Ce^{4+} after the injection of 0.75 mL 0.002 M solution of $Ce(SO_4)_2$ into 14.2 mL of BrMA solution (leading to initial concentrations of $[Ce^{4+}]_0 = 1\times10^{-4}$ M and $[BrMA]_0 = 0.06$ M). When we treat the curve according to a first order kinetics, a deviation from the straight line after the first half life of the reaction appears (see Figure 3-29). This indicates that the back reaction has to be taken account.

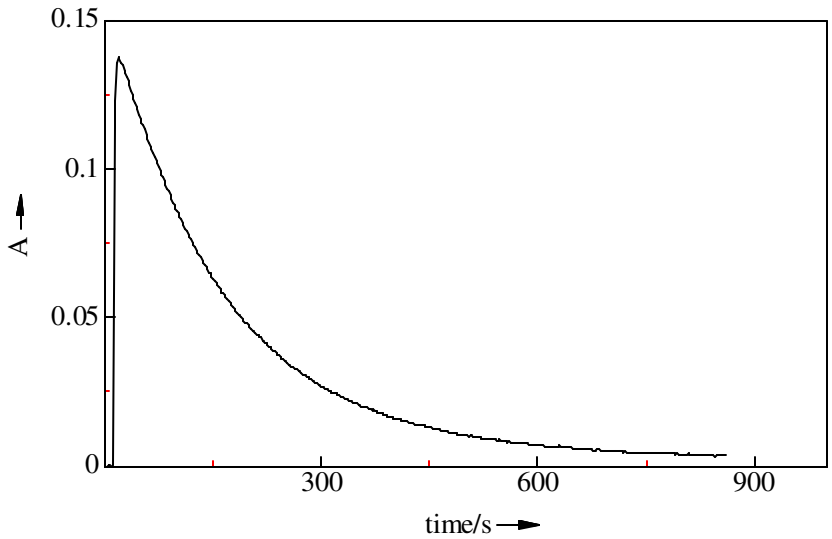

Figure 3-28: Absorbance A of Ce^{4+} at $\lambda = 401$ nm after the injection of $Ce(SO_4)_2$ into BrMA – sulphuric acid solution.

The experiment was performed with a cell of 1.9 cm optical path length (15 mL volume) in 1 M H_2SO_4 at 20°C in the absence of oxygen. The absorbance change due to Ce^{4+} was followed at 401 nm with the dual-wavelength method. $[BrMA]_0 = 0.06$ M; $[Ce^{4+}]_0 = 1\times10^{-4}$ M.

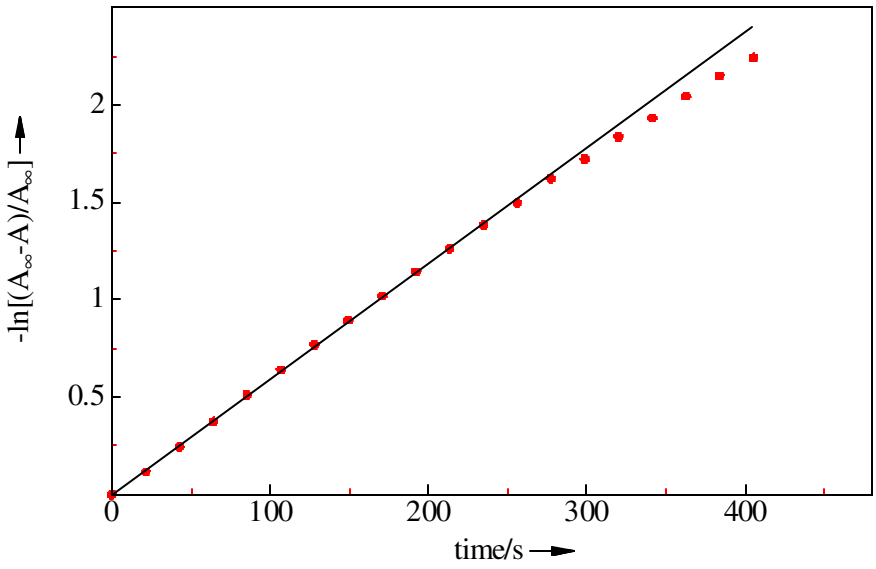

Figure 3-29: Logarithmic plot for the reaction of 1×10^{-4} M Ce^{4+} with 0.06 M BrMA in 1 M H_2SO_4.

The dots are calculated from the curve in Figure 3-28. The solid line corresponds to the regression curve.

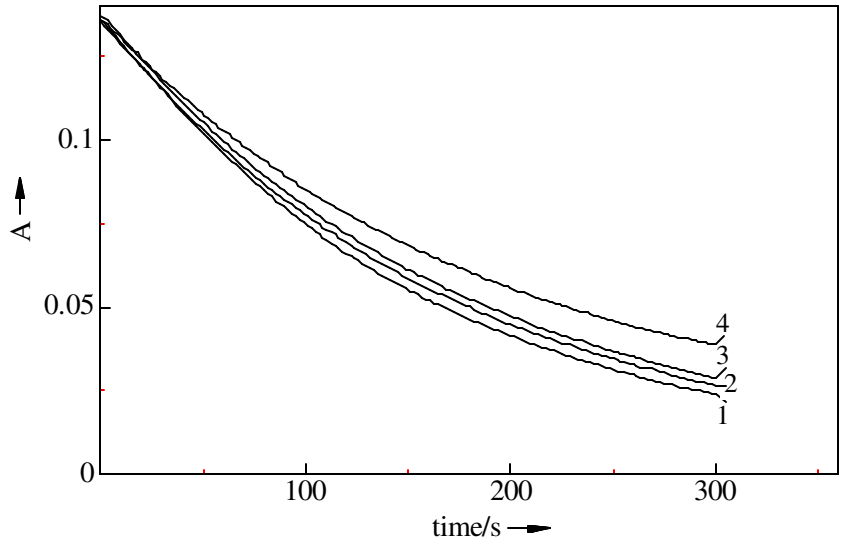

Figure 3-30: The effect of adding Ce^{3+}: decay of Ce^{4+} in subsequent injections of Ce^{4+} into a 0.06 M solution of BrMA.

The experimental conditions are the same as in Fig. 328. $[BrMA]_0$ = 0.06 M, the concentration of Ce^{4+} for each injection is 1×10^{-4} M. Before injections 3 and 4 additional amounts of Ce^{3+} (5×10^{-4}, 1.5×10^{-3}M) were injected.

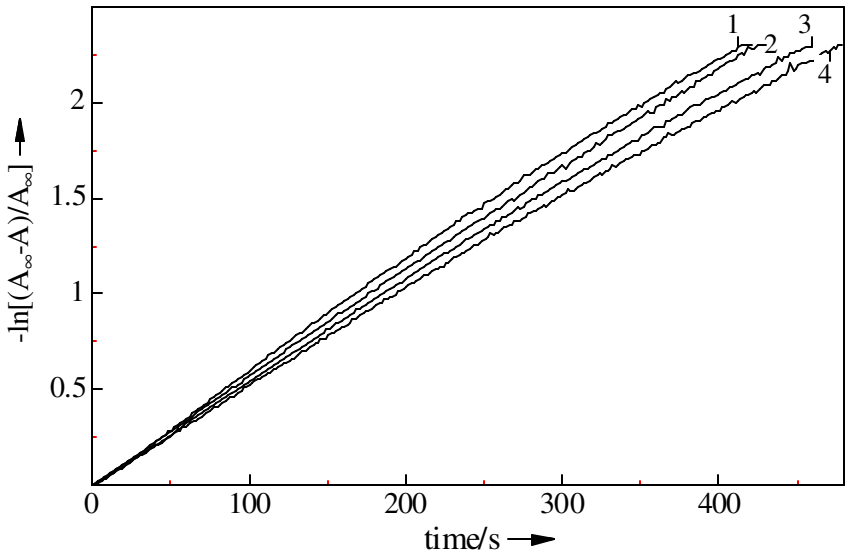

Figure 3-31: Logarithmic plots as a function of time for the experimental curves 1 – 4 in Figure 3-30.

To check for the back reaction, we carried out the experiment with several subsequent injections of 1×10^{-4} M $Ce(SO_4)_2$ into the same BrMA solution ($[BrMA]_0$ = 0.06 M) and by adding additional amounts of Ce^{3+}. The results are displayed in Figure 3-30. The curves (before injections 3 and 4 additional amounts of Ce^{3+} were added) demonstrate that the Ce^{4+} decay is slowed down by Ce^{3+}. The first order plots of these curves (curves 1-4 in Figure 3-30) are shown in Figure 3-31. With increasing $[Ce^{3+}]_0$ the logarithmic plots deviate more and more from the straight lines.

Evaluation of k_8

Using the two-step mechanism, R_8 and R_9,

$$BrMA + Ce^{4+} \rightarrow Ce^{3+} + BrMA^{\bullet} + H^{+} \qquad R_8$$

$$2\ BrMA^{\bullet} \rightarrow BrEETRA + CO_2 + Br^{-} + H^{+} \qquad R_9$$

the reaction rate in terms of Ce^{4+} and bromomalonyl radicals can be written as:

$$\frac{d[Ce^{4+}]}{dt} = -k_8[Ce^{4+}][BrMA] + k_{-8}[Ce^{3+}][BrMA^{\bullet}][H^{+}] \tag{3.36}$$

$$\frac{d[BrMA^{\bullet}]}{dt} = k_8[Ce^{4+}][BrMA] - k_{-8}[Ce^{3+}][BrMA^{\bullet}][H^{+}] - 2k_9[BrMA^{\bullet}]^2 \tag{3.37}$$

Based on the stationary-state method, the rate of formation of the bromomalonyl radicals is zero:

$$k_8[Ce^{4+}][BrMA] - k_{-8}[Ce^{3+}][BrMA^{\bullet}]_{ss}[H^{+}] - 2k_9[BrMA^{\bullet}]_{ss}^{\ 2} = 0 \tag{3.38}$$

Assuming that the second term in Equation (3.38) is negligible (this assumption will be justified at the end of this section), we obtain the stationary-state concentration of bromomalonyl radicals

$$[BrMA^{\bullet}]_{ss} = \sqrt{\frac{k_8[Ce^{4+}][BrMA]}{2k_9}} \tag{3.39}$$

Substituting $[BrMA^{\bullet}]_{ss}$ into (3.36) yields

$$\frac{d[Ce^{4+}]}{dt} = -k_8[Ce^{4+}][BrMA] + k_{-8}[Ce^{3+}][H^+]\sqrt{\frac{k_8[Ce^{4+}][BrMA]}{2k_9}} \qquad (3.40)$$

If no additional Ce^{3+} is added before the reaction, $[Ce^{3+}]$ will be very small, and the last term in Equation (3.40) can be neglected. Thus, rate Equation (3.40) can be simplified to (3.41).

$$-\frac{d[Ce^{4+}]}{dt} = k_8[Ce^{4+}][BrMA] \qquad (3.41)$$

Using the relation

$$A = d\varepsilon[Ce^{4+}]$$

for the absorbance of Ce^{4+}(ε = extinction coefficient, d= optical path length) we obtain Equation (3.42) by integration.

$$\ln\frac{A_\infty - A}{A_\infty} = -k_{obs}t \qquad (3.42)$$

$$k_{obs} = k_8[BrMA]_0 \qquad (3.43)$$

According to Equation (3.42) in the case of excess BrMA the first order rate constant k_{obs} can be obtained fom the slope of the logarithmic plot and leads to the second order rate constant k_8 via Equation (3.43).

A series of experiments was performed by varying the concentration of BrMA from 0.008 to 0.18 M. To get a straight logarithmic plot we always evaluate the first order rate constant within the first half life of the reaction. The experimental results are displayed in Table 3-11. From (3.43) we expect that k_{obs} increases linearly with $[BrMA]_0$. Figure 3-32 shows, however, that there is a deviation at higher concentrations: in the range of $[BrMA]_0 \leq 0.1$ M, k_{obs} increases linearly with $[BrMA]_0$ just as expected from (3.43), the slope is 0.10 M^{-1} s^{-1}; for $[BrMA]_0 > 0.1$ M, k_{obs}

becomes smaller than expected from the straight line indicating that the mechanism of R_8 is more complex. In the BZ system [BrMA] is always smaller than 0.1 M, therefore we restrict our concentration to the linear part in Fig. 3-32.

Table 3-11: The first order rate constants for the reaction of Ce^{4+} with BrMA.

The experiments were performed as Figure 3-28. $[Ce^{3+}]_0 = 0$. The values of k_{obs} were evaluated from the initial slopes of the logarithmic plots according to (3.42). k_8 was calculated from k_{obs} according to (3.43).

No.	$[Ce^{4+}]_0/(10^{-4}M)$	$[BrMA]_0/(10^{-2}M)$	$k_{obs}/(10^{-3}s^{-1})$
1	1.0	0.84	0.74
2	1.0	1.70	1.71
3	1.0	3.4	3.34
4	1.0	6.0	6.03
5	1.3	6.7	6.63
6	1.3	12	10.5
7	1.0	14	12.1
8	1.3	18	13.3

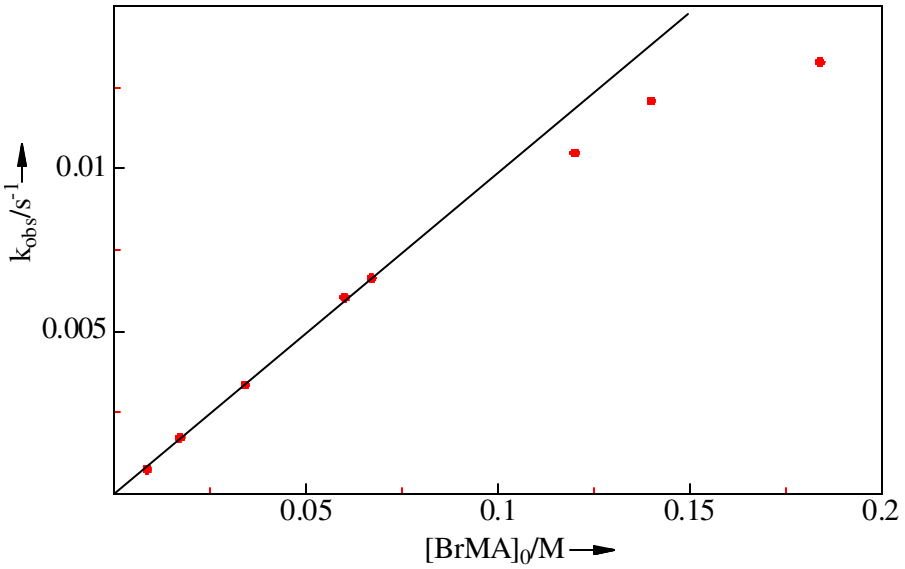

Figure 3-32: Determination of rate constant k_8: k_{obs} as a function of $[BrMA]_0$.

The data are taken from Table 3-11. From the slope of the straight line (solid line) an experimental value of the rate constant $k_8 = 0.10\ M^{-1}\ s^{-1}$ is derived.

Evaluation of k_{-8}

In the case that additional amounts of Ce^{3+} were injected before the reaction, the last term of (3.40) cannot be neglected. Rearranging Equation (3.40) yields

$$-\frac{d[Ce^{4+}]}{dt}=\left(k_8[BrMA]_0-k_{-8}[Ce^{3+}][H^+]\sqrt{\frac{k_8[BrMA]_0}{2[Ce^{4+}]k_9}}\right)[Ce^{4+}] \qquad (3.44)$$

For a rough estimate of k_{-8} we set $[Ce^{3+}] = [Ce^{3+}]_0$. Furthermore, $[Ce^{4+}]$ in the square root expression is set to $[Ce^{4+}]_0$. Then the second term inside the parentheses of (3.44) is a constant (denoted by k'), and rate Equation (3.44) becomes first order in Ce^{4+}.

$$-\frac{d[Ce^{4+}]}{dt}=k'[Ce^{4+}] \qquad (3.45)$$

$$k'=k_8[BrMA]_0-k_{-8}[Ce^{3+}]_0[H^+]\sqrt{\frac{k_8[BrMA]_0}{2[Ce^{4+}]_0 k_9}} \qquad (3.46)$$

According to (3.45), k' can be evaluated from the first-order plots of Ce^{4+}. Equation (3.46) indicates that the plot of k' versus $[Ce^{3+}]_0$ should be a straight line with a slope of

$$k_{-8}[H^+]\sqrt{\frac{k_8[BrMA]_0}{2[Ce^{4+}]_0 k_9}} \qquad (3.47)$$

Experiments as already described by Figs.3-30 and 3-31 were performed with the same concentration of BrMA and Ce^{4+}, but adding various amount of Ce^{3+} before the injection of Ce^{4+}. The results are displayed in Table 3-12a. Plotting k' as a function of $[Ce^{3+}]_0$ in Figure 3-33, we obtain a straight line as expected from (3.46). From the slope 0.28 M^1s^{-1} of the straight line k_{-8} = 400 M^1s^{-1} is obtained (with k_9 = 1×10^9 $M^{-1}s^{-1}$, k_8 = 0.10 $M^{-1}s^{-1}$, $[BrMA]_0$ = 0.06 M, $[H^+]$ = 1.29 M and $[Ce^{4+}]_0 = 1\times10^{-4}$ M).

Using the values of k_8 and k_{-8} obtained here and k_9 = 1×10^9 $M^{-1}s^{-1}$, we performed numerical simulations on the basis of R_8 and R_9. It turns out that the experimental curve is very well reproduced by the calculation (dots in Figure 3-34).

Table 3-12a: Subsequent injections of $Ce(SO_4)_2$ into a 0.06 M BrMA solution.

The experiments were performed as in Figure 3-28 but adding various amount of Ce^{3+} before the injection of Ce^{4+}. The values of k' were evaluated from the initial slopes of the logarithmic plots.

No.	$[Ce^{4+}]_0/10^{-4}$M	$[Ce^{3+}]_0/10^{-4}$M	$k'/10^{-3}$ s^{-1}
1	1.0	1.0	5.68
2	1.0	4.0	5.57
3	1.0	7.0	5.46
4	1.0	9.9	5.42
5	1.0	18.0	5.18

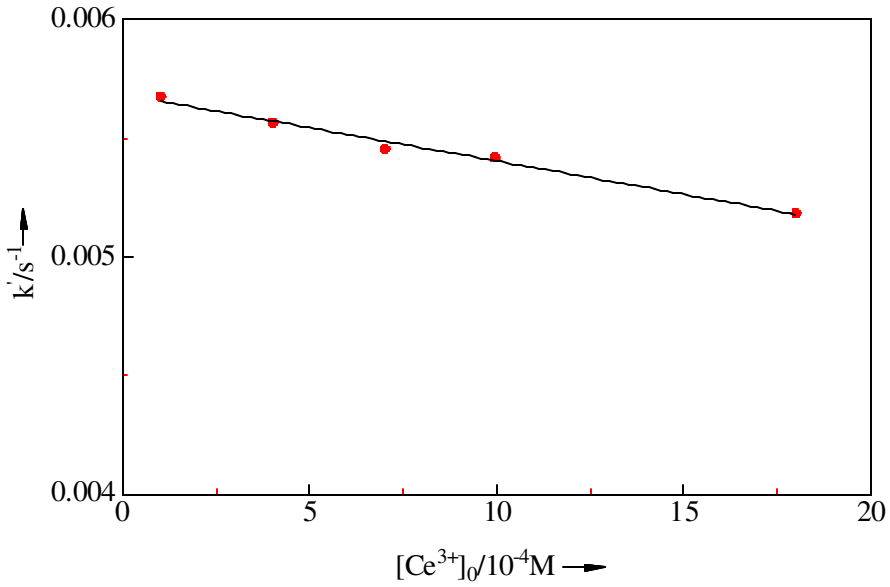

Figure 3-33: Evaluation of the rate constant k_{-8}: the first order rate constant k' as a function of the initial concentration of Ce^{3+}.

The data are taken from Table 3-12a. From the slope 0.28 $M^{-1}s^{-1}$ of the straight line the rate constant $k_{-8} = 400$ $M^{-1}s^{-1}$ is evaluated.

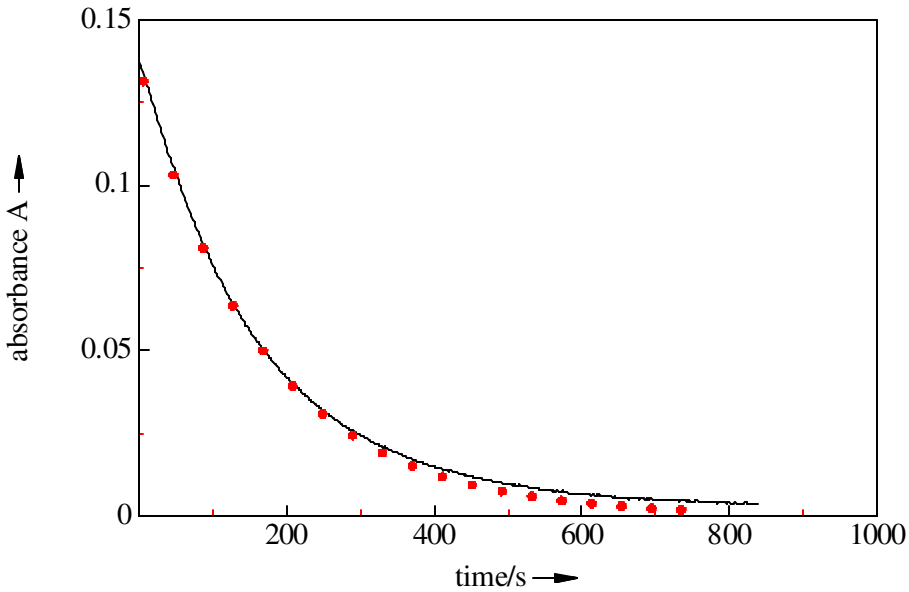

Figure 3-34: Decay of the absorbance A due to Ce^{4+} during the reaction with BrMA - numerical simulation.

The experiment (solid line) is curve 4 in Figure 3-30. $[BrMA]_0$ = 0.06 M, $[Ce^{4+}]_0$ = 1×10^{-4} M. Optical pathlength d = 1.9 cm, λ = 401 nm. The calculation (dots) is obtained with scheme R_8 ~ R_9 and the rate constants k_8 = 0.1 $M^{-1}s^{-1}$, k_{-8}= 400 $M^{-1}s^{-1}$, k_9= 1×10^9 $M^{-1}s^{-1}$.

Justification of Equation (3.39)

The steady state concentration of bromomalonyl radical, Equation (3.39), was obtained by assuming that the second term in Equation (3.38) can be neglected. If we take the second term into account, we get

$$[BrMA^{\bullet}]_{ss}' = -\frac{k_{-8}[Ce^{3+}][H^+]}{4k_9} + \sqrt{\left(\frac{k_{-8}[Ce^{3+}][H^+]}{4k_9}\right)^2 + \frac{k_8[Ce^{4+}][BrMA]}{2k_9}} \qquad (3.39a)$$

At the half life of the reaction, half of the Ce^{4+} is converted to Ce^{3+} and the concentrations of Ce^{4+} and Ce^{3+} are $[Ce^{4+}]_{t_{1/2}}$ and $[Ce^{3+}]_{t_{1/2}}$, respectively. The steady

state concentration of the bromomalonyl radicals can be calculated according to (3.39) or (3.39a). Table 3-12b shows the values of the bromomalonyl radical concentration calculated from (3.39) ($[BrMA^{\bullet}]_{ss}$) and from (3.39a) ($[BrMA^{\bullet}]'_{ss}$) using the conditions of the experiments in Table 3-12a and k_8 = 0.1 $M^{-1}s^{-1}$, k_{-8} = 400 $M^{-1}s^{-1}$, $k_9 = 1\times10^9$ $M^{-1}s^{-1}$. We can see that the calculations with and without approximation are indeed comparable even in the case that a large amount of Ce^{3+} is added before the reaction (experiment 5). Therefore, the assumption made for Equation (3.38) is reasonable.

Table 3-12b: Calculated values of $[BrMA^{\bullet}]_{ss}$ according to Equations (3.39) and (3.39a).

$[BrMA^{\bullet}]_{ss}$ and $[BrMA^{\bullet}]'_{ss}$ are calculated from the experimental conditions in Table 3-12a according to (3.39) and (3.39a), respectively, using k_8 = 0.1 $M^{-1}s^{-1}$, k_{-8} = 400 $M^{-1}s^{-1}$, $k_9 = 1\times10^9$ $M^{-1}s^{-1}$ and [BrMA] = 0.06 M.

No.	$[Ce^{4+}]_0$ /(10^{-4}M)	$[Ce^{3+}]_0$ /(10^{-4}M)	$[Ce^{4+}]_{t_{1/2}}$ /(10^{-4}M)	$[Ce^{3+}]_{t_{1/2}}$ /(10^{-4}M)	$[BrMA^{\bullet}]_{ss}$ /(10^{-8} M)	$[BrMA^{\bullet}]'_{ss}$ /(10^{-8} M)	Deviation /(%)
1	1.0	1.0	0.5	1.5	1.22	1.22	- 0.23
2	1.0	4.0	0.5	4.5	1.22	1.22	0.086
3	1.0	7.0	0.5	7.5	1.22	1.22	0.40
4	1.0	9.9	0.5	10.4	1.22	1.21	0.71
5	1.0	18.0	0.5	18.5	1.22	1.20	1.57

3.2.2 Reaction of Ce^{4+} with Dibromomalonic Acid

It is well known that bromomalonic acid can be further brominated by bromine and hypobromous acid to give dibromomalonic acid[45]. As bromomalonic acid is present in a high concentration dibromomalonic acid can accumulate. We followed the reaction of Ce^{4+} with dibromomalonic acid in 1 M H_2SO_4 as for R_8, and found that Ce^{4+} can indeed oxidize dibromomalonic acid, but the rate constant, 0.004 $M^{-1}s^{-1}$, is too small to be important for the mechanism of the BZ reaction.

3.2.3 Reaction of Ce^{4+} with Oxalic Acid

Recently Hegedüs et al.[46] found by using HPLC technique that oxalic acid (OA) is an important flow-through intermediate of the BZ reaction. The oxidation of OA by Ce^{4+} has been investigated by Kansal et al.[47] two decades ago with a titration method. A molar ratio 1:2 between oxalic acid and Ce^{4+} was determined, and the following mechanism was assumed:

$$OA + Ce^{4+} \rightarrow Ce^{3+} + CO_2 + COOH^{\bullet} + H^{+} \qquad R_{18}$$

$$COOH^{\bullet} + Ce^{4+} \rightarrow CO_2 + Ce^{3+} + H^{+} \qquad R_{19}$$

This way the second feedback loop (the Radicalator type feedback) in the BZ reaction would be strengthened by the OA /Ce^{4+} reaction, because $COOH^{\bullet}$ can capture $BrO_2^{\bullet}$ radicals.

The kinetics of the OA-Ce^{4+} reaction was studied in 1 M H_2SO_4 under nitrogen atmosphere. Oxalic acid is always in large excess over Ce^{4+}. The experimental setup and conditions are the same as described in Chapter 3.2.1.

For evaluating k_{18} the proposed mechanism, R_{18}~R_{19}, is considered. What must be mentioned is the neglect of the $COOH^{\bullet}$ recombination reaction. The reaction of Ce^{4+} with $COOH^{\bullet}$ is extremely fast[13] and the concentration of $COOH^{\bullet}$ in this system is far smaller than that of Ce^{4+}, thus the fate of $COOH^{\bullet}$ is dominated by the Ce^{4+}/ $COOH^{\bullet}$ reaction. Then,

$$\frac{d[Ce^{4+}]}{dt} = -k_{18}[Ce^{4+}][OA] - k_{19}[COOH^{\bullet}][Ce^{4+}] \qquad (3.48)$$

Based on the stationary-state method, the rate of $COOH^{\bullet}$ formation is set to zero and its steady-state concentration is derived:

$$\frac{d[COOH^{\bullet}]}{dt} = k_{18}[Ce^{4+}][OA] - k_{19}[COOH^{\bullet}][Ce^{4+}] = 0$$

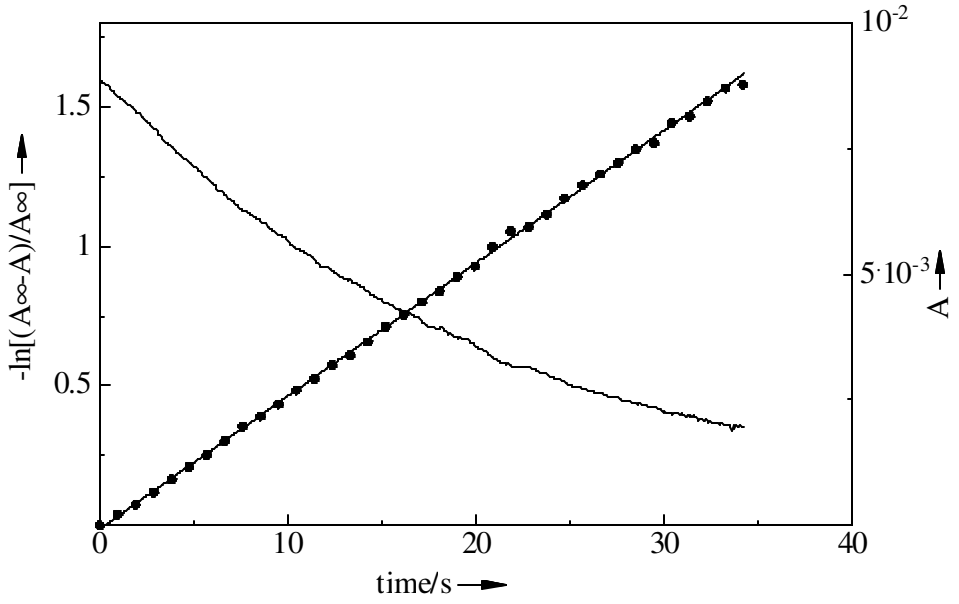

Figure 3-35: Reaction of Ce^{4+} with OA. Absorbance A (right hand scale) and logarithmic plot (left hand scale).

The experiment was performed with an optical cell with 1.9 cm path length (15 mL volume). H_2SO_4 = 1 M, T = 20°, oxygen was excluded by bubbling nitrogen. $[OA]_0 = 0.88 \times 10^{-3}$ M, $[Ce^{4+}]_0 = 6.25 \times 10^{-6}$ M. Dual-wavelength method at 401 nm (reference wavelength 670 nm) was used to follow the concentration change of Ce^{4+} with time.

$$[COOH^{\cdot}]_{ss} = \frac{k_{18}[OA]}{k_{19}} \tag{3.49}$$

We obtain rate equation (3.50) by substituting (3.49) into (3.48).

$$\frac{d[Ce^{4+}]}{dt} = -2k_{18}[OA]_0[Ce^{4+}] \tag{3.50}$$

Equation (3.50) means when oxalic acid is in large excess over Ce^{4+} the reaction is first order in Ce^{4+}, and the first order rate constant k_{obs} is

$$k_{obs} = 2k_{18}[OA]_0 \tag{3.51}$$

Table 3-13: Reaction of Ce^{4+} with OA: first order rate constants.

The experiments were performed as in Figure 335. The values of k_{obs} were evaluated from the slopes of the logarithmic plots .

No.	$[Ce^{4+}]_0/10^{-6}$M	$[OA]_0/10^{-3}$M	$k_{obs}/10^{-2}s^{-1}$
1	6.25	0.44	2.70
2	6.25	0.88	4.82
3	6.25	1.76	7.84
4	6.25	2.64	9.82

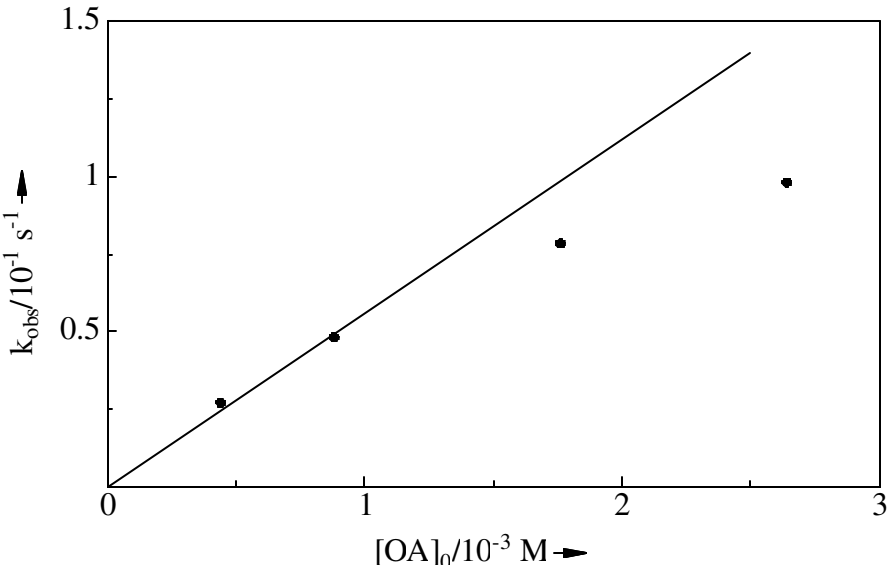

Figure 3-36: Determination of rate constant k_{18} : k_{obs} as a function of $[OA]_0$.

The data are taken from Table 313. From the slope 56.0 $M^{-1}s^{-1}$ of the straight line (solid line) and Equation (3.51) an experimental value of the rate constant $k_{18} = 28\ M^{-1}\ s^{-1}$ is derived.

Figure 3-35 demonstrates that this reaction is indeed first order indicating that the reverse reaction does not occur or is negligible.

Additional experiments with different initial concentrations of oxalic acid are summarized in Table 3-13. The first order rate constants k_{obs} are plotted as a function of $[OA]_0$ in Figure 3-36. We found that when $[OA]_0 > 1\times 10^{-3}$ M k_{obs} becomes smaller than expected from Equation (3.51). The rate constant k_{18} = 28 $M^{-1}s^{-1}$ is evaluated from the slope 56.0 $M^{-1}s^{-1}$ of the linear part of the complete curve. For the rate constant k_{19} we follow GTF[13], 1×10^{7} $M^{-1}s^{-1}$ is used. It is remarkable that R_{18} is a very fast reaction compared with R_8.

3.2.4 Reaction of Ce^{4+} with Mesoxalic Acid

So far, there has been no report about the kinetics of the reaction between Ce^{4+} and mesoxalic acid. GTF[13] argued that in aqueous solution MOA exists in the form of the hydrate, and hydrogen abstraction from such a hydrate is expected to be from an alcoholic OH rather than from –COOH; the resulting intermediate may then decompose into $COOH^{\bullet}$ and $(COOH)_2$, followed by reactions of $COOH^{\bullet}$ and $(COOH)_2$ with Ce^{4+} (R_{19} and R_{18}):

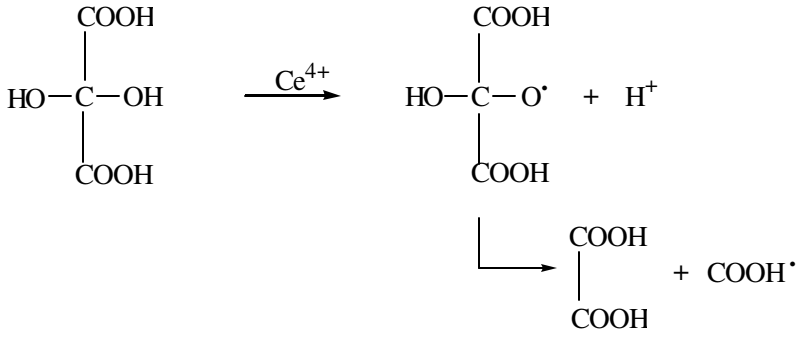

R_{20}

$$OA + Ce^{4+} \rightarrow Ce^{3+} + CO_2 + COOH^{\bullet} + H^{+} \qquad R_{18}$$

$$COOH^{\bullet} + Ce^{4+} \rightarrow CO_2 + Ce^{3+} + H^{+} \qquad R_{19}$$

We investigated the kinetics of the MOA-Ce^{4+} reaction in the absence of oxygen. The experiments were performed as described in Chapter 3.2.1 but with a large optical cell of 10.8 cm path length (140 mL volume). This was necessary to detect Ce^{4+} at a very low concentration level.

According to the suggested mechanism, the rate of Ce^{4+} disappearance is:

$$\frac{d[Ce^{4+}]}{dt} = -k_{20}[Ce^{4+}][MOA] - k_{18}[OA][Ce^{4+}] - k_{19}[COOH^{\bullet}][Ce^{4+}] \qquad (3.52)$$

Using the stationary-state method, the steady-state concentration of $COOH^{\bullet}$ is:

$$\frac{d[COOH^{\bullet}]}{dt} = k_{20}[Ce^{4+}][MOA] + k_{18}[OA][Ce^{4+}] - k_{19}[COOH^{\bullet}][Ce^{4+}] = 0$$

$$[COOH^{\bullet}]_{ss} = \frac{k_{20}[MOA] + k_{18}[OA]}{k_{19}} \qquad (3.53)$$

Thus the rate equation for Ce^{4+} becomes

$$\frac{d[Ce^{4+}]}{dt} = -\left(2k_{20}[MOA] + 2k_{18}[OA]\right)[Ce^{4+}] \qquad (3.54)$$

The resulting Equation (3.54) indicates that the first order rate constant evaluated from the Ce^{4+} curve includes the contribution of oxalic acid formed in step R_{20}. According to the stoichiometry of R_{20} one Ce^{4+} reacting with MOA produces one OA. Thus in the case of mesoxalic acid in excess [OA] is very small, the second term in the parentheses of (3.54) can be neglected, and the first order rate constant is determined by k_{20} and $[MOA]_0$.

$$k_{obs} = 2k_{20}[MOA]_0 \qquad (3.55)$$

To obtain the rate constant k_{20}, the experiment was repeated with different initial concentrations of mesoxalic acid and constant initial concentration of Ce^{4+}. These experiments are summarized in Table 3-14. The logarithmic plot (Figure 3-37 shows experiment 1 in Table 3-14) confirms that the reaction is first order. From the slope 0.14×10^{5} $M^{-1}s^{-1}$ of the k_{obs} – $[MOA]_0$ plot (Figure 3-38) we obtain $k_{20} = 7.0\times10^{3}$ $M^{-1}s^{-1}$ according to Equation (3.55). This is the highest rate constant found for reactions of Ce^{4+} with organic intermediates in the BZ reaction.

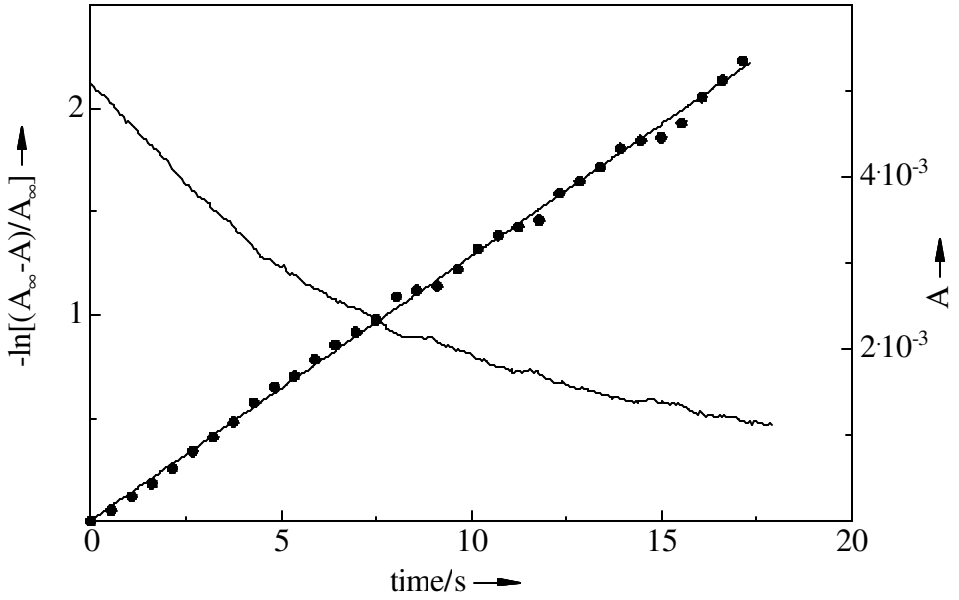

Figure 3-37: Reaction of Ce^{4+} with MOA. Absorbance A (right hand scale) and logarithmic plot (left hand scale).

The experiment was performed as in Figure 335 but with a big optical cell of 10.8 cm path length (volume 140 mL). $[MOA]_0 = 0.79\times 10^{-5}$ M, $[Ce^{4+}]_0 = 7.1\times 10^{-7}$ M. The solid line is absorbance change due to Ce^{4+} (right hand side scale). The dots are the logarithmic plot (left hand side scale).

Table 3-14: Reaction of Ce^{4+} with MOA: first order rate constants.

The experiments were performed as described in Figure 337. The values of k_{obs} were evaluated from the slopes of the logarithmic plots .

No.	$[Ce^{4+}]_0/10^{-7}$M	$[MOA]_0/10^{-5}$M	k_{obs}/s^{-1}
1	7.10	0.79	0.128
2	7.10	1.05	0.148
3	7.10	1.32	0.169
4	7.10	1.60	0.220

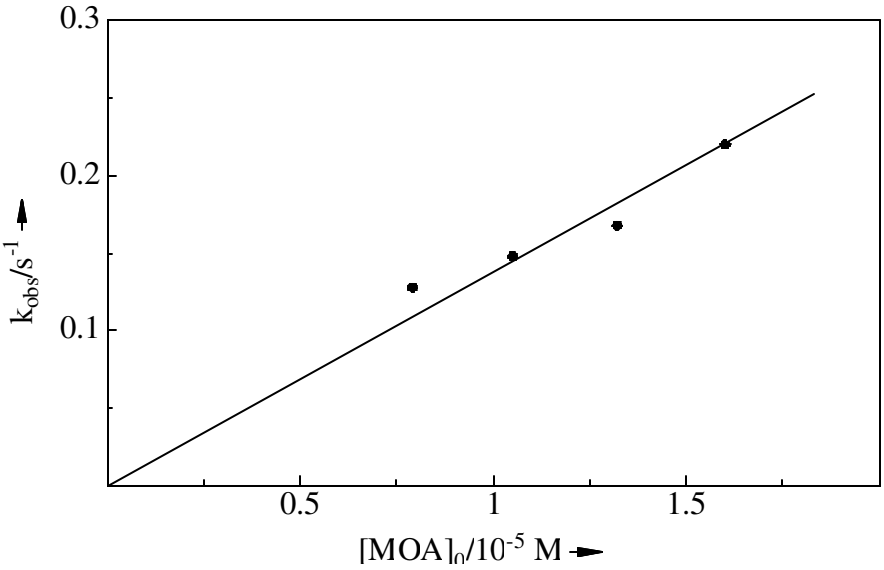

Figure 3-38: Determination of rate constant $k_{20} : k_{obs}$ as a function of $[MOA]_0$.

The data are taken from Table 314. From the slope 0.14×10^5 $M^{-1}s^{-1}$ of the straight line (solid line) and Equation (3.55) an experimental value of the rate constant $k_{20} = 7.0 \times 10^3$ $M^{-1} s^{-1}$ is obtained.

3.2.5 Evidence of the COOH•-BrMA Reaction

From the oxidation of MOA and OA $COOH^•$ radicals are naturally introduced into the BZ system. We notice that the $COOH^•$ radical is different from other organic radicals as it is capable to reduce Ce^{4+} very fast (R_{19}). We agree with GTF[13]'s suggestion that $COOH^•$ will act as a reducing agent by donating its unpaired electron rather than as an oxidizing agent by abstracting a hydrogen. GTF[13] also assumed that BrMA (known to be a good electron acceptor) is rapidly reduced by $COOH^•$ giving Br^- and $MA^•$

$$COOH^• + BrMA \rightarrow Br^- + MA^• + CO_2 + H^+ \qquad R_{21}$$

On the basis of this assumed radical transfer reaction, not only the formation of HCOOH is avoided (which is not found among the BZ reaction products), but also the negative feedback loop (reaction of $MA^•$ with $BrO_2^•$) is strengthened. However, so far there has been no direct experimental evidence supporting this reaction.

To obtain direct evidence for R_{21}, the generation of malonyl radicals and bromide by reaction of carboxyl radicals with bromomalonic acid, we carried out a batch experiment by oxidizing a 1:1-mixture of oxalic acid and bromomalonic acid by Ce^{4+}. In this system the carboxyl radicals appear as soon as Ce^{4+} is injected into the mixture of oxalic acid and bromomalonic acid because Ce^{4+} reacts with oxalic acid much faster than with BrMA (results obtained in Chapters 3.2.1 and 3.2.3). We anticipated that if R_{21} did not take place, most of the Ce^{4+} would be consumed by OA giving Ce^{3+} and carbon dioxide; the BrMA consumption by reaction between Ce^{4+} and BrMA can be neglected. Then the HPLC of the product solution should show a remarkable decrease on the oxalic acid peak corresponding to a concentration change of half of the added Ce^{4+} (as the stoichiomitry of the oxalic acid-Ce^{4+} reaction is 1:2[47]); little change on the BrMA and Br^- peaks; no any product peak. On the other hand, if $COOH^\bullet$ is capable to oxidize BrMA to $MA^\bullet$ and Br^- (R_{21} takes place), not only a significant increase of the Br^- peak and a decrease of the oxalic acid and BrMA peaks, but also peaks of recombination products of $MA^\bullet$ radicals (ETA, EETA and MAMA) should be detected.

Now we focus on the experiment. The experiment was carried out at room temperature and N_2 atmosphere. A HPLC apparatus (Shimadzu with SPD-10A dual wavelength UV detector working at 220 nm and equipped with an ion exchange column at 45 °C) was applied. The eluent is 0.01 M H_2SO_4, flow rate 0.40 mL/min. Samples containing 1 M H_2SO_4 were diluted to 0.01 M to be equal to the eluent concentration (100-µL aliquots were diluted to 10 mL). The eluent and the measured solutions were filtered with membrane filters (pore size 0.2 µm) to remove solid particles. The chromatograms were recorded with high and low sensitivity to measure various components of the sample which are present in a wide concentration and absorbance range.

First a mixture of 3.54×10^{-2} M OA and 3.52×10^{-2} M BrMA in 1 M H_2SO_4 was bubbled with N_2 for 15 min, its chromatogram is displayed in Figure 3-39a. Then 3 mL 0.1 M solution of Ce^{4+} was added into the mixture to start the reaction. Assuming an instantaneous mixing of the reagents without reaction the initial concentrations are $[OA]_0 = [BrMA]_0 = 3.0\times 10^{-2}$ M and $[Ce^{4+}]_0 = 1.53\times 10^{-2}$ M. After the completion of the reaction a HPLC sample was taken (Figure 3- 39b). Abbreviations of the intermediates

belonging to the separate peaks are given in the figures. Full name, retention times and final concentration for the intermediates are given in Table 3-16.

Comparing Fig. 3-39 a and b it can be seen that the height of the Br^- peak significantly increases corresponding to a concentration change of 6.7×10^{-3} M; the BrMA peak is apparently smaller in the product solution than it is in the original solution, corresponding to a concentration change of 7.4×10^{-3} M (see Table 3-16). These changes are clearly not only caused by direct reaction of BrMA with Ce^{4+} since only 3% of the Ce^{4+} have a chance to react with BrMA directly. Moreover, the ratio of the concentration changes of OA and Ce^{4+} is about 1:1 (instead of 1:2) indicating that most $COOH^\bullet$ radicals formed in the first step are consumed by BrMA rather than by Ce^{4+}.

Besides the changes of the peak heights of Br^-, OA and BrMA, some recombination products of $MA^\bullet$ radicals in the product solution are detected by the HPLC (Fig.3-39b): MAMA, a recombination product of an alkyl and a carboxylato malonyl radicals; MA, a recombination-decarboxylation product of $COOH^\bullet$ and $MA^\bullet$ radicals; EETA, a recombination product of $BrMA^\bullet$ and $MA^\bullet$ radicals (loosing one HBr). However, the peak of ETA (a recombination product of two alkyl malonyl radicals) can not be seen as it has the same retention time as OA. Fortunately, the contribution of ETA to the peak at 600 s can be calculated from the MAMA peak as the ETA/MAMA peak ratio is a stable value of 1.6 due to a mesomeric equilibrium between the two different forms of the malonyl radical[56]. The OA concentration is calculated from the remaining absorbance. All these facts demonstrate that carboxyl radicals react with bromomalonic acid giving malonyl radicals and bromide.

To confirm the result further, numerical simulation were performed on the Ce^{4+}- (OA+ BrMA) reaction. The individual reactions involved in the Ce^{4+}- (OA+ BrMA) reaction are shown in Table 3-15, they are the basis of simulations. It should be mentioned that the rate constant of the Ce^{4+}/OA reaction depends on the initial concentration of oxalic acid (see Figure 3-36), it slows down by a factor of 10 at $[OA]_0 = 3.0\times10^{-2}$ M. We performed the simulation first without R_{21} by setting $k_{21} = 0$. The results are presented by $\Delta c_{cal,1}$ in Table 3-16 (column 6). Obviously, all the calculated concentration changes

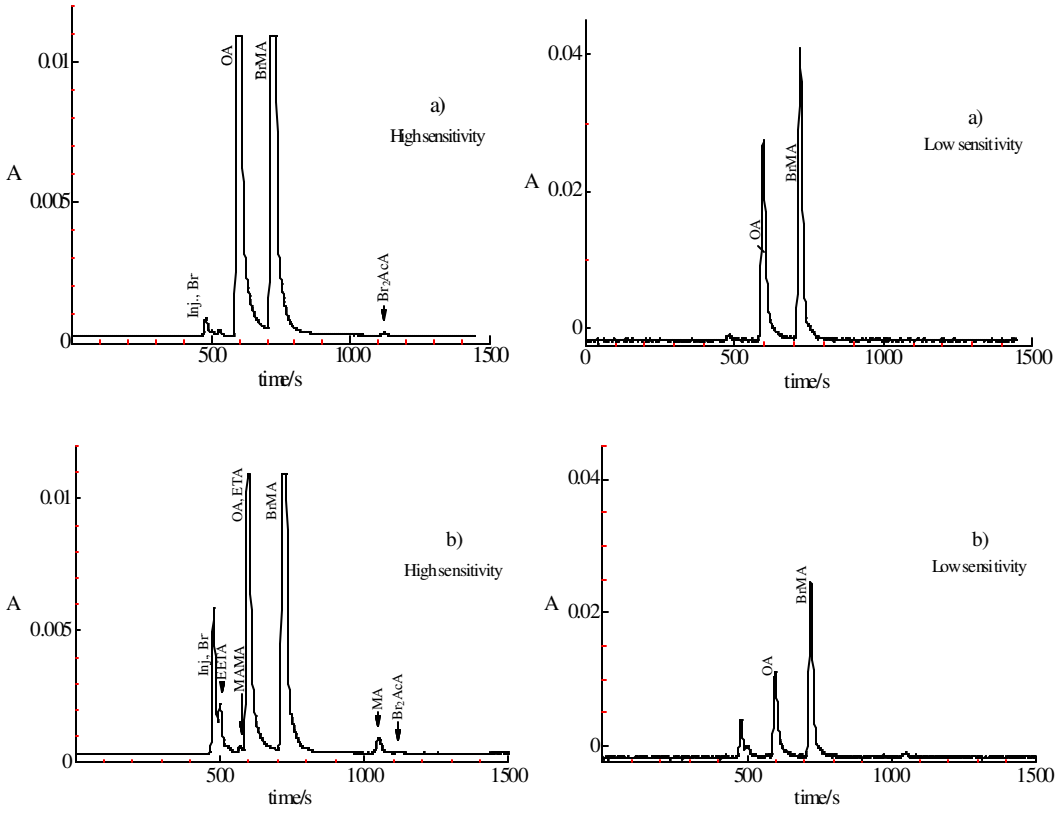

Figure 3-39: Chromatograms of the Ce^{4+}/(OA + BrMA) reaction solutions 100 times diluted by water.

A dilution of solutions before a) and after b) the reaction. Assuming an instantaneous mixing of the reagents without reaction the initial concentrations are $[OA]_0 = [BrMA]_0 = 3.0 \times 10^{-2}$ M and $[Ce^{4+}]_0 = 1.53 \times 10^{-2}$ M. See Table 3-16 for assignment of the various peaks.

are far away from the experiment: no product peak is predicted and the concentration change of Br^-, BrMA and OA are much less than the experimental values. The simulation is repeated by including R_{21} (setting $k_{21} = 1.0 \times 10^7$ $M^{-1}s^{-1}$ [13]). The calculated results are designated with $\Delta c_{cal,2}$ in Table 3-16 (column 7). It turns out that the calculations including R_{21} give values of each component comparable with the experiment. The reason that ETA and EETA are higher in the calculation than in the experiment may be the path leading to MAMA is not yet included in the mechanism.

Table 3-15: Reactions and rate constants involved in the Ce^{4+}/(OA + BrMA) reaction.

Reactions			Rate constants	
			Forward/ $M^{-1}s^{-1}$	Backward
BrMA + Ce^{4+}	$\rightleftharpoons$	Ce^{3+} + $BrMA^{\bullet}$ + H^{+}	0.1	400 $M^{-2}s^{-1}$
2 $BrMA^{\bullet}$	$\rightarrow$	Br^{-} + BrEETRA + CO_2	1×10^{9}	0
OA + Ce^{4+}	$\rightarrow$	Ce^{3+} + CO_2 + $COOH^{\bullet}$ + H^{+}	2.8	0
$COOH^{\bullet}$ + Ce^{4+}	$\rightarrow$	Ce^{3+} + CO_2 + H^{+}	1.0×10^{7}	0
2 $COOH^{\bullet}$	$\rightarrow$	OA	5×10^{9}	0
$COOH^{\bullet}$ + $BrMA^{\bullet}$	$\rightarrow$	BrMA + CO_2	5×10^{9}	0
$COOH^{\bullet}$ + BrMA	$\rightarrow$	Br^{-} + $MA^{\bullet}$ + CO_2 + H^{+}	1×10^{7}	0
$COOH^{\bullet}$ + $MA^{\bullet}$	$\rightarrow$	MA + CO_2	5×10^{9}	0
2 $MA^{\bullet}$	$\rightarrow$	ETA	3.2×10^{9}	0
$MA^{\bullet}$ + $BrMA^{\bullet}$	$\rightarrow$	EETA + Br^{-} + H^{+}	1×10^{9}	0

Table 3-16: Comparison of experimental and calculated concentrations for intermediates found in the experiment.

Retention time/s	Symbol	Component name	ΔA_{exp}	Concentration change/M		
				Δc_{exp}	$\Delta c_{cal.\,1}$	$\Delta c_{cal.\,2}$
480	Inj.	Injection				
480	Br^{-}	Bromide	4.92×10^{-3}	6.7×10^{-3}	0.13×10^{-3}	14×10^{-3}
500	EETA	1,1,2-Ethenetetracarboxylic acid	1.71×10^{-3}	4×10^{-5}	0	48×10^{-5}
570	MAMA	Monomalonyl malonate	3.23×10^{-4}			
600	OA	Oxalic acid	-1.68×10^{-2}	-1.46×10^{-2}	-0.75×10^{-2}	-1.6×10^{-2}
600	ETA	1,1,2,2-Ethanetetracarboxylic acid	5.3×10^{-4}	0.9×10^{-3}	0	4.3×10^{-3}
723	BrMA	Bromomalonic acid	-1.66×10^{-2}	-0.74×10^{-2}	-2.6×10^{-4}	-1.4×10^{-2}
1049	MA	Malonic acid	5.65×10^{-4}	5.6×10^{-3}	0	4.2×10^{-3}

3.2.6 Reaction of Bromate with Tartronic Acid

It has been proved that potassium bromate is capable to oxidize aliphatic alcohols to the corresponding ketones[50,51]. Although tartronic acid (TA) is a secondary alcohol, there has been no report so far about its reaction with bromate and thus only its oxidation by Ce^{4+} is involved in the mechanism of the classical BZ reaction.

In order to experimentally check whether acidic bromate can oxidize TA or not, we injected a small amount of TA (leading to an intial concentration of 8.7×10^{-4} M) into a solution of excess bromate (1 M BrO_3^- in 1 M H_2SO_4). According to the mechanism proposed by Natarajan et al.[50], the first product of the TA-bromate reaction is $HBrO_2$. It is well known that $HBrO_2$ reacts with bromate and disproportionates, $BrO_2^\bullet$ is expected as an intermediate and HOBr as a final product. The dual-wavelength method was used to follow the kinetics at 480 nm (Figure 3-40a solid line, ΔA_{480} due to $BrO_2^\bullet$); the absorbance of the reaction mixture was also measured at 330 nm to check for the formation of HOBr (Figure 3-40 b, ΔA_{330}).

$TA + BrO_3^- + H^+$	$\rightarrow$	$MOA + HBrO_2 + H_2O$	R_{22}
$HBrO_2 + H^+$	$\rightleftharpoons$	$H_2BrO_2^+$	R_{4a}
$HBrO_2 + H_2BrO_2^+$	$\rightleftharpoons$	$HOBr + BrO_3^- + 2\,H^+$	R_{4b}
$HBrO_2 + BrO_3^- + H^+$	$\rightleftharpoons$	$Br_2O_4 + H_2O$	R_{5a}
Br_2O_4	$\rightleftharpoons$	$2\,BrO_2^\bullet$	R_{5b}

We can see from Figure 3-40 that after the injection of TA into bromate ΔA_{480} increases to a maximum value $\Delta A_{480} = 0.003$, and ΔA_{330} increases monotonically. To make sure that ΔA_{480} is indeed due to $BrO_2^\bullet$, the kinetics was also measured at a wavelength range (340 nm ~ 700 nm). We found that the spectrum of the formed intermediate is in good agreement with that of $BrO_2^\bullet$ (curve not shown).

From the value $\Delta A_{330,\infty} = 0.13$ (which is reached at t = 15000 s = 250 min) and ε_{HOBr} =32 $M^{-1}cm^{-1}$ the final concentration of HOBr, $[HOBr]_\infty = 4.0\times10^{-4}$ M was calculated, this value is about one half of the initial concentration of TA. On the other hand, the maximum concentration of $BrO_2^\bullet$, $[BrO_2^\bullet]_{max} = 1.2\times10^{-6}$ M was calculated (from $\Delta A_{480} = 0.003$ and $\varepsilon_{BrO_2} = 994\ M^{-1}cm^{-1}$), it is about 0.3% of $[HOBr]_\infty$ indicating that the TA-bromate reaction is rather slow and R_5 is negligible when the overall reaction is under consideration. Thus, we obtain the stoichiomitry of the overall reaction which can explain the experimental fact that $[HOBr]_\infty = \frac{1}{2}[TA]_0$:

$$2\,TA + BrO_3^- + H^+ \rightarrow 2\,MOA + HOBr + H_2O$$

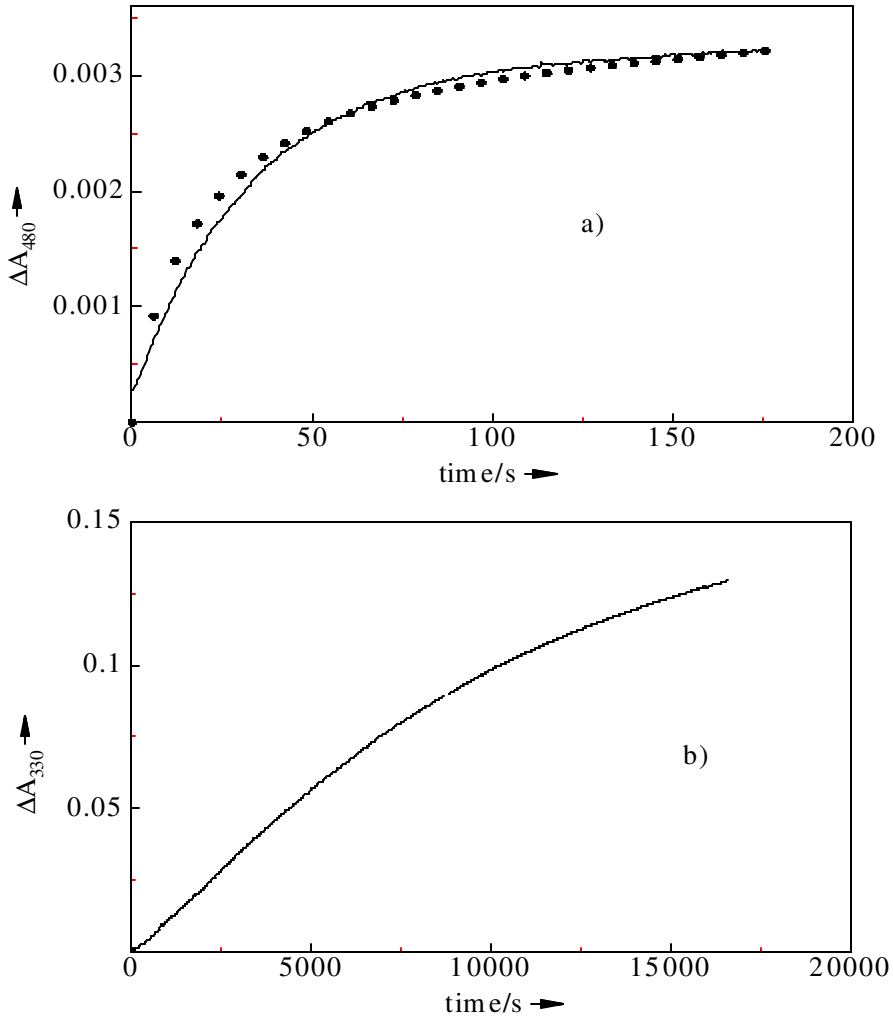

Figure 3-40: Change of the absorbance Δ A in the reaction of TA with bromate.

The solution was bubbled with nitrogen to exclude the oxygen. Temperature 20 °C. H_2SO_4 = 1 M, $[BrO_3^-]_0$ = 1 M, $[TA]_0 = 8.7\times 10^{-4}$ M. Curve a: optical path length 2.5 cm, dual-wavelength method monitoring wavelength 480 nm. The dots are calculated with R_{22}, R_4 and R_5. For rate constant of R_4 and R_5 see Table 3-9, $k_{22} = 5\times 10^{-5}$ $M^{-2}s^{-1}$. Curve b: optical path length 10 cm, double beam spectrophotometer monitoring wavelength 330 nm.

To get the value of rate constant k_{22}, a simulation based on R_{22}, R_4 and R_5 is performed by setting k_{22} as a parameter. It turns out that the value, $k_{22} = 5\times 10^{-5}$ $M^{-2}s^{-1}$ fits the experimental ΔA_{480} very well (dots in Figure 3-40a).

3.3 The Oscillations

In the previous chapters we have investigated the inorganic and organic subsets separately. However, the full oscillatory reaction is much more complicated. GTF[13] has presented a detailed mechanism of the complete organic and inorganic chemistry for the cerium catalyzed system containing 26 dynamic variables and 80 elementary reactions. But this powerful model failed to predict any oscillation in the system started with BrMA as a organic substrate[14]. Moreover, some radical transfer reactions important in the GTF mechanism have later been disproved[14]; without those reactions, the GTF model cannot even explain oscillations in the MA system.

Recently, Gao and Försterling[24] successfully explained their observations in a BZ system with bromomalonic acid as organic substrate and $[Ru(bipy)_3]^{2+}$ as a catalyst by a simple model (18 elementary reactions GF model) involving two different negative feedback loops: removal of $HBrO_2$ by Br^- and removal of $BrO_2^\bullet$ by organic radicals. Adopting this theory (GF model) Szalai et al.[20] were successful in modelling the observed oscillations in a similar system but with $[Ru(phen)_3]^{2+}$ as the catalyst. However, Oslonivitch[52] came into difficulties with ferroin as the catalyst.

In this section, we establish a new model with 46 elementary reactions containing both negative feedback loops. The new model is discussed using a 4 step procedure. First we test the validity of the GF model in a BrMA -BrO_3-Ce^{4+}system. Second, we modify the inorganic subset of the GF model by incorporating the results obtained in Chapter 3.1 (the resulting model is called the modified GF model). Third, we include all reactions necessary to model a BZ system starting with bromomalonic acid as the only organic substrate. Finally, we test the new model by its ability of reproducing observations in a BZ system starting with a mixture of MA and BrMA or pure MA.

As will be seen the new model works very well. Not only cerium catalyzed BrMA and MA systems but also systems with other catalysts (ruthenium and ferroin) can be explained.

3.3.1 The Oscillations Started with BrMA

3.3.1.1 Maps of Oscillation Limits

Although oscillations can take place in many solutions containing sulfuric acid, bromate ion, a one-equivalent redox couple with a reduction potential of about 1.0 to 1.5 V, and an organic compound that can be brominated by an enolization mechanism, there is a limit beyond which oscillations can no more occur, we call it "oscillation limit". The area within the limit is called "the oscillation region". To obtain the oscillation region of the cerium catalyzed BZ system with BrMA as a substrate, we considered experiments within a wide range of initial concentrations. 1 M sulfuric acid is always used, the temperature is 20 °C. The concentration of sodium bromate is in the range from 0.02 M to 0.2 M, that of bromomalonic acid is in the range from 0.01 M to 0.2 M, and that of $Ce(SO_4)_2$ is in the range from 1.5×10^{-4} M to 4.7×10^{-4} M.

A cell with 40 mL volume equipped with a magnetic stirrer was used, through which a nitrogen stream was bubbled throughout the solution 15 minutes before the reaction and was sufficient to provide an inert gas blanket above the solution during the reaction. The solution of $Ce(SO_4)_2$ was bubbled with nitrogen for 40 minutes before the injections. The fresh solutions were introduced into the cell always in the same order: sulfuric acid, aqueous bromate and bromomalonic acid. The reaction was started by injecting Ce^{4+}. A AgBr electrode was used to follow the development of the reaction with time.

Figure 3-42 displays the results of the experiments. The x-axis represents the concentration of bromate, the y-axis represent bromomalonic acid while Ce^{4+} is constant (1.5×10^{-4} M (a), 3.5×10^{-4} M (b), 4.7×10^{-4} M (c)). The dots denote oscillations under the corresponding conditions and the crosses denote no regular oscillations. The solid lines beyond which the oscillations can no more occur are drawn according to the dots and crosses. We can see that the sizes of oscillating areas closely relate to the concentration of Ce^{4+}: when $[Ce^{4+}]_0 = 1.5\times10^{-4}$ M (a), only 2 out of 20 experiments show oscillations, and the resulting oscillating area is so small that all the oscillating conditions are near to the boarder line. Increasing Ce^{4+} to 3.5×10^{-4} M (b), 8 out of 16 experiments show stable

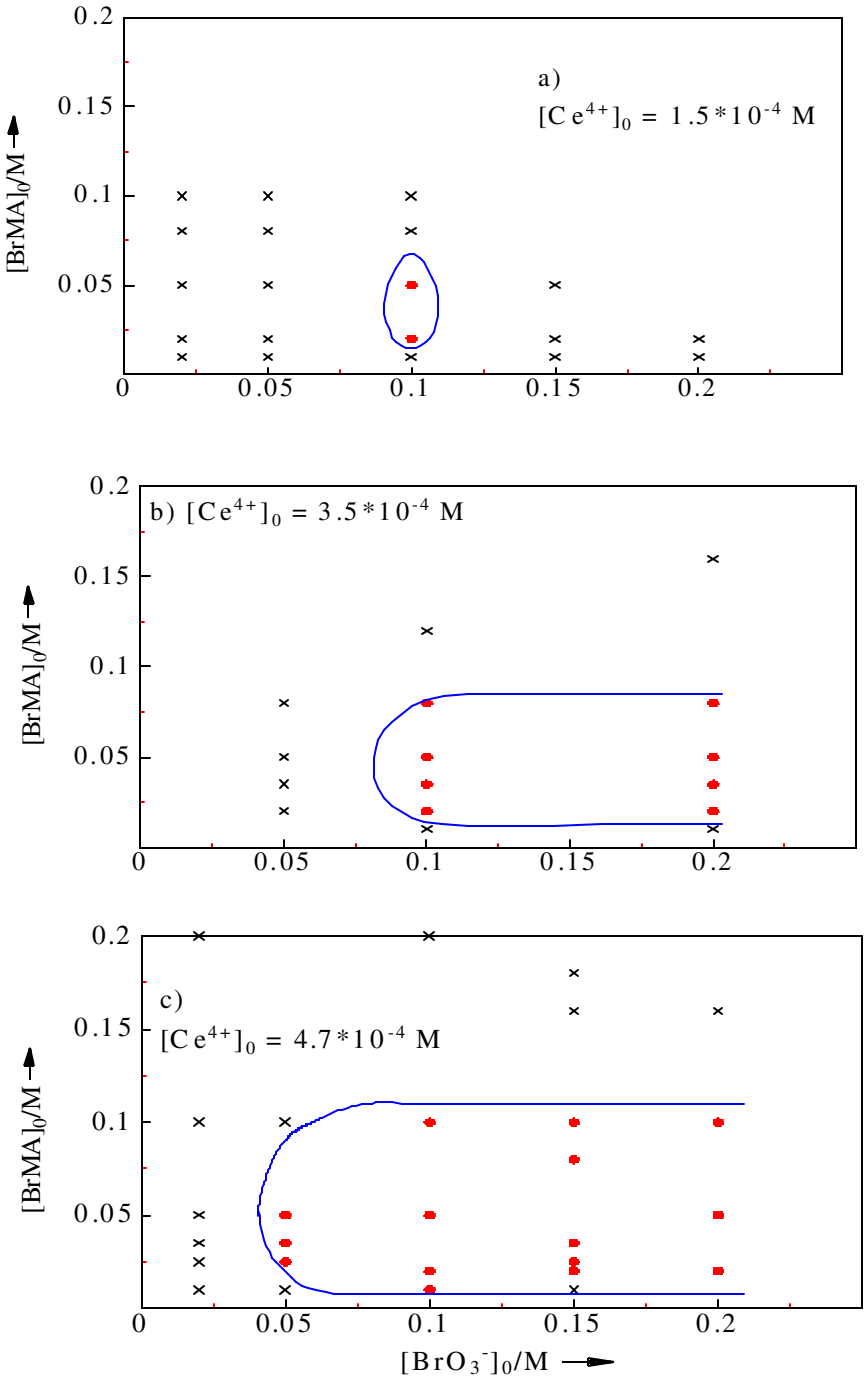

Figure 3-42: Obtaining the oscillation limit.

The experiments were performed with a well stirred cell in 1 M H_2SO_4 at 20 °C under nitrogen atmosphere. The kinetics was followed by a AgBr electrode. The concentration range of bromate is from 0.02 M to 0.1 M, of bromomalonic acid is from 0.01 M to 0.2 M while Ce^{4+} was kept constant 1.5×10^{-4} M (a), 3.5×10^{-4} M (b), 4.7×10^{-4} M (c). Dots: oscillations. Crosses: no oscillations. Solid lines: oscillation limits.

oscillations, and the size of the oscillating area expands accordingly, thus the space within the limit is enough for studying the development of the oscillatory behavior with the initial conditions. The limit is expanded further when $[Ce^{4+}]_0$ was increased to 4.7×10^{-4} M (c).

3.3.1.2 The Experimental Oscillations

The behavior of the BrMA-BrO_3-Ce^{4+} oscillation system was investigated. The general experimental conditions are the same as described in Chapter 3.3.1.1 but a photospectrometer was used to follow the kinetics of the reactions at 401 nm (detection of Ce^{4+}) and at 550 nm (detection of $BrO_2^{\bullet}$) simultaneously with a cell of 25 mL volume (optical path length of 2.5 cm). The concentration change of Ce^{4+} and $BrO_2^{\bullet}$ is calculated from the measured absorbance according to Equations (3.3) and (3.4) (described in Chapter 3.1.1).

As a standard experiment, 0.071 mL of 0.1 M Ce^{4+} oxygen free solution was injected into the cell holding 20 mL of a solution of 0.15 M bromate / 0.05 M BrMA/ 1 M H_2SO_4 to start the reaction (leading to a initial concentration of $[Ce^{4+}]_0 = 3.56 \times 10^{-4}$ M). The observed oscillations are depicted in Figure 3-43b. The upper curve is the concentration change of Ce^{4+} and the lower one is that of $BrO_2^{\bullet}$. We can see that the oscillations start immediately after the addition of the catalyst, and continue with a stable period and amplitude.

The experiments were repeated by using different concentrations of bromate. Figure 3-43 ($[BrO_3^-]_0$ = 0.1 M (a), 0.15 M (b) and 0.2 M (c)) shows that with increasing the concentration of bromate the inhibition on the autocatalytic process becomes smaller and the oscillatory period becomes shorter. The oscillatory amplitude is not significantly effected in this case.

In analogy, 0.025 M and 0.08 M bromomalonic acid were used to investigate the effect of bromomalonic acid concentration on the oscillations. The concentrations of bromate

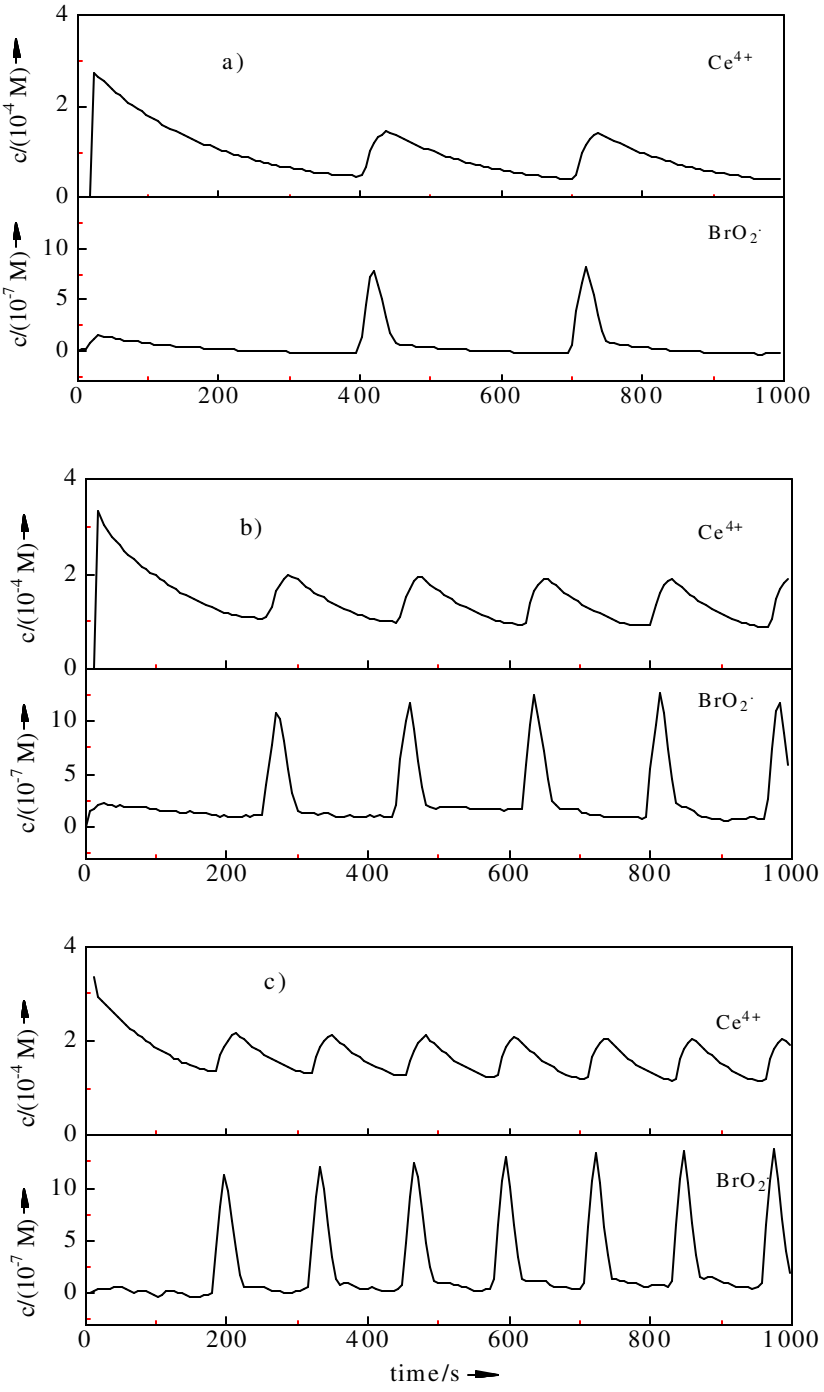

Figure 3-43: Oscillations in the systems with different concentration of bromate.

The experiments were performed at 20 °C in 1 M H_2SO_4 with a cell of 25 mL volume (2.5 cm optical path length). The kinetics was followed by measuring the absorbance change at 401 nm and 550 nm. The concentrations of Ce^{4+} and $BrO_2^{\bullet}$ are calculated from the measured absorbance according to Equations (3.3) and (3.4). The initial concentrations are $[BrMA]_0 = 0.05$ M, $[Ce^{4+}]_0 = 3.56\times10^{-4}$ M, $[BrO_3^-]_0 = 0.10$ M (a) ; 0.15 M (b) ; 0.20 M (c).

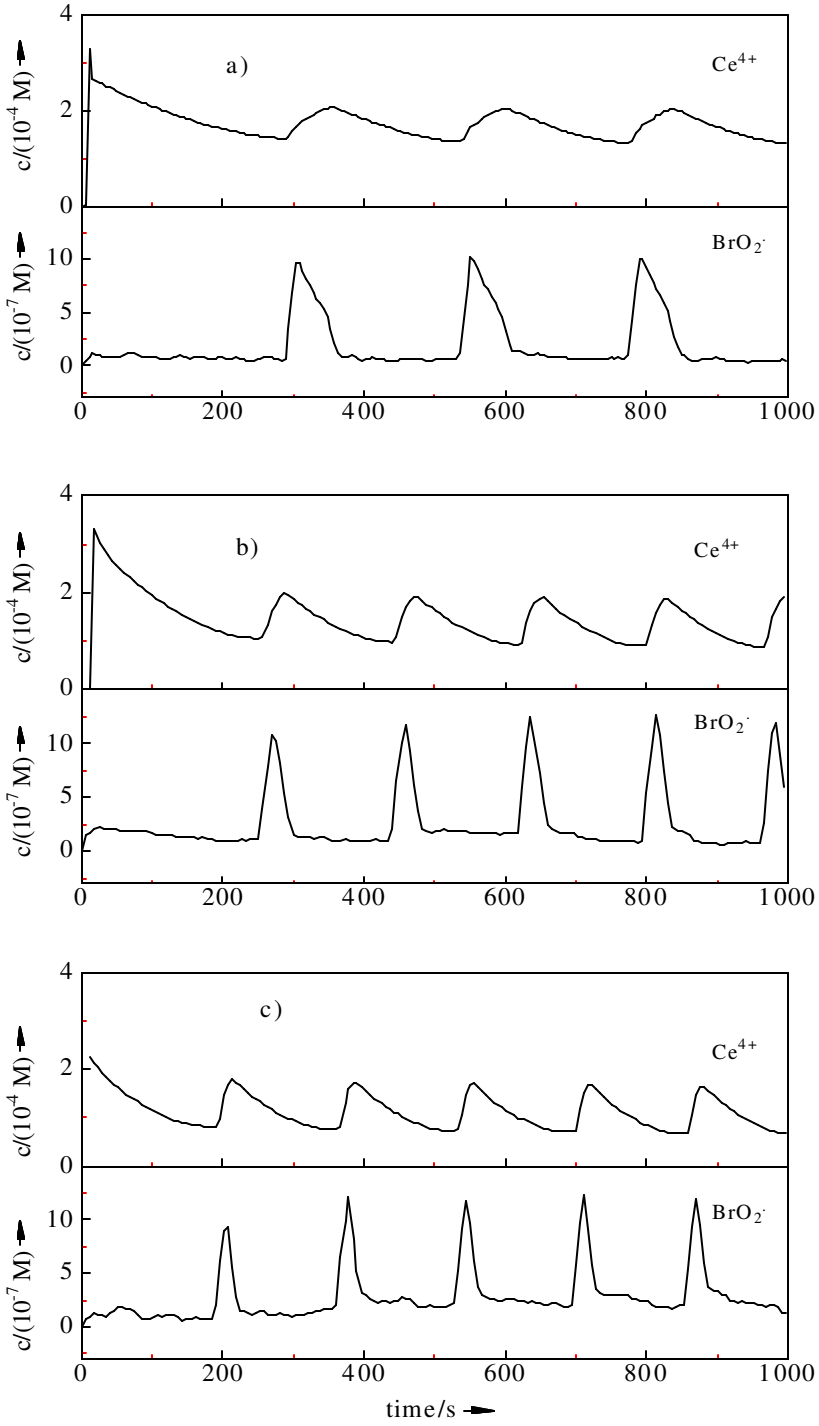

Figure 3-44: Oscillations in the systems with different concentration of bromo-malonic acid.

The experimental conditions and the evaluation of data are the same as in Figure 3-43. The initial concentrations: $[BrO_3^-]_0 = 0.15$ M, $[Ce^{4+}]_0 = 3.56 \times 10^{-4}$ M, $[BrMA]_0 = 0.025$ M, (a) ; 0.05 M (b) ; 0.08 M (c).

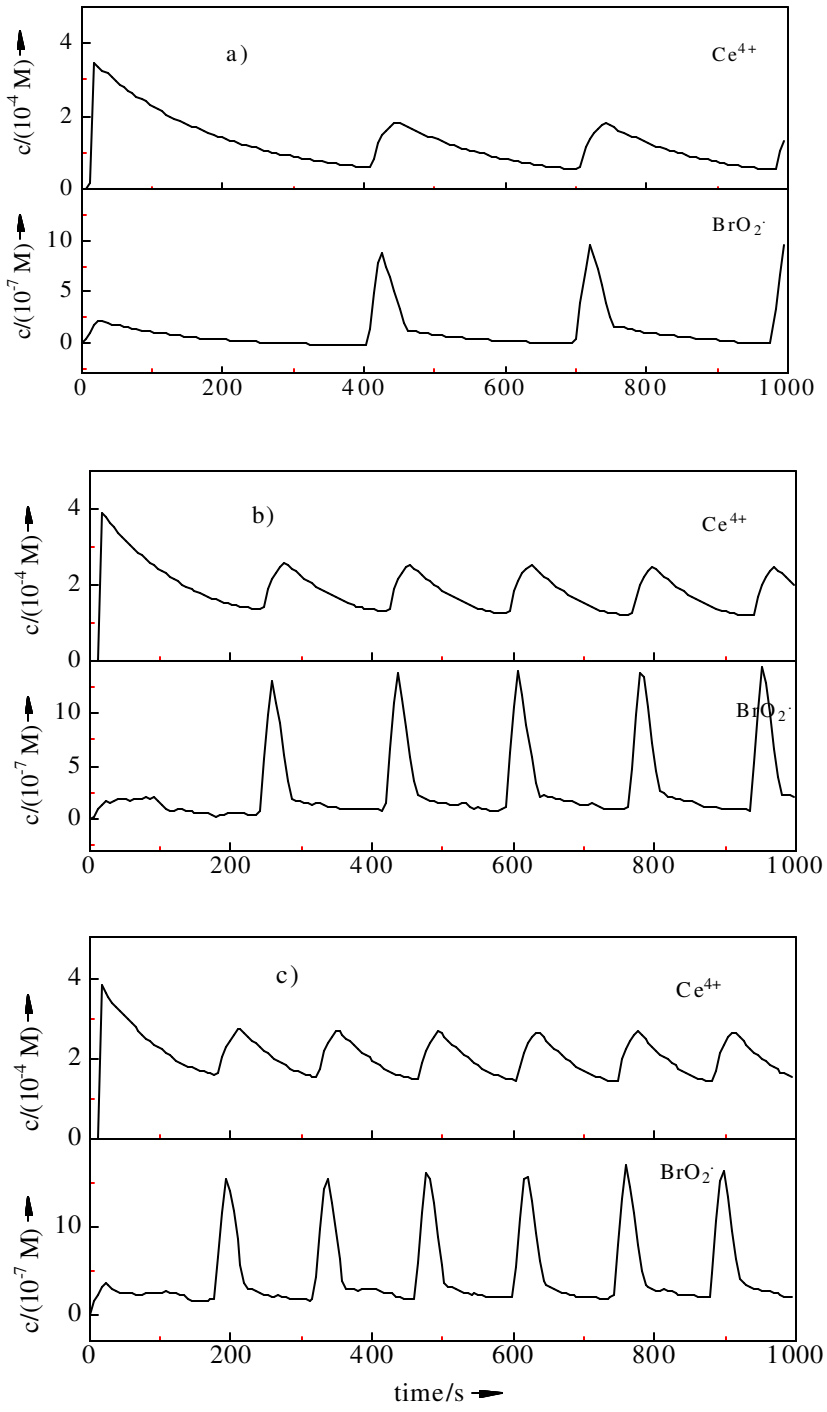

Figure 3-45: Oscillations in the systems with 4.7×10^{-4} M Ce^{4+} and different $[BrO_3^-]_0$.

The conditions of experiments and the evaluation of data are the same as in Figure 3-43 but with higher Ce^{4+} concentration: $[BrMA]_0$ = 0.05 M, $[Ce^{4+}]_0 = 4.7\times10^{-4}$ M, $[BrO_3^-]_0$ = 0.10 M, (a) ; 0.15 M (b) ; 0.20 M (c).

and Ce^{4+} are the same as in the standard case. The results are shown in Figure 3-44 and compared with the standard case (b). We found that changing the bromomalonic acid concentration caused a quite similar effect with that of changing bromate except that the amplitude in this case becomes slightly larger with increasing the initial concentration of bromomalonic acid.

To study the case of higher initial concentrations of Ce^{4+}, additional experiments were carried out with 4.7×10^{-4} M Ce^{4+} and 0.05 M BrMA. Different concentrations of bromate were used (from 0.1 M to 0.2 M). No essential difference except the absolute amplitude was observed on the oscillation behaviour when $[Ce^{4+}]_0$ increases from 3.56×10^{-4} M (Figure 3-43) to 4.7×10^{-4} M (Figure 3-45).

3.3.1.3 Simulations with the Current GF Model

We first simulate the experiments with the current GF model[24], since it has successfully explained the oscillations in BZ systems with ruthenium as the catalyst. For simulating the cerium system, reactions of $[Ru(bipy)_3]^{2+}$/ $[Ru(bipy)_3]^{3+}$ are replaced with those of Ce^{3+}/Ce^{4+}, the resulting model is shown in Table 3-17.

The initial conditions of the simulations are set just as for the experiments: $[Br^-]_0 = 1.5\times10^{-2}\times[BrMA]_0$ (1.5% bromide impurity in bromomalonic acid product), the concentration of Ce^{4+} is set to $[Ce^{4+}]_0 = 3.56\times10^{-4}$ M (or 4.7×10^{-4} M) 15 minutes after mixing BrMA and bromate.

The calculated results for systems with different concentrations of bromate, bromomalonic acid and Ce^{4+} are shown in Figure 3-46, Figure 3-47 and Figure 3-48, respectively, and compared with the experiments. It turns out that in the current GF model the calculations for the cerium system are far away from the experiments: the negative feedback loops are not sufficient to inhibit the autocatalytic reaction properly. 5 cases are completely contrary to the experiments (no oscillation at all in the model); although oscillations appear in the other 3 cases, the autocatalytic reaction starts too

early and the amplitude is much smaller than that in the experiments. These results demonstrate convincingly that the current GF model does not work in the cerium catalyzed BZ system despite the fact that it is capable of reproducing the behavior of a variety of BZ systems.

Table 3-17: The current GF Model for the cerium catalyzed BZ reaction.

Nr.	Reaction			Rate constants k_+ / ($M^{-1} s^{-1}$)	k_- / ($M^{-1} s^{-1}$)
R_1	$Br^- + HOBr + H^+$	$\rightleftharpoons$	$Br_2 + H_2O$	8×10^9 M^{-1}	80 M
R_2	$Br^- + HBrO_2 + H^+$	$\rightleftharpoons$	2 HOBr	2.5×10^6 M^{-1}	2×10^{-5}
R_3	$Br^- + BrO_3^- + 2\ H^+$	$\rightleftharpoons$	$HOBr + HBrO_2$	1.2 M^{-2}	3.2
R_{4a}	$HBrO_2 + H^+$	$\rightleftharpoons$	$H_2BrO_2^+$	2×10^6	1×10^8 M
R_{4b}	$HBrO_2 + H_2BrO_2^+$	$\rightleftharpoons$	$HOBr + BrO_3^- + 2\ H^+$	1.7×10^5	0
R_{5a}	$HBrO_2 + BrO_3^- + H^+$	$\rightleftharpoons$	$Br_2O_4 + H_2O$	48 M^{-1}	3200 M
R_{5b}	Br_2O_4	$\rightleftharpoons$	$2\ BrO_2^\bullet$	7.5×10^4 M	1.4×10^9
R_6	$Ce^{3+} + BrO_2^\bullet + H^+$	$\rightleftharpoons$	$Ce^{4+} + HBrO_2$	6.0×10^4 M^{-1}	8.9×10^3
R_7	$2\ BrO_3^- + 2\ H^+$	$\rightarrow$	$2\ HBrO_2 + 2\ O_2$	6×10^{-10} M^{-2}	
R_8	$BrMA + Ce^{4+}$	$\rightleftharpoons$	$Ce^{3+} + BrMA^\bullet + H^+$	0.1	400
R_9	$2\ BrMA^\bullet$	$\rightarrow$	$Br^- + BrEETA + CO_2$	1×10^8	0
R_{10}	BrTA	$\rightarrow$	Br^- + MOA	1.5 M	0
R_{11}	BrMA	$\rightleftharpoons$	BrMAE	1.2×10^{-2} M	800 M
R_{12}	$BrMAE + Br_2$	$\rightarrow$	$Br_2MA + Br^-$	3.5×10^6	0
R_{13}	BrMAE + HOBr	$\rightarrow$	Br_2MA	1.1×10^6	0
R_{14}	$BrMA^\bullet + BrO_2^\bullet$	$\rightarrow$	$BrMABrO_2$	4×10^9	0
R_{15}	$BrMABrO_2 + H_2O$	$\rightarrow$	$BrTA + HBrO_2$	0.46 M	0
R_{16}	$BrMABrO_2$	$\rightarrow$	$Br^- + H^+ + P_1$	0.62 M	0

The abbreviations are as follows:

k_+: forward rate constants, k: backward rate constants.

BrMA = bromomalonic acid, BrEETRA = bromoethenetricarboxylic acid, $BrMA^\bullet$ = bromomalonyl radical, BrTA = bromotartronic acid, MOA = mesoxalic acid.

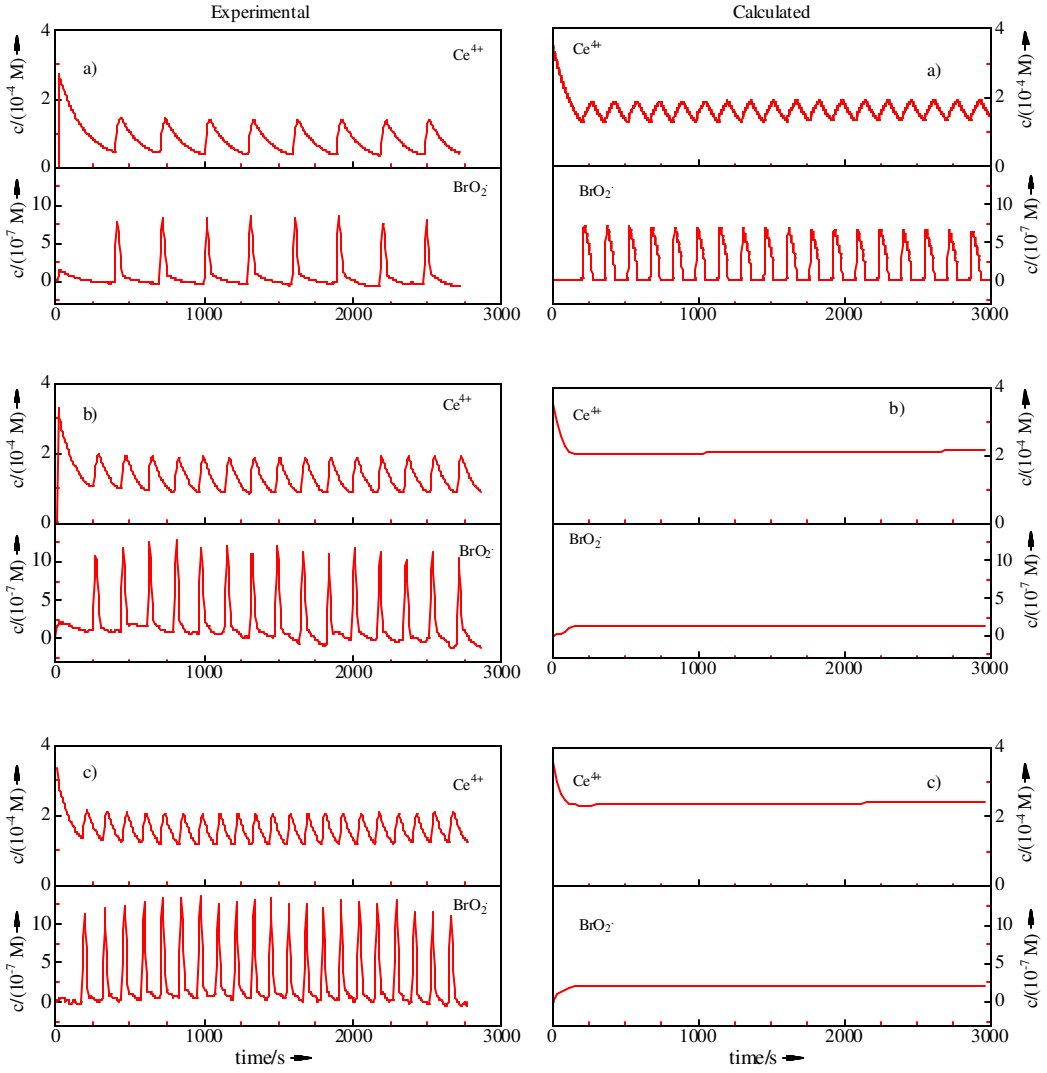

Figure 3-46: Oscillations in the systems with different initial concentration of bromate - prediction by the current GF model.

The same experiments as in Figure 3-43. The calculated curves are obtained on the basis of the current GF model (Table 3-17). The initial conditions are $[BrMA]_0$ = 0.05 M; $[Ce^{4+}]_0 = 3.56 \times 10^{-4}$ M; $[H^+]$ = 1.29 M; $[BrO_3^-]_0$ = 0.10 M (a), 0.15 M (b), 0.20 M (c).

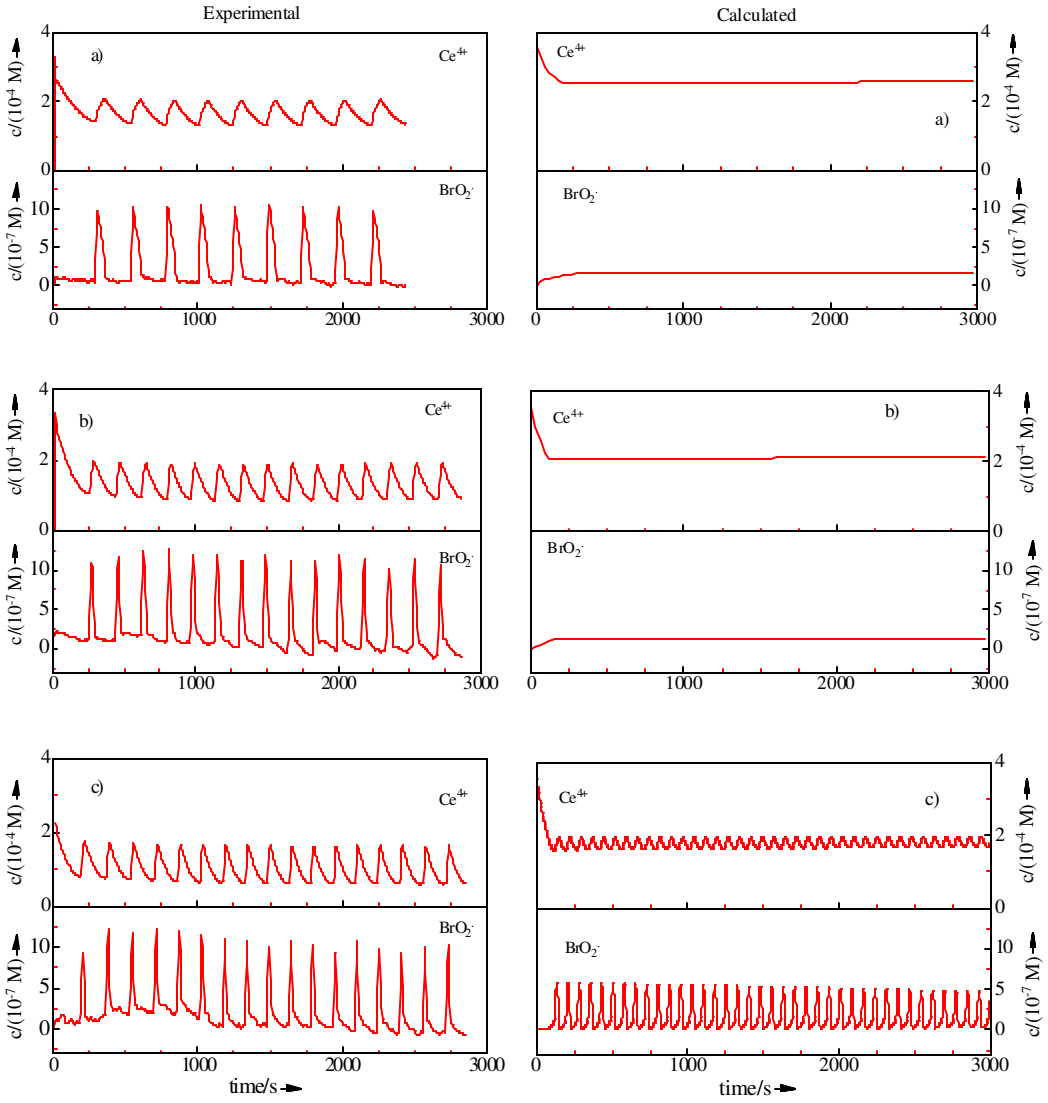

Figure 3-47: Oscillations in the systems with different initial concentration of bromomalonic acid – prediction of the current GF model.

The same experiments as in Figure 3-44. The calculated curves are obtained as in Figure 3-46. The initial conditions are $[BrO_3^-]_0$ = 0.15 M; $[Ce^{4+}]_0$ = 3.56×10^{-4} M; $[H^+]$ = 1.29 M; $[BrMA]_0$ = 0.025 M (a), 0.05 M (b), 0.08 M (c).

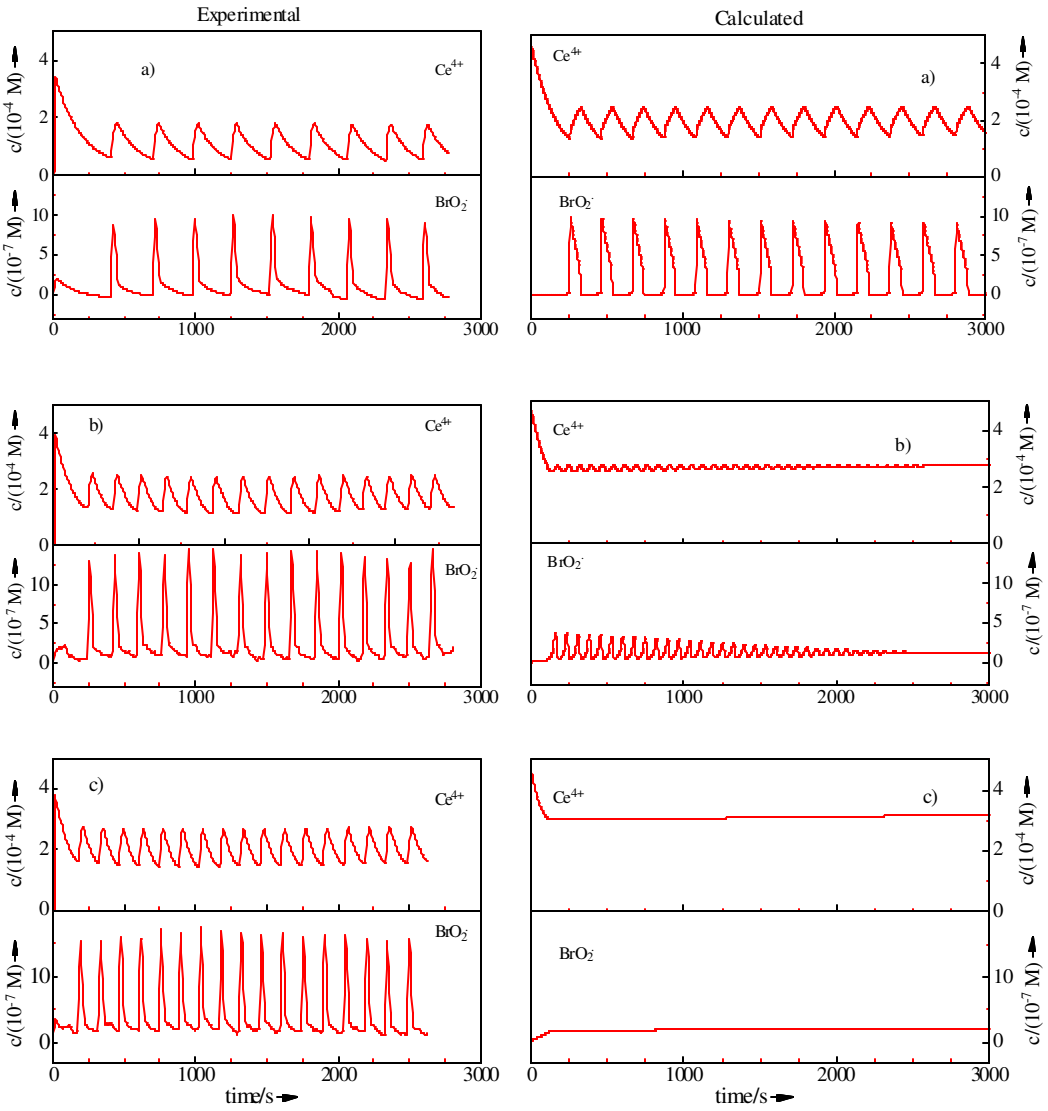

Figure 3-48: Oscillations in higher Ce^{4+} systems with different initial concentration of bromate – predition of the current GF model.

The same experiments as in Figure 3-45. The calculated curves are obtained as in Figure 3-46. The initial conditions are $[BrMA]_0$ = 0.05 M; $[Ce^{4+}]_0 = 4.7\times10^{-4}$ M; $[BrO_3^-]_0$ = 0.10 M (a), 0.15 M (b), 0.20 M (c).

3.3.1.4 Simulations with the Modified GF Model

As we found in Chapter 3.1 a decisive change has to be made on rate constant k_3, the reaction of bromide with bromate in excess. The problems in the inorganic subset of the BZ reaction can be removed by incorporating the experimental results of reactions involved in the autocatalytic reaction into the current GF model and keeping the organic subset as it is. The modifications are put in a nutshell as the following:

On the rate constant k_3. Our experimental results clearly show that reaction R_3 is not an elementary reaction, but follows a complex kinetics. The rate constant k_3 depends on the initial concentrations of bromide and bromate in the typical concentration range of the BZ system. The dependency on the bromide concentration can be described by a power series (see Chapter 3.1.4).

On the rate constant k_6. The experimental values resulting from two different methods demonstrate that the rate constant of the Ce^{4+}-$HBrO_2$ reaction (k_{-6}) strongly depends on the ionic strength of the solution. k_{-6} decreases with increasing the ionic strength according to a power series (see Chapter 3.1.3).

On the decomposition of $BrO_2^{\bullet}$. Since $BrO_2^{\bullet}$ is a crucial species in the BZ system, the reaction of its decomposition should be taken into account although it proceeds very slowly ($k_{17} = 0.06\ s^{-1}$).

Thus, we obtained the modified GF model (R_1~R_{17}; the rate constants of the inorganic subset use the values in Table 3-9, of the organic subset use the values in Table 3-17).

The simulations were repeated with the modified model. The calculated results are shown in Figure 3-49, Figure 3-50 and Figure 3-51 for oscillations with different concentrations of bromate, bromomalonic acid and Ce^{4+}, respectively, and compared with the experiments. Obviously, a significant progress is achieved after modifying the inorganic subset: the negative feedback loops are significantly strengthened such that the model turns to the oscillatory regime for all the selected conditions; the dependency of the oscillation characteristics on the initial conditions is well reproduced. For

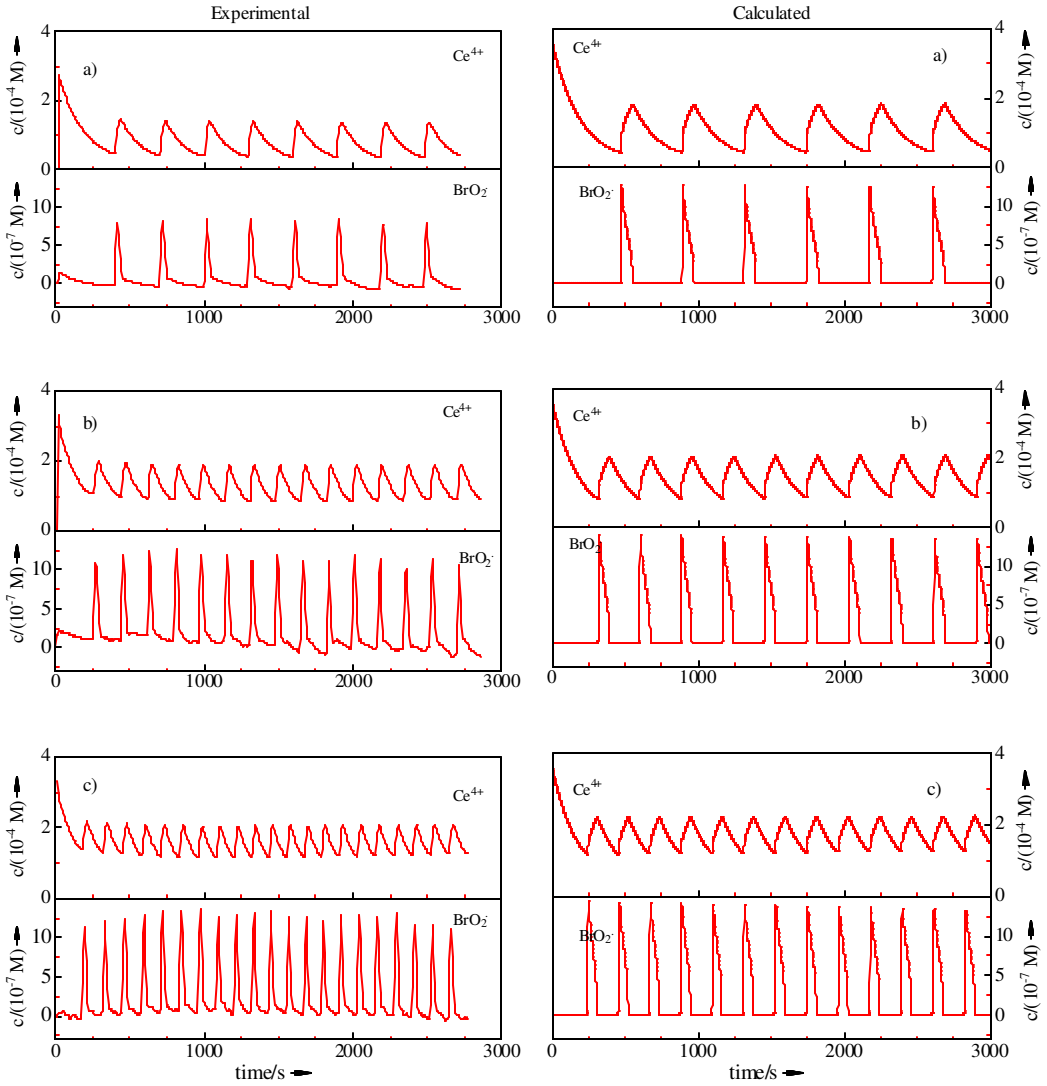

Figure 3-49: Oscillations in the systems with different initial concentrations of bromate - prediction of the modified GF model.

The same experiments as Figure 3-43. The calculated curves are obtained based on reactions R_1~R_{17} and rate constants for R_1~R_7 in Table 3-9, for R_8~R_{16} in Table 3-17, k_{17} = 0.06 s^{-1}. $[BrMA]_0$ = 0.05 M; $[Ce^{4+}]_0 = 3.56 \times 10^{-4}$ M; $[H^+]$ = 1.29 M; $[BrO_3^-]_0$ = 0.10 M (a), 0.15 M (b), 0.20 M (c).

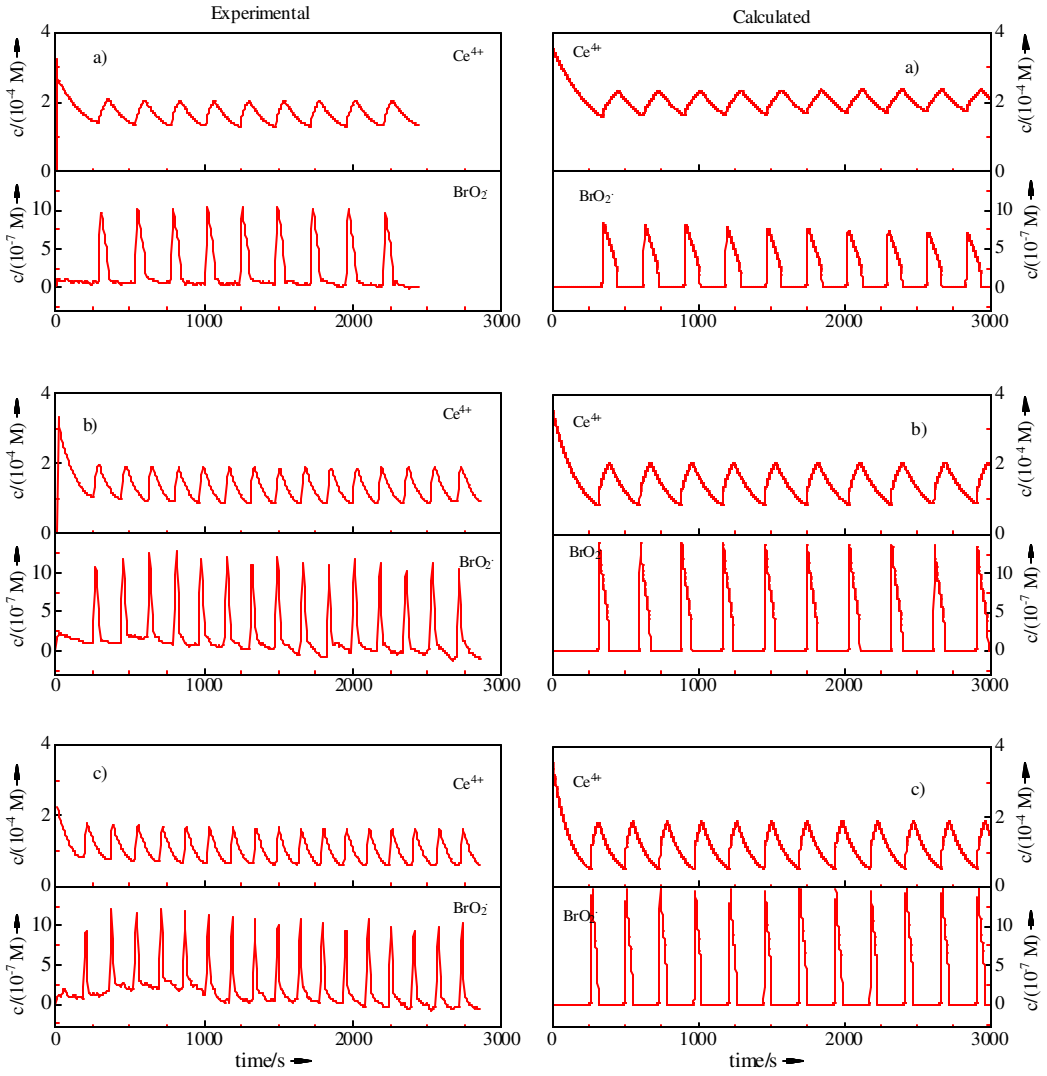

Figure 3-50: Oscillations in the systems with different initial concentrations of bromo-malonic acid – prediction of the modified GF model.

The same experiments as Figure 3-44. The calculated curves are obtained as in Figure 3-49. The initial conditions are $[BrO_3^-]_0$ = 0.15 M; $[Ce^{4+}]_0$ = 3.56× 10^{-4} M; $[H^+]$ = 1.29 M; $[BrMA]_0$ = 0.025 M (a), 0.05 M (b), 0.08 M (c).

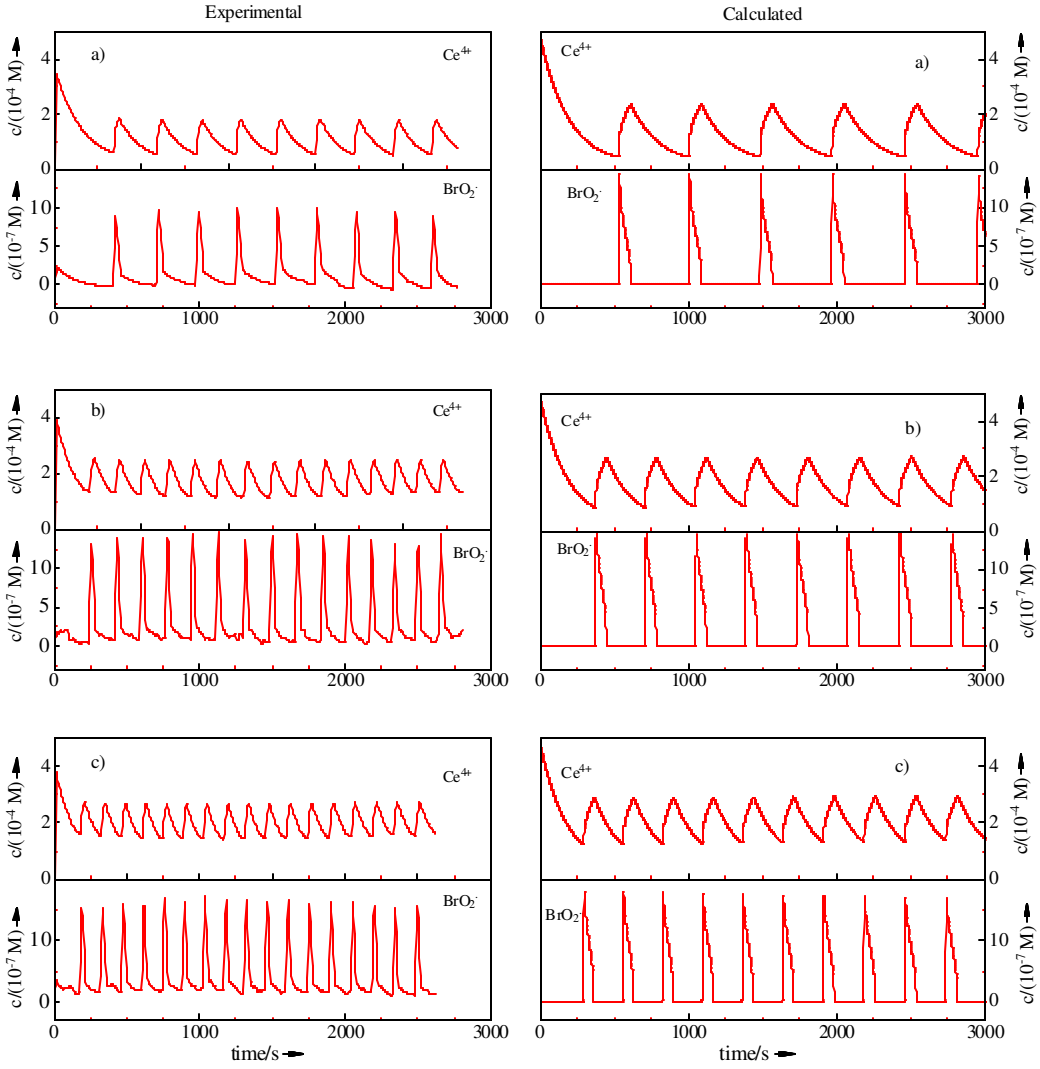

Figure 3-51: Oscillations in higher Ce^{4+} systems with different initial concentrations of bromate – prediction of the modified GF model.

The same experiments as Figure 3-45. The calculated curves are obtained as Figure 3-49. The initial conditions are $[BrMA]_0$ = 0.05 M; $[Ce^{4+}]_0 = 4.7\times 10^{-4}$ M; $[BrO_3^-]_0$ = 0.10 M (a), 0.15 M (b), 0.20 M (c).

instance, increasing the concentration of bromate or BrMA the oscillatory period becomes shorter and the frequency becomes higher.

However, modifications on the inorganic subset are not sufficient: the calculated oscillating peak is less sharp-pointed than in the observations; the period needed to switch off the autocatalytic reaction in each oscillation cycle is two times longer than that of experiments, as a result the calculated oscillatory period is longer and the oscillating frequency is lower. These shortcomings of the calculations implicate that there are still problems with the negative feedback loops. While the chemistry and kinetics of the inorganic subset has been clarified, our interest must be focused on the organic subset.

3.3.1.5 Expanded GF Mechanism

The Basis of the Expanded GF Mechanism

It has been known[6] that organic radicals can recombine with $BrO_2^{\bullet}$ radicals and this is the basis of the second negative feedback loop and the radical controlled oscillations[53]. Nevertheless the subsequent decomposition of the recombination intermediate was an open problem. For bromomalonyl bromite ($BrMABrO_2$, the recombination product of $BrMA^{\bullet}$ and $BrO_2^{\bullet}$), GTF[13] included only its hydrolysis route (leading to bromotartronic acid and $HBrO_2$) in the mechanism although they have speculated about another possible route which would produce OA, Br^-, CO_2 and HOBr. GF[24] assumed two different decomposition routes for $BrMABrO_2$ too, the first one (R_{15}) is the same as in GTF; the other one (R_{16}) leads to Br^-, H^+ and an unknown inert product P_1 without explicit mechanism. It seems no argument against the hydrolysis route, for the second route we adopt GTF's supposition as it is an oxygen atom transfer reaction.

One product of the $BrMABrO_2$ hydrolysis, bromotartronic acid (BrTA), is an unstable compound decomposing to Br^- and mesoxalic acid (MOA)[24]. As discussed in Chapter 3.2 mesoxalic acid can be rapidly oxidized to $COOH^{\bullet}$ and oxalic acid by Ce^{4+}. The

negative feedback loop is strengthened by the subsequent reaction of $COOH^{\bullet}$ radicals, generating $MA^{\bullet}$ and Br^{-} through the reduction of BrMA (see Chapter 3.2.5).

$MA^{\bullet}$ radicals have been found to react with $BrO_2^{\bullet}$ at a very high rate[6], the primary product, malonyl bromite decomposes in two different paths[13] leading to tartronic acid and mesoxalic acid. TA can be oxidized to MOA by Ce^{4+} [13] and by bromate (see Chapter 3.2.6). Moreover, the reaction of $MA^{\bullet}$ radicals with acidic bromate has been detected by ESR spectroscopy[6, 11], the products were assumed to be tartronic acid and $BrO_2^{\bullet}$ [6, 13].

It was previously assumed that organic radicals disproportionate rather than recombine[13]. However, the identification of ethanetetracarboxylic acid (ETA, a recombination product of two alkyl malonyl radicals)[42] and malonyl malonate (MAMA, a recombination product of an alkyl and a carboxylato malonyl radicals)[55] as the products of the Ce^{4+}-malonic acid reaction supply a strong basis for radical recombination. Later on Oslonovitch et al.[43], identified bromoethenetricarboxylic acid (BrEETRA), CO_2 and Br^{-} as the products of the Ce^{4+}-bromomalonic acid reaction indicating that bromomalonyl radicals disappear also in a recombination path. Thus it is reasonable to believe that all organic radicals recombine rather than disproportionate.

As for the mechanism of recombination of radicals, Oslonovitch et al.[43] proposed two slightly different mechanisms for explaining the formation of BrEETRA, but they had no basis to prefer one or the other as both of them had problems. The first proposal is: two alkyl bromomalonyl radicals recombine to form dibromo-1,1,2,2-ethanetetracarboxylic acid (Br_2ETA). Br_2ETA decarboxylates to give 1,2-dibromoethanetricarboxylic acid (Br_2ETRA), and Br_2ETRA loses HBr to give rise to the end product BrEETRA. The problem of this mechanism is that an unusually fast decarboxylation of Br_2ETA, which is much faster than that of the other polycarboxylic acid, must be assumed. The second proposal is that, before the recombination, one of the bromomalonyl radicals decarboxylates first. The resulting alkybromoacetyl radical recombines with a bromomalonyl radical to form Br_2ETRA, Br_2ETRA next loses HBr as in the first mechanism. The problem with this proposal is that no self-recombination products of the assumed alkybromoacetyl radical has been found.

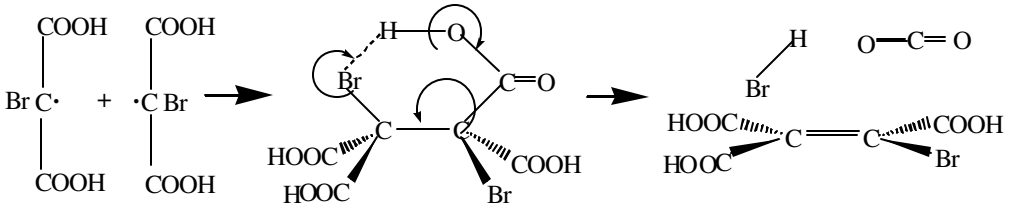

Figure 3-52: Suggested route for the formation of bromoethenetricarboxylic acid (BrEETRA) from alkyl bromomalonyl radicals.

We prefer an intramolecular hydrogen abstraction and decarboxylation mechanism: two alkyl bromomalonyl radicals recombine to form Br_2ETA as in the first mechanistic proposal of Oslonovitch et al. The strongly eletronegative substituent -Br abstracts an electropositive alcoholic -H configuring a hexacyclic ring, then Br_2ETA decarboxylates and loses HBr simultaneously to give the end product BrEETRA. This path is shown in Figure 3-52. This way both problems of Oslonovitch et al's proposal are resolved: decarboxylation accompanied by HBr abstraction could be unusually fast; BrEETRA is surely the only recombination product.

The intermediates formed from $BrMA^{\bullet}/TTA^{\bullet}$ and $TTA^{\bullet}/TTA^{\bullet}$ may decarboxylate in a similar way as Br_2ETA because –Br or –OH are strongly eletronegative substituents.

The bromination of malonic acid, bromomalonic acid and tartronic acid by bromine and hypobromous acid was proved to occur all via the enol form of the acid, and the reaction products are brominated species[45].

Based on the aforementioned theory, 39 elementary reactions (Table 3-18) are assumed to be involved in the organic chemistry of a BZ system starting with BrMA.

Table 3-18: The organic subset of the expanded GF mechanism model.

				k_+/($M^{-1}s^{-1}$)	k_-/($M^{-1}s^{-1}$)	Ref.
R_8	BrMA + Ce^{4+}	⇌	Ce^{3+} + $BrMA^{\bullet}$ + H^+	0.1	400 M^{-1}	a
R_9	2 $BrMA^{\bullet}$	→	Br^- + BrEETRA+ CO_2	1×10^9	0	24[b]
R_{10}	BrTA	→	Br^- + MOA	1.5 M	0	24
R_{11}	BrMA	⇌	BrMAE	1.2×10^{-2} M	800 M	45
R_{12}	BrMAE + Br_2	→	Br_2MA + Br^-	3.5×10^6	0	45
R_{13}	BrMAE + HOBr	→	Br_2MA + H_2O	1.1×10^6	0	45
R_{14}	$BrMA^{\bullet}$ + $BrO_2^{\bullet}$	→	$BrMABrO_2$	2×10^9	0	24[b]
R_{15}	$BrMABrO_2$ + H_2O	→	BrTA + $HBrO_2$	0.46 M	0	24
R_{16}	$BrMABrO_2$	→	Br^- + OA + HOBr + CO_2 + H^+	0.62 M	0	24,13
R_{17}	$BrO_2^{\bullet}$	→	½ Br_2 + O_2	0.06 M	0	a
R_{18}	OA + Ce^{4+}	→	Ce^{3+}+CO_2+$COOH^{\bullet}$ + H^+	28	0	a
R_{19}	$COOH^{\bullet}$ + Ce^{4+}	→	Ce^{3+} + CO_2 + H^+	1.0×10^7	0	13
R_{20}	MOA + Ce^{4+}	→	Ce^{3+}+OA+$COOH^{\bullet}$ + H^+	7.0×10^3	0	a
R_{21}	$COOH^{\bullet}$ + BrMA	→	Br^- + $MA^{\bullet}$ + CO_2 + H^+	1×10^7	0	13, a
R_{22}	TA + BrO_3^- + H^+	→	MOA + $HBrO_2$	5×10^{-5} M^{-1}	0	a
R_{23}	$COOH^{\bullet}$ + $BrMA^{\bullet}$	→	BrMA + CO_2	3×10^9	0	13[b]
R_{24}	$COOH^{\bullet}$ + $MA^{\bullet}$	→	MA + CO_2	4×10^9	0	13[b]
R_{25}	$COOH^{\bullet}$ + $BrO_2^{\bullet}$	→	$HBrO_2$ + CO_2	5×10^9	0	13
R_{26}	2 $COOH^{\bullet}$	→	OA	5×10^9	0	13[b]
R_{27}	2 $MA^{\bullet}$	→	ETA	3.2×10^9	0	54
R_{28}	$MA^{\bullet}$ + $BrO_2^{\bullet}$	→	MA-BrO_2	5×10^9	0	6
R_{29}	$MA^{\bullet}$ + $BrMA^{\bullet}$	→	EETA + Br^- + H^+	2×10^9	0	13[b]
R_{30}	$MA^{\bullet}$ + BrO_3^- + H^+	→	TA + $BrO_2^{\bullet}$	160 M^{-1}	0	6[b]
R_{31}	MA-BrO_2	→	MOA + HOBr	0.55 M	0	13[b]
R_{32}	MA-BrO_2	→	TA + $HBrO_2$	1 M	0	13
R_{33}	TA + Ce^{4+}	⇌	$TA^{\bullet}$ + Ce^{3+} + H^+	0.66	1.7×10^4 M^{-1}	13
R_{34}	2 $TA^{\bullet}$	→	EEHTRA + CO_2 + H_2O	1×10^9	0	13[b]
R_{35}	$TA^{\bullet}$ + $BrMA^{\bullet}$	→	BrEETRA + CO_2 + H_2O	1×10^9	0	13[b]
R_{36}	$TA^{\bullet}$ + $MA^{\bullet}$	→	EETA + H_2O	3×10^9	0	13[b]
R_{37}	$TA^{\bullet}$ + $COOH^{\bullet}$	→	TA + CO_2	3×10^9	0	13[b]
R_{38}	$TA^{\bullet}$ + $BrO_2^{\bullet}$	→	TA-BrO_2	5×10^9	0	13
R_{39}	TA-BrO_2	→	$HBrO_2$ + MOA	1 M	0	13
R_{40}	TA	⇌	TAEnol	0.023 M	1.5 M	45
R_{41}	TAEnol + Br_2	→	BrTA + Br^- + H^+	3×10^5	0	45
R_{42}	TAEnol + HOBr	→	BrTA + H_2O	2×10^5	0	45
R_{43}	MA + Ce^{4+}	⇌	$MA^{\bullet}$ + Ce^{3+} + H^+	0.23	2.1×10^4 M^{-1}	13
R_{44}	MA	⇌	MAEnol	0.0026 M	180 M	45
R_{45}	MAEnol + Br_2	→	BrMA + Br^- + H^+	2.0×10^6	0	45
R_{46}	MAEnol + HOBr	→	BrMA + H_2O	6.7×10^5	0	45

The abbreviations are as follows:

a) This work. b) Adjusted here.

$COOH^{\bullet}$ = carboxyl radical, EEHTRA = ethenehydroxytricarboxylic acid, EETA = ethenetetra-carboxylic acid, ETA = ethanetetracarboxylic acid, MA = malonic acid, $MA^{\bullet}$ = malonyl radical, OA = oxalic acid, TA = tartronic acid, $TA^{\bullet}$ = tartronyl radical.

Selection of Rate Constant Values

The final model consists of 46 elementary reactions and their rate constants. The value and source of each rate constant are given in Table 3-9 (for R_1~R_7) and Table 3-18 (for R_8~R_{46}). It should be pointed out that all rate constants in the inorganic reactions (Table 3-9) are derived from direct measurements and thus have fixed values in the model. However, in the organic subset the rate constants for some reactions are difficult to be measured, and have to be assigned by analogy to similar reactions.

There are five kinds of radicals and thus 15 recombination reactions arise in our new model. Among these reactions only two rate constants are known from direct experiments, namely, the malonyl radical self-recombination (3.2×10^9 $M^{-1}s^{-1}$)[54] and recom-ination with $BrO_2^\bullet$ (5×10^9 $M^{-1}s^{-1}$)[6]. The others were set on the basis of the stability and the spatial obstruction of the radicals involved. For example, the rate constant of the bromomalonyl radical reaction with $BrO_2^\bullet$ was set to 4×10^9 $M^{-1}s^{-1}$ by GF[24], this value seems a little too high as $BrMA^\bullet$ is more stable than $MA^\bullet$, we use a smaller value 2×10^9 $M^{-1}s^{-1}$; 1×10^8 $M^{-1}s^{-1}$[13, 24] for $BrMA^\bullet$ self-recombination seems too low, we use 1×10^9 $M^{-1}s^{-1}$.

For the rate constant of the $MA^\bullet$-bromate reaction 800 $M^{-1}s^{-1}$ was obtained as an upper limit in an ESR spectroscopy experiment[6]; we use a smaller value 160 $M^{-1}s^{-1}$.

The recombination product of $MA^\bullet$ and $BrO_2^\bullet$ radicals, malonyl bromite, was assumed to decompose in two different paths, the probabilities of these two routes were obtained on the basis of fitting experimental data[59]. However, we found that the inhibition is too strong when using the original value, $k_{31} = k_{32} = 1$ $M^{-1}s^{-1}$; decreasing k_{31} to 0.55 $M^{-1}s^{-1}$ fits our experimental induction period of MA systems very well.

Simulations

As for the current and modified GF model, the expanded GF model (R_1~R_7 in Table 3-9 and R_8~R_{46} in Table 3-18) is tested using the BrMA-BrO_3^-- Ce^{4+} system. Figures 3-53, 3-54 and 3-55 show the simulated concentration curves for systems with different initial

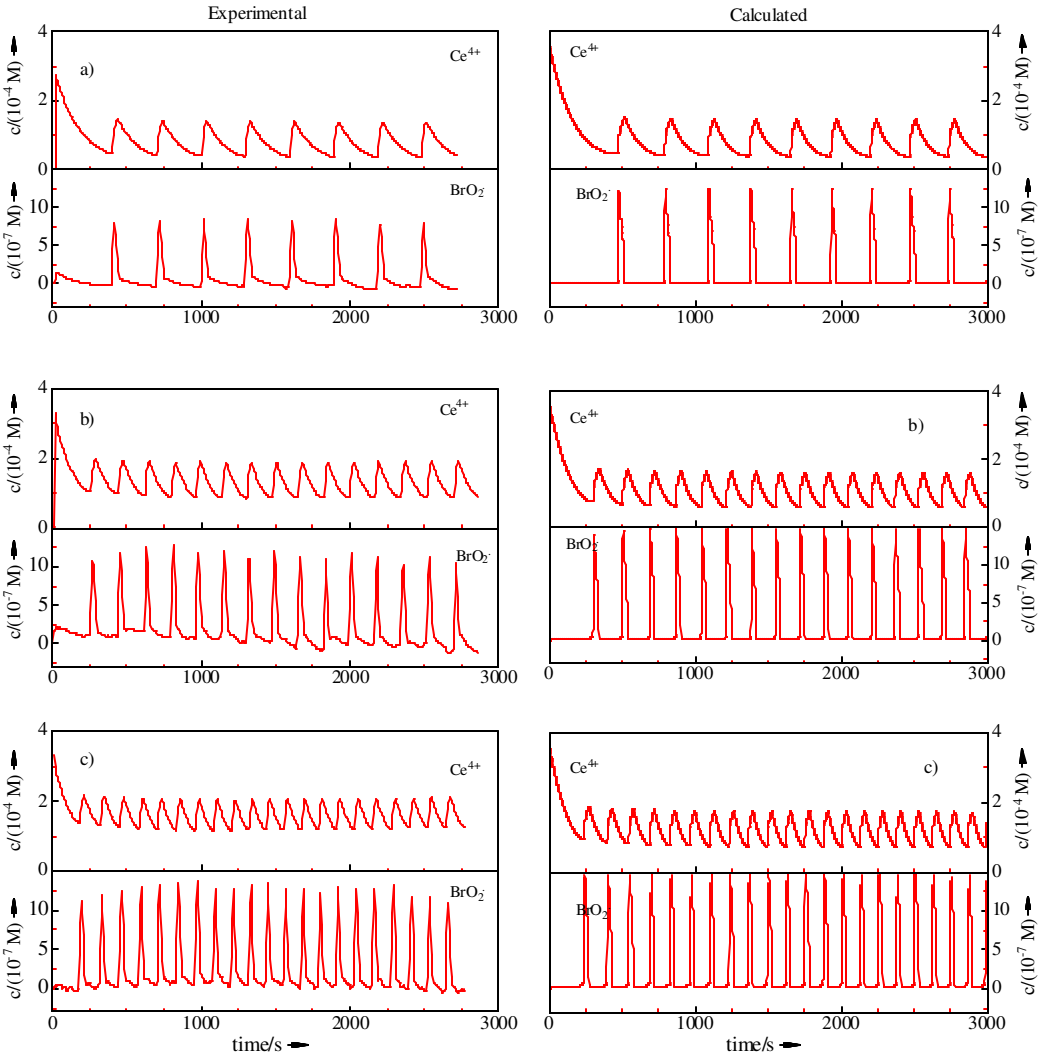

Figure 3-53: Oscillations in the systems with different initial concentrations of bromate - simulations with expanded GF model.

The same experiments as Figure 3-43. The calculated curves are obtained based on reactions R_1~R_{46} and rate constants for R_1~R_7 in Table 3-9, for R_8~R_{46} in Table 3-18. $[BrMA]_0$ = 0.05 M; $[Ce^{4+}]_0 = 3.56\times10^{-4}$ M; $[H^+]$ =1.29 M; $[BrO_3^-]_0$ = 0.10 M (a), 0.15 M (b), 0.20 M (c).

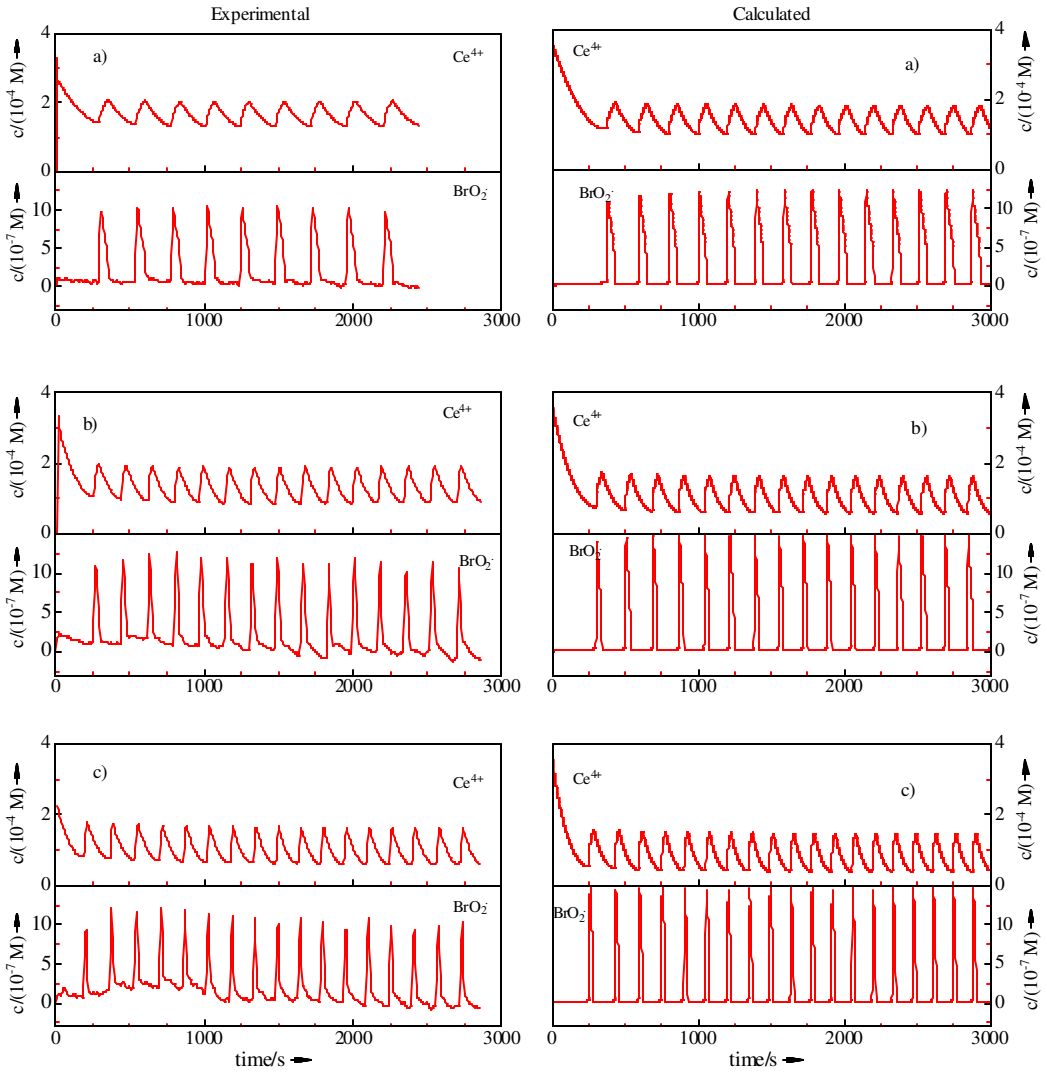

Figure 3-54: Oscillations in the systems with different initial concentrations of bromomalonic acid – simulations with expanded GF model.

The same experiments as Figure 3-44. The calculated curves are obtained as in Figure 3-53. The initial conditions are $[BrO_3^-]_0$ = 0.15 M; $[Ce^{4+}]_0 = 3.56\times 10^{-4}$ M; $[H^+]$ = 1.29 M; $[BrMA]_0$ = 0.025 M (a), 0.05 M (b), 0.08 M (c).

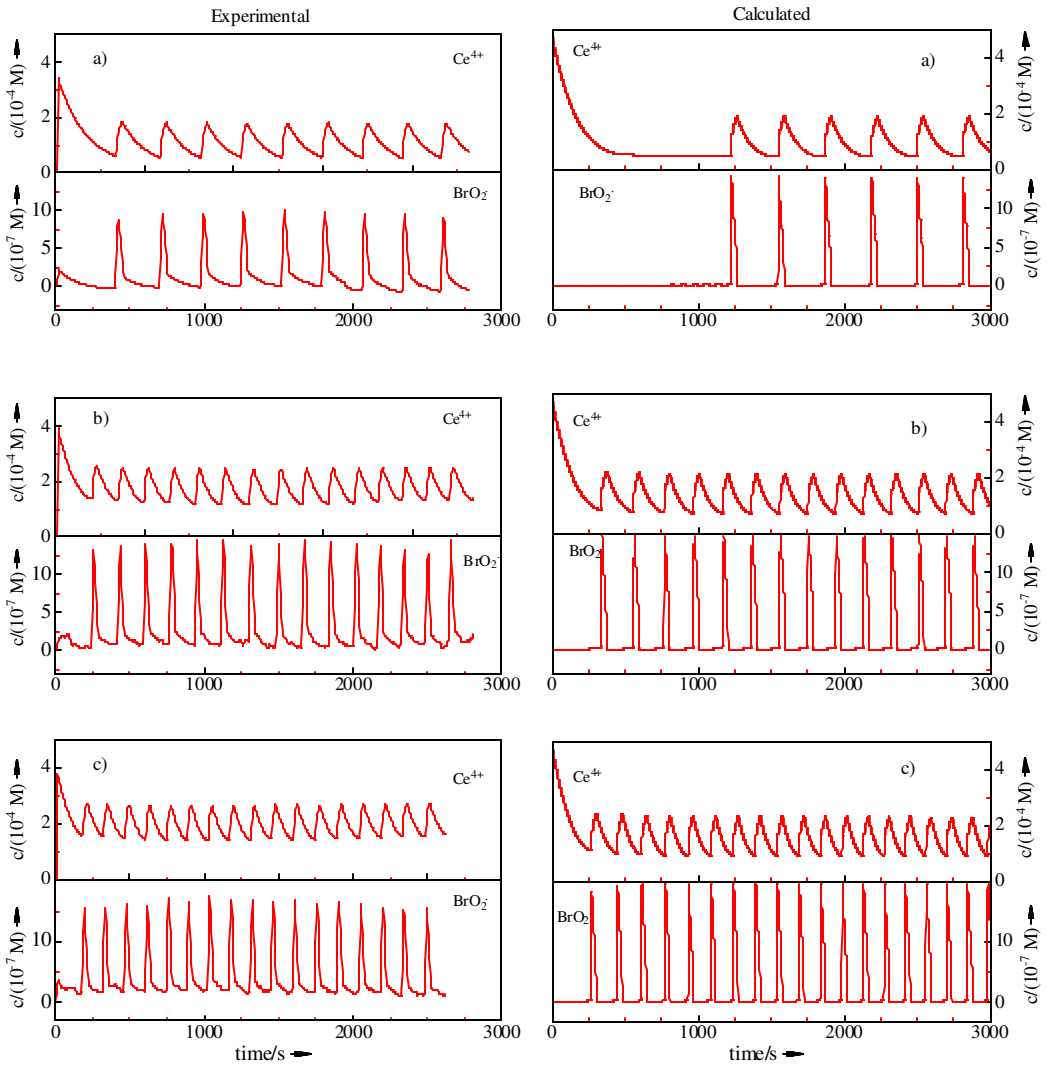

Figure 3-55: Oscillations in higher Ce^{4+} systems with different initial concentrations of bromate – simulations with expanded GF model.

The same experiments as Figure 3-45. The calculated curves are obtained as Figure 3-53. The initial conditions are [BrMA]$_0$ = 0.05 M; $[Ce^{4+}]_0 = 4.7\times 10^{-4}$ M; $[BrO_3^-]_0$ = 0.10 M (a), 0.15 M (b), 0.20 M (c).

concentrations of bromate, bromomalonic acid and Ce^{4+}. It turns out that the ability of the new model to reproduce the observations is significantly improved by extending the mechanism of the organic chemistry. It can be seen in Figures 3-53 and 3-54 that at lower Ce^{4+} concentration (3.56×10^{-4} M) the agreement between theory and experiment is excellent. The peak shape and oscillatory period, which showed problems in the modified model, are just as those observed in the experiments. There is one exception at higher Ce^{4+} concentration (4.7×10^{-4} M, Figure 3-55): in the case of low bromate concentration (0.1 M) the inhibition is too strong in the model such that the oscillations start too late. The reason for this is not clear.

In the classical theory of the BZ reaction it is assumed that bromide ions are exclusively responsible for the inhibition of the autocatalytic reaction. To test this assumption as in the work of Gao et al.[24], we repeated the simulations by setting the rate constant for the $BrMA^{\bullet} - BrO_2^{\bullet}$ reaction, $k_{14} = 0$. It turns out that without the help of bromomalonyl radicals the inhibitor bromide cannot stop the autocatalytic reaction and no oscillations are allowed for all experimental conditions (curves not shown).

3.3.2 The Oscillations with BrMA/MA Mixtures or Pure MA as the Organic Substrate

In this section, we study the oscillatory behavior of the cerium-catalyzed BZ system starting with a mixture of malonic acid and bromomalonic acid or with pure MA. In the previous chapter we have established a new model, which successfully explains the oscillations in a BZ system starting with bromomalonic acid as the only organic substrate; in this case oscillations start immediately after the addition of the catalyst. Now we use this model to simulate BZ systems starting with a mixture of malonic acid and bromomalonic acid or with pure molonic acid. The calculated results are compared with experimental data for selected initial conditions.

We first observe the effect of added MA on the oscillations of the standard case (Fig. 3-43b: 0.15 M BrO_3^-, 3.56×10^{-4} M Ce^{4+} and 0.05 M BrMA) in the experiments. The concentrations of bromate and cerium are kept constant (just as in the standard case), BrMA was replaced by MA stepwise until MA becomes the only organic substrate (in

all cases the total amount of organic substrates is the same, namely $[BrMA]_0 + [MA]_0 = 0.05$ M). The operation procedure, the experiment setup and the evaluation of the data are the same as described in Chapter 3.3.1.

If up to 30% BrMA is replaced by MA there is no essential difference in the oscillatory behavior, only the oscillatory frequency becomes higher. When the content of MA in the organic substrate increases to 50%, an induction period appears (a period with a steady state concentration of Ce^{4+}) indicating that oscillations can only start if additional organic intermediates appear. At the end of the induction period oscillations with stable amplitude start. Above 50% of added MA, the induction period increases with increasing content of MA (e.g. the induction time increases from 50s to 2300s when the MA content increases from 50% to 100%). Another characteristic of the MA system is that the curve for the Ce^{4+} concentration can pass a minimum before reaching the steady state value. In other words, one single oscillation occurs immediately after injecting Ce^{4+} into the reaction mixture. This feature is more pronounced at lower content of MA and disappears at higher MA content. Figure 3-56 a), b) and c) depict, respectively, the experimental oscillations with MA accounts for 30%, 70% and 100% of the total amount of organic substrate.

The simulations of the mixed MA/BrMA oscillations are performed on the basis of the new model (R_1~R_{46}). The calculated results of systems containing 30%, 70% and 100% malonic acid in the organic substrates are displayed in Figure 3-56 a, b and c in comparison with the experiments. We see that the model calculations agree with the experiments. Most of the important features of this system are well modeled, for example, the single oscillation before the induction period for different conditions are in good agreement with the experiments; the length of the induction period in each case is quantitatively predicted. However, the agreement between theory and experiment for the pure malonic acid substrate is not as good as for the bromomalonic acid substrate: the oscillatory period in the model calculations is somewhat longer than in the experiments. That may be due to some consecutive reactions not involved in our model (for example ETA).

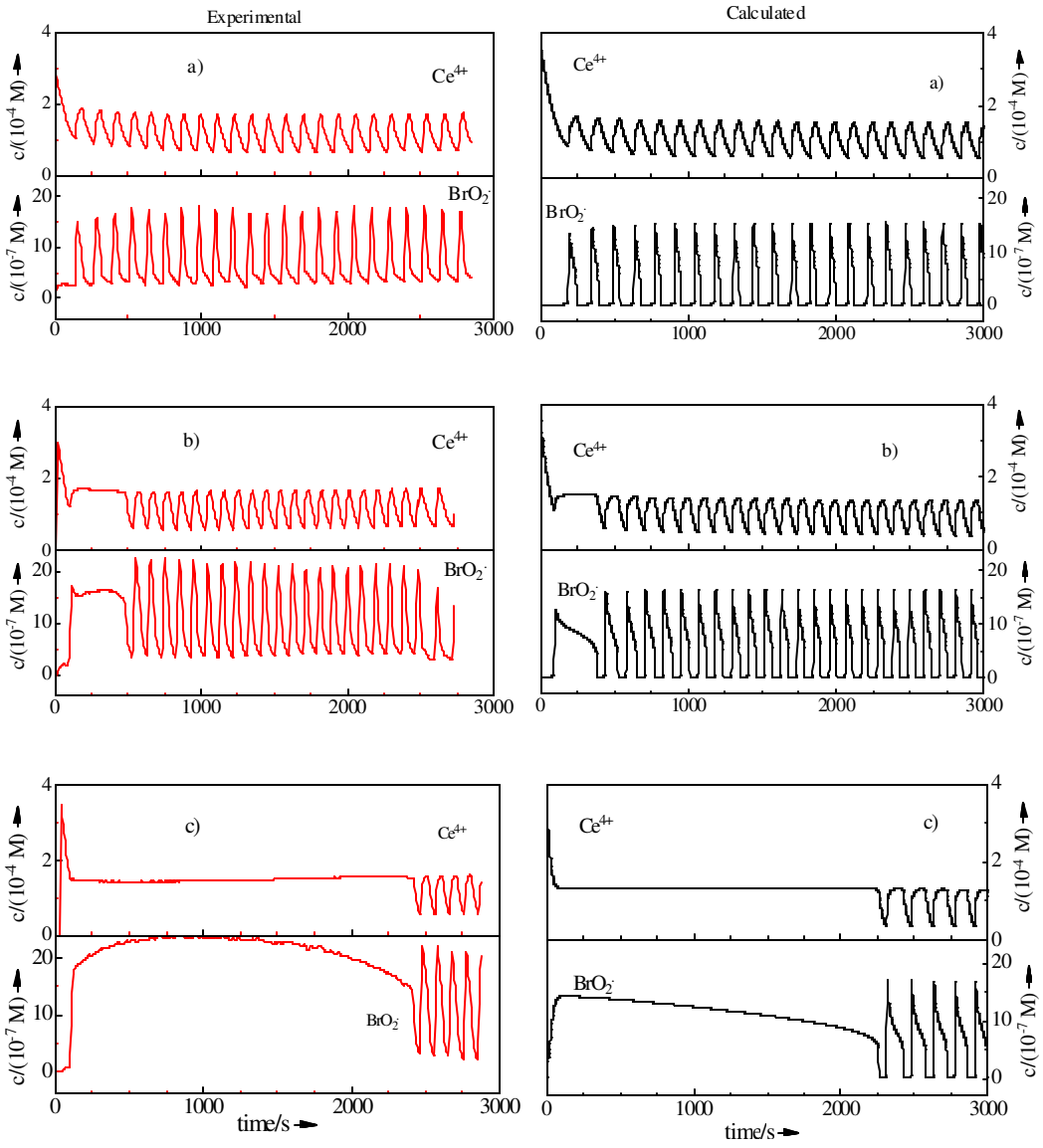

Figure 3-56: The oscillations started with different concentrations of BrMA and MA.

The experiments were performed at 20 °C in 1 M H_2SO_4 with a cell of 25 mL volume and 2.5 cm optical path length. The kinetics was followed by measuring the absorbance change at 401 nm (for Ce^{4+}) and 550 nm (for $BrO_2^{\bullet}$). $[BrO_3^-]_0 = 0.15$ M; $[Ce^{4+}]_0 = 3.56\times10^{-4}$ M; (a) MA 30% ($[BrMA]_0 = 0.035$ M, $[MA]_0 = 0.015$); (b) MA 70% ($[BrMA]_0 = 0.015$ M, $[MA]_0 = 0.035$ M); (c) MA 100% ($[BrMA]_0 = 0$, $[MA]_0 = 0.05$ M).

The calculated curves are obtained by using the entire mechanism R_1~R_{46} and rate constants for R_1~R_7 in Table 3-9, and for R_8~R_{46} in Table 3-18.

3.3.3 Work in Literature

For a further check of the new model work in literature is included.

3.3.3.1 HPLC Measurement

Recently, Hegedüs et al.[46] found by HPLC study that in the classical BZ reactions (malonic acid-bromate-cerium-sulfuric acid) the concentration of oxalic acid grows in the induction period together with that of bromomalonic acid and tartronic acid when the autocatalytic reaction is switched on. They assume two possibilities for the malonyl bromite (formed from $MA^{\bullet}$–$BrO_2^{\bullet}$ reaction) decomposition to explain the accumulation of oxalic acid. One leads to MOA as in R_{31} of our model, the other one leads to oxalic acid and bromide.

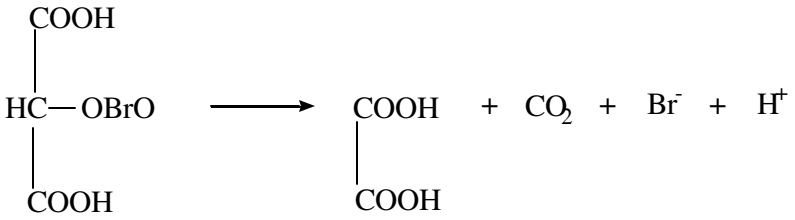

A high catalyst concentration was applied in their experiment, the initial conditions are $[BrO_3^-]_0$ = 0.1 M, $[MA]_0$ = 0.5 M, and $[Ce^{4+}]_0$ = 0.005 M. We simulate this experiment with our new model, Figure 3-57 shows the calculated concentrations of bromomalonic acid, oxalic acid and tartronic acid from the start of the reaction to the end of the induction period. Just as Hegedüs et al.[46] found, the concentrations of all the 3 intermediates grow during the induction period in the model. Especially, the calculated concentration of oxalic acid (2.6×10^{-3} M) at 2 min reaction time agrees with that of the experiment (3.2×10^{-3} M).

The result of our model calculation means that it is not necessary to assume a new route for malonyl bromite decomposition to account for the appearance of oxalic acid. According to our model the oxalic acid is an indirect product of the decomposition of malonyl bromite: in the induction period the BZ system is in its oxidized state, and the autocatalytic reaction is "switched on" establishing a relatively high $BrO_2^{\bullet}$ level. $BrO_2^{\bullet}$

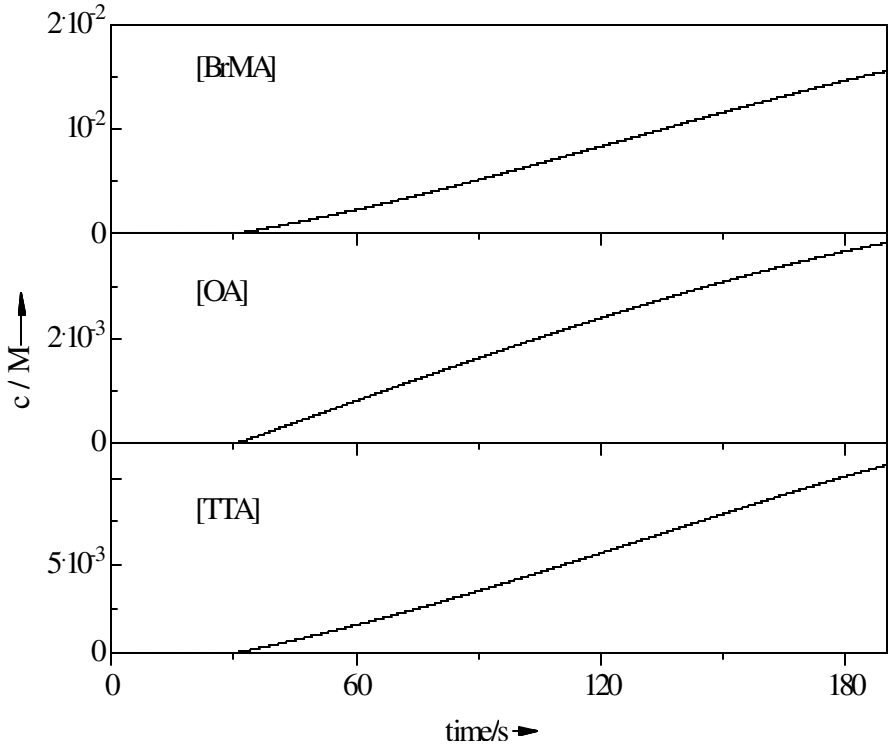

Figure 3-57: Calculated curves of BrMA, OA and TTA concentrations.

The calculated curves were obtained by simulations with the reaction scheme R_1-R_{46} and the corresponding rate constants in Tables 3-9 and 3-18. The initial conditions are $[BrO_3^-]_0$ = 0.1 M, $[MA]_0$ = 0.5 M, and $[Ce^{4+}]_0$= 0.005 M.

radicals react with malonyl radicals in a fast diffusion controlled way (R_{28}) thus the self-recombination route (R_{27}) is suppressed. The generated malonyl bromite decomposes to mesoxalic acid in R_{31}, then Ce^{4+} oxidizes MOA rapidly to oxalic acid and $COOH^{\bullet}$. $COOH^{\bullet}$ self-recombination gives oxalic acid too.

3.3.3.2 Formation of Carbon Dioxide

In the BZ reaction a large amount of the organic substrate is oxidized to carbon dioxide[46, 60]. Thus simulating the rate of CO_2 evolution is also a good test for our new model. Försterling et al.[57] and Noszticzius[58] have intensively measured the rate of

CO_2 evolution in the BZ system, the rate of CO_2 evolution is very small in the beginning of the reaction, and a sharp increase is observed as soon as the autocatalytic reaction starts. This result cannot be understood within the framework of the FKN-theory, which gives a calculated value being smaller by two orders of magnitude than the experimental one[57]. The "Radicalator" model[59] has made some progress by assuming that the primary product of $MA^{\bullet}$-$BrO_2^{\bullet}$ reaction decomposes into glyoxalic acid (GOA), HOBr and CO_2. Provided that their assumption is true, the calculated values are still lower by a factor of 4 compared with the experiments.

We simulate the experiments of Försterling et al.[57], which were monitored by a flame-ionization detector, with our new model. Within this model the rate of CO_2 evolution is given by the following equation involving 11 reactions:

$$\frac{d[CO_2]}{dt} = v_9 + v_{16} + v_{18} + v_{19} + v_{21} + v_{23} + v_{24} + v_{25} + v_{34} + v_{35} + v_{37} \qquad (3.56)$$

where v_i is the reaction rate while i refers to the numbering of reactions in Table 3-18.

Table 3-19: The calculated and measured values for rate of CO_2 formation

The experimental values which are taken from Försterling et al.'s work[57] are valid at the end of the induction period. The calculations are obtained with our new model (R_1-R_{46} and corresponding rate constants in Tables 3-9 and 3-18) and the initial concentrations of bromate, MA and cerium.

No.	$[BrO_3^-]_0$ / M	$[MA]_0$ / M	$[Ce^{4+}]_0$ / $10^{-4}\,M$	$(d[CO_2]/dt) \times 10^6$ M s^{-1}	
				Experiment[57]	Calculation
1	0.1	0.1	1	2.5	2.4
2	0.1	0.1	2	5.3	4.9
3	0.1	0.1	5	11.0	10.1
4	0.1	0.1	10	19.0	19.6
5	0.03	0.1	3.45	2.9	2.7
6	0.3	0.1	1.32	5.0	6.0

Table 3-19 summarizes the details of the experiments and the results of d[CO2]/dt for both theory and experiments[57]. These values are valid at the end of the induction period. It turns out that the values calculated from Equation (3.56) agree very well with those measured in the experiments. They demonstrate that mesoxalic acid and oxalic

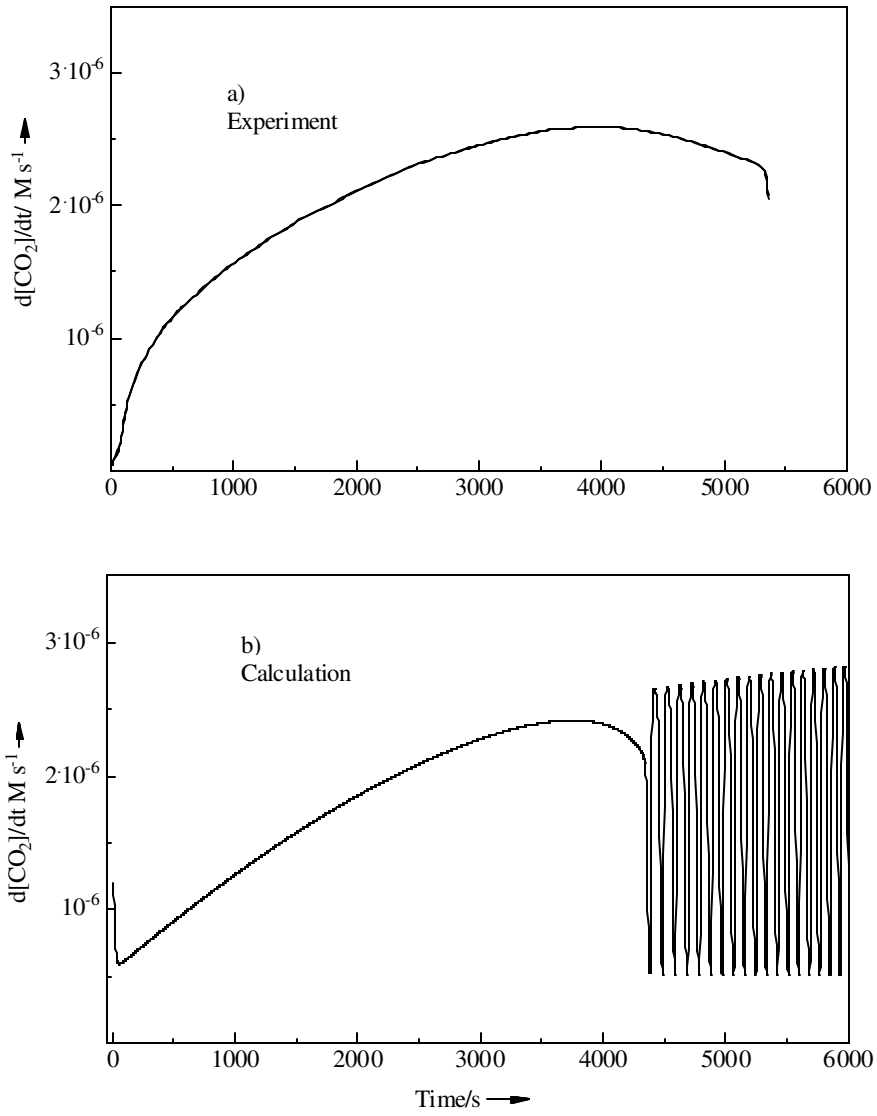

Figure 3-58: Calculation of $d[CO_2]/dt$ as a function of time.

The experiment (due to Försterling et al.[57]) was performed in 1 M H_2SO_4 at 20 °C in the absence of oxygen. CO_2 was followed by bubbling a stream of hydrogen through the solution and measuring the current in a flame ionization detector (FID) after reducing the CO_2 catalytically to CH_4. The initial concentrations are $[BrO_3^-]_0 = 0.1$ M; $[MA]_0 = 0.1$ M; $[Ce^{4+}]_0 = 1 \times 10^{-4}$ M; $[H^+]_0 = 1.29$ M.

The calculated curve is obtained with the complete model (R_1~R_{46} and the corresponding rate constants in Tables 3-9 and 3-18).

acid are the major source of carbon dioxide: 7 out of the 11 reactions involved in the CO_2 evolution are related with OA or $COOH^{\bullet}$; the ratio of these 7 reactions to the total $d[CO_2]/dt$ is 73%.

Moreover, the agreement between theory and experiment can also be seen from the characteristic feature of the diagram. Figure 3-58 depicts the experimental (due to Försterling et al.[57]) and calculated curves of $d[CO_2]/dt$ for conditions 1 in Table 3-19. The calculated overall trend of CO_2 evolution is just as observed in the experiment, the $d[CO_2]/dt$ is strongly increasing after the start of the autocatalytic reaction, and becoming nearly constant at the end of the induction period. Unfortunately, we cannot see the large amplitude of the oscillations in the experiment as the response time of the instrument (flame ionization detector) is too long.

3.3.3.3 Simulated Oscillations in the $[Ru(bipy)_3]^{2+}$ or Ferroin Catalyzed BZ systems

It is well known that there are differences in the behavior of oscillators using various catalysts[22, 52]. While the cerium catalyzed oscillations with various organic substrates could be simulated it would be a good test for our model to simulate systems catalyzed by other catalysts. The experiments due to Gao[22] for ruthenium-catalyzed, and due to Oslonovitch[52] for ferroin-catalyzed oscillations are ideal for testing our model as they are started with bromomalonic acid and carried out under N_2 atmosphere.

$[Ru(bipy)_3]^{2+}$/ bromomalonic acid/bromate BZ system has been intensively studied by Gao[22], Figure 3-59 displays one set of their experiments for $[BrMA]_0$ = 0.0089 M, $[Ru^{2+}]_0 = 5\times 10^{-5}$ M, and $[BrO_3^-]_0$ = 0.18 M a) 0.089 M b) 0.041 M c) in 0.91 M sulfuric acid at 20 °C (Figure 3-24 in reference 22). In that case, the absorbance was measured at 450 nm (for Ru^{2+}) and simultaneously the potential *U* of a AgBr electrode was followed (for Br^- and HOBr). Gao found that with decreasing bromate concentration the oscillatory period increases and the inhibition effect on the autocatalytic process becomes larger.

The difference of the oscillatory behavior between ruthenium-catalyzed and cerium-catalyzed systems are dramatic: the autocatalytic process proceeds to a profound level (low Ru^{2+} concentration) before it is inhibited in the ruthenium-catalyzed system, and switches on again after all Ru^{3+} is reduced to Ru^{2+}. Thus, most of the time the system remains in the reduced state and the oscillatory amplitudes are very large. This oscillatory behavior has been explained by GF with the aforementioned GF model.

We modified our new model by replacing the Ce^{4+}/Ce^{3+} reactions in Table 3-18 with those of Ru^{3+}/Ru^{2+} for the case of ruthenium as a catalyst. Table 3-20 gives the modified reactions and the corresponding rate constants. What must be mentioned is that the rate constants for reactions R_6, R_8, R_{18} and R_{20} are drawn from direct experiments, for R_{19}, R_{33} and R_{43} the values of cerium reactions are used as no experimental result available. This will not introduce big errors because neither MA nor TA are important in the bromomalonic acid system.

The simulations were performed with the modified reaction scheme R_1~R_{46} to calculate the concentrations of Ru^{2+}, Br^-, and HOBr; from the Br^- and HOBr concentrations the change ΔU of the electrode potential was calculated as described in Chapter 3.1.5. The calculated concentration change of Ru^{2+} and the potential change of the electrode are shown in Figure 3-59. It turns out that the new model is also capable to generate oscillations in BZ system with ruthenium as the catalyst but that the agreement between theory and experiment is not as good as in the cerium system: the oscillatory period in the model calculations is longer than that in the experiments.

Table 3-20: Chemical reactions and corresponding rate constants for the Ru^{3+}/Ru^{2+} system.

	Modified reactions			$k_+/(M^{-1}s^{-1})$	$k_-/(M^{-1}s^{-1})$	Ref.
R_6	$Ru^{2+} + BrO_2^{\bullet} + H^+$	$\rightleftharpoons$	$Ru^{3+} + HBrO_2$	$4.0\times10^6\ M^{-1}$	0	[24]
R_8	$BrMA + Ru^{3+}$	$\rightleftharpoons$	$Ru^{2+} + BrMA^{\bullet} + H^+$	55	$1.3\times10^5\ M^{-1}$	[24]
R_{18}	$OA + Ru^{3+}$	$\rightarrow$	$Ru^{2+}+CO_2+COOH^{\bullet} + H^+$	20		a
R_{19}	$COOH^{\bullet} + Ru^{3+}$	$\rightarrow$	$Ru^{2+}+ CO_2 + H^+$	1.0×10^7		[2]
R_{20}	$MOA + Ru^{3+}$	$\rightarrow$	$Ru^{2+}+OA+COOH^{\bullet} + H^+$	2.8×10^3		a
R_{33}	$TA + Ru^{3+}$	$\rightleftharpoons$	$TA^{\bullet} + Ru^{2+} + H^+$	0.66	$1.7\times10^4\ M^{-1}$	[2]
R_{43}	$MA + Ru^{3+}$	$\rightleftharpoons$	$MA^{\bullet} + Ru^{2+} + H^+$	0.23	$2.1\times10^4 M^{-1}$	[2]

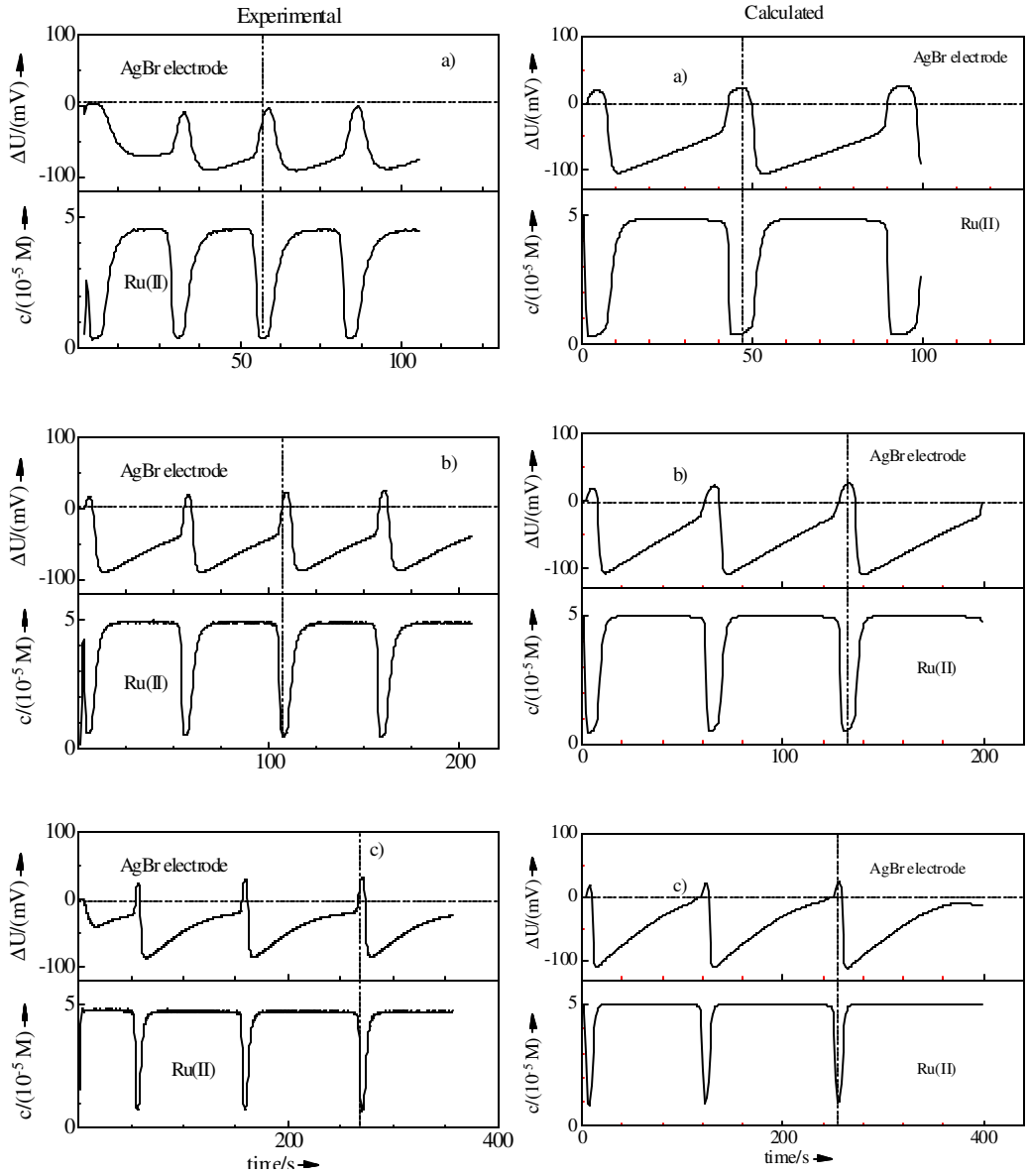

Figure 3-59: Ruthenium catalyzed oscillations in systems started with different initial concentration of bromate in 0.91 M H_2SO_4.

The experiments are taken from Gao's work, which were performed at 20 °C with a 15 mL volume cell (optical pathlength 1.9 cm). Oxygen was excluded with bubbling N_2. The kinetics was followed by measuring the absorbance change at 450 nm and the potential change of a bromide-selective electrode simultaneously. $[BrMA]_0$ = 0.0089 M, $[Ru^{2+}]_0 = 5\times 10^{-5}$ M, and $[BrO_3^-]_0$ = 0.18 M a) 0.089 M b) 0.041 M c).

The calculated curves are obtained with our new model (R_1~R_{46}) after modification of the catalyst reactions (see Table 3-20).

Ferroin/ bromomalonic acid/bromate BZ system. Besides the presence of the organic ligands which can take part in the mechanism, the ferroin catalyst differs from cerium also in the redox potential:

Ce^{4+}	$+ e$	$\rightarrow$	Ce^{3+}	1.41 V
$Fe(phen)_3^{3+}$	$+ e$	$\rightarrow$	$Fe(phen)^{2+}$	1.056 V

The low redox potential of the ferroin/ferriin pair shifts the equilibrium of the elementary steps in the oscillatory reaction towards the oxidized form of the catalyst, so the mechanism is more complex than for the cerium-system and ruthenium-system: not only $BrO_2^{\bullet}$ but also $HBrO_2$, HOBr, Br_2 , and BrO_3^- can oxidize Fe^{2+} to Fe^{3+}. The modifications to our model are listed in Table 3-21.

Oslonovitch[52] discovered that under identical experimental conditions the oscillatory behavior of the ferroin system is different from the cerium system as well as from the ruthenium system. Figure 3-60 shows two experiments of Oslonovitch for $[BrO_3^-]_0$ = 0.09 M, $[Fe(phen)_3^{2+}]_0 = 7\times 10^{-5}$ M, and $[BrMA]_0$ = 0.02 M (a) and 0.09 M (b) in 0.94 M sulfuric acid at 20 °C. The catalyst tends to stay in the oxidized state, the oscillatory amplitude of the $Fe(phen)_3^{2+}$ concentration is very small and strongly depends on the initial concentration of bromomalonic acid.

The simulations were performed on the basis of reaction scheme R_1~R_{51} after modifying the catalyst related reactions as shown in Table 3-21. It should be pointed out that the rate constants of some reactions (k_{18}, k_{19}, k_{33} and k_{43}) are not available and have to be assigned by analogy to the corresponding cerium reactions. A much smaller value, k_{20} = 70 $M^{-1}s^{-1}$ is set for the ferriin-MOA reaction as MOA can be detected only in the ferroin catalysed BZ system indicating that the ferriin-MOA reaction is much slower than the Ce^{4+}-MOA. Special in this system are the reactions of ferroin with bromine and hypobromous acid (R_{49} and R_{50}). The mechanism of these two reactions are[52]:

Fe^{2+}	$+ Br_2$	$\rightleftharpoons$	$Fe^{3+} +$	$Br_2^{-\bullet}$				
$Br_2^{-\bullet}$		$\rightleftharpoons$	$Br^- +$	$Br^{\bullet}$	$Fe^{2+} + HOBr + H^+$	$\rightarrow$	$Fe^{3+} + Br^{\bullet} + H_2O$	
$Fe^{2+} + Br^{\bullet}$		$\rightleftharpoons$	$Fe^{3+} +$	Br^-	$2\ Br^-$	$\rightarrow$	Br_2	
$2\ Fe^{2+}$	$+ Br_2$	$\rightleftharpoons$	$2\ Fe^{3+} + 2\ Br^-$		$2\ Fe^{2+} + 2\ HOBr + 2\ H^+$	$\rightarrow$	$2Fe^{3+} + Br_2 + 2H_2O$	

To avoid too many variables being introduced into the model, only the overall reactions are used. The calculated results are shown in Figure 3-60, in comparison with the experiments. We found that the new model can predict the most important features of this system but the inhibition of the autocatalytic reaction in the model is less than in the experiments. The concentrations of $Fe(phen)_3^{2+}$ reach zero before the autocatalytic reaction is inhibited. The cause of this discrepancy may be more the uncertainty of ferroin related rate constants than the overall mechanism. For example, different values of the rate constant k_8 for the ferriin-BrMA reaction are reported, this constant seriously effects the level of the reduction of the catalyst. The value 0.1 $M^{-1}s^{-1}$ reported by Oslonovitch is too small to generate enough bromide to inhibit the autocatalytic reaction while the value 11.3 $M^{-1}s^{-1}$ reported by Jwo et al.[61] seems to be too large (dashed line in Fig. 3-60a). To fit the experimental amplitude a medium value 2 $M^{-1}s^{-1}$ (between Oslonovitch's and Jwo et al.'s reports) is used in our simulations (solid line in Fig. 3-60a).

Table 3-21: Chemical reactions and corresponding rate constants for Fe^{3+}/Fe^{2+}system

				$k_+/(M^{-1}s^{-1})$	$k_-/(M^{-1}s^{-1})$	Ref.
R_6	$Fe^{2+} + BrO_2^{\bullet} + H^+$	$\rightleftharpoons$	$Fe^{3+} + HBrO_2$	$5.0\times10^7\ M^{-1}$	0	[52]
R_8	$BrMA + Fe^{3+}$	$\rightleftharpoons$	$Fe^{2+} + BrMA^{\bullet} + H^+$	2	0	a
R_{18}	$OA + Fe^{3+}$	$\rightarrow$	$Fe^{2+} + CO_2 + COOH^{\bullet} + H^+$	28	0	a
R_{19}	$COOH^{\bullet} + Fe^{3+}$	$\rightarrow$	$Fe^{2+} + CO_2 + H^+$	1.0×10^7	0	[13]
R_{20}	$MOA + Fe^{3+}$	$\rightarrow$	$Fe^{2+} + OA + COOH^{\bullet} + H^+$	70	0	a
R_{33}	$TA + Fe^{3+}$	$\rightleftharpoons$	$TA^{\bullet} + Fe^{2+} + H^+$	0.66	$1.7\times10^4 M^{-1}$	[13]
R_{43}	$MA + Fe^{3+}$	$\rightleftharpoons$	$MA^{\bullet} + Fe^{2+} + H^+$	0.23	$2.1\times10^4 M^{-1}$	[13]
R_{47}	$Fe^{2+} + HBrO_2 + H^+$	$\rightarrow$	$Fe^{3+} + BrO^{\bullet} + H_2O$	$550\ M^{-1}$	0	[52]
R_{48}	$Fe^{2+} + BrO^{\bullet} + H^+$	$\rightarrow$	$Fe^{3+} + HOBr$	$1\times10^8 M^{-1}$	*0*	[52]
R_{49}	$2\ Fe^{2+} + Br_2$	$\rightleftharpoons$	$2Fe^{3+} + 2\ Br^-$	2.5	$0.23\ M^{-1}$	[52]
R_{50}	$2\ Fe^{2+} + 2\ HOBr + 2H^+$	$\rightarrow$	$Fe^{3+} + Br_2 + H_2O$	$3\ M^{-4}$	0	[52]
R_{51}	$Fe^{2+} + BrO_3^- + 2H^+$	$\rightarrow$	$Fe^{3+} + BrO_2^{\bullet}$	$0.02\ M^{-2}$	0	[52]

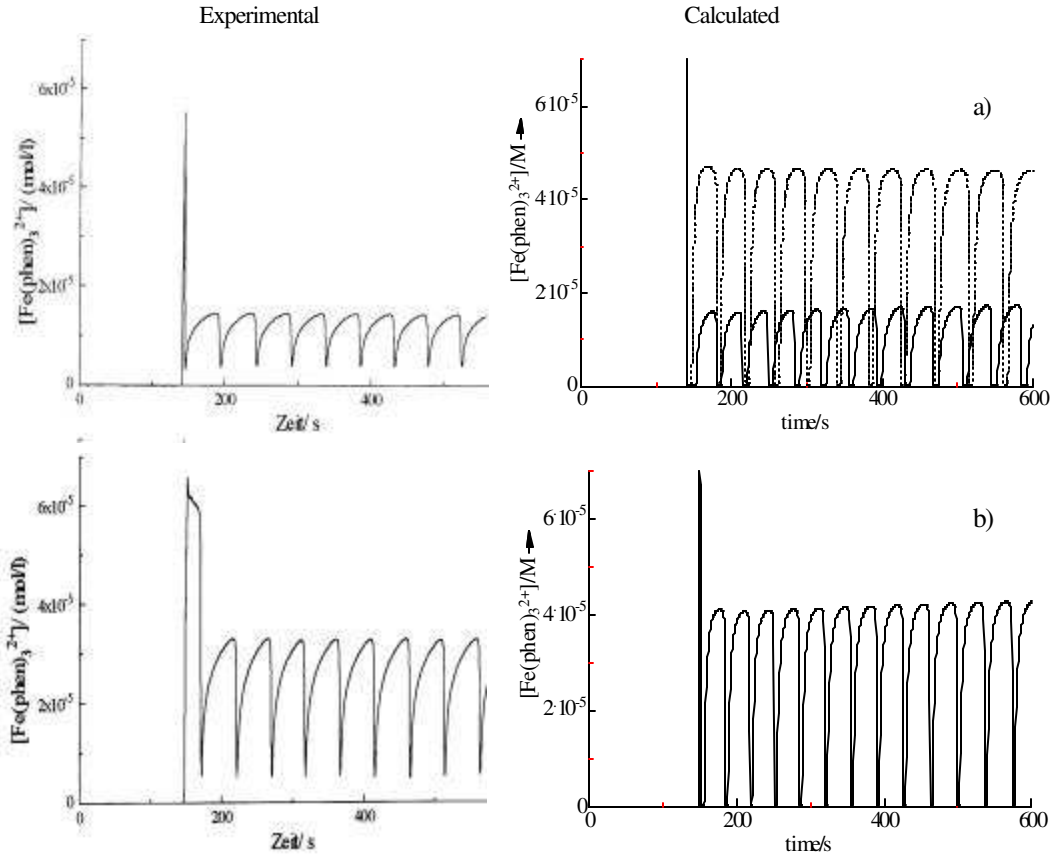

Figure 3-60: Ferroin catalyzed oscillations – experiments and simulations.

The experiments (taken from Oslonovitch's work) were performed at 20 °C with a 15 mL volume cell (optical pathlength 1.9 cm). Oxygen was excluded with bubbling N_2. The kinetics was followed by measuring the absorbance change at 516 nm. $[BrO_3^-]_0$ = 0.09 M, $[Fe^{2+}]_0$ = 7×10^{-5} M, and $[BrMA]_0$ = 0.02 M a) 0.09 M b). $[H_2SO_4]$ = 0.94 M.

The calculated curves are obtained with our new model (R_1~R_{46}) after modification for the catalyst reactions (see Table 3-21).

Chapter 4

Preparation and Purification of Chemicals

4.1 Preparation of Bromomalonic Acid

Potassium salt of bromomalonic acid (K_2BrMA) used in the experiments was prepared according to the method reported by Försterling and Stuk [14, 16].

10.2 g of malonic acid (Fluka pa.) was dissolved in 200 mL of diethylether. 5 mL of Br_2 was dissolved in 30 mL of CCl_4. The flask containing the MA/ether solution was placed in an ice bath with magnetic stirring, and the Br_2/CCl_4 solution was added dropwise. The ratio of Br_2 and MA was 1:1. At the end of the reaction, the solvent was evaporated by a vacuum line, with the flask still in the ice bath.

The yellowish product was dissolved in about 10 mL of double distilled water, followed by filtration. The filtrate was added to a saturated solution of 30 g potassium acetate in 500 mL of ethanol. The white precipitate of K_2BrMA formed immediately and was separated from the ethanol by filtration.

The product was further purified by dissolving it in 100 mL of distilled water and precipitating with 500 mL of ethanol, followed by filtration. This procedure was repeated three times in order to remove most of the bromide impurity from the product. The end product was dried in a vacuum desiccator at room temperature, and kept in a refrigerator.

The purity of the product was checked by HPLC and UV-VIS spectroscopy. The absorption spectrum of BrMA in 0.01 M H_2SO_4 (Figure 4-1) is in good agreement with the result reported in literature[57]. Bromide (retention time 480 s), dibromomalonic acid

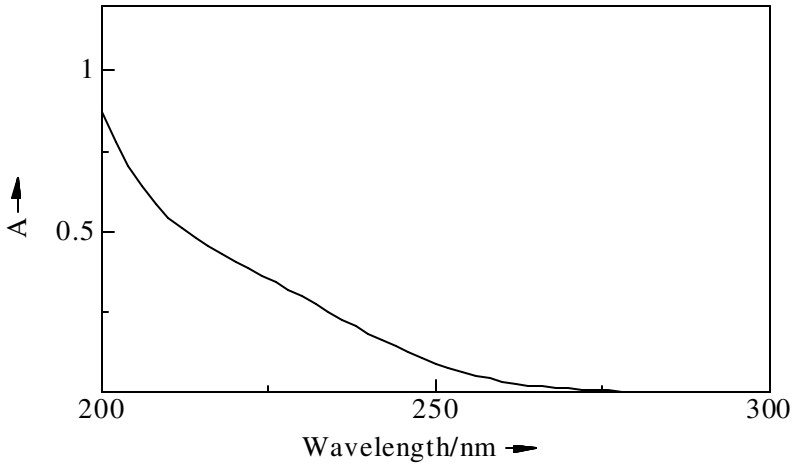

Figure 4-1: The spectrum of bromomalonic acid in 0.01 M H_2SO_4.

Bromomalonic acid prepared with the Försterlingand Stuk method[14, 16]. [BrMA] = 6.9×10^{-4} M. A diode array spectrophotometer with a cell of 1 cm optical path length was used.

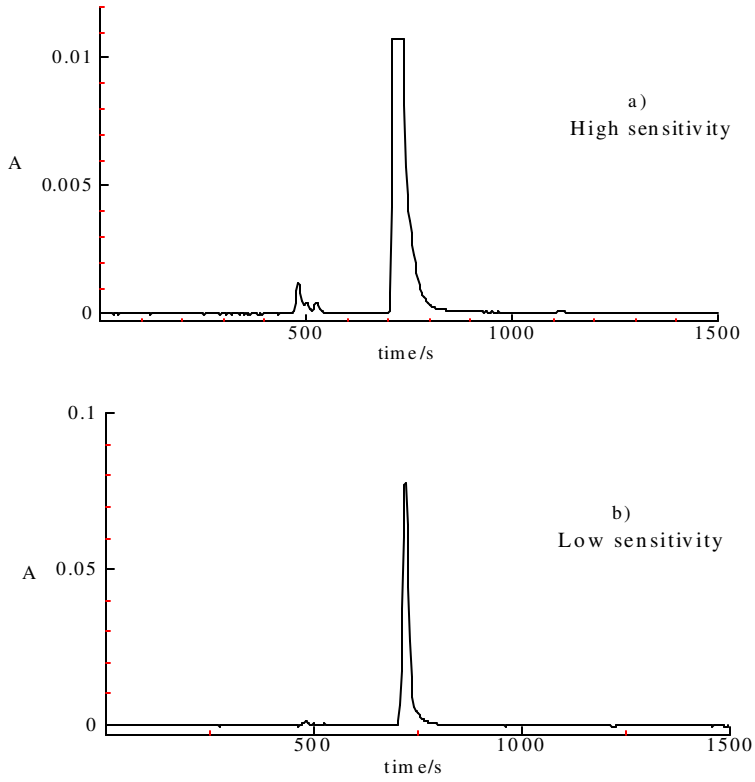

Figure 4-2: The chromatograms of bromomalonic acid in 0.01 M H_2SO_4.

HPLC-chromatograms taken with Shimadzu instrument (UV detector working at 220 nm). Injection volume 20µL; flow rate 0.40 mL / min; temperature 45 °C; the eluent is 0.01 M H_2SO_4. $[BrMA]_0 = 6.9\times 10^{-4}$ M.

(retention time 500 s) and dibromoacetic acid (retention time 1120 s) were found as trace contaminations by HPLC (see Figure 4-2). Dibromomalonic acid and dibromoacetic acid cannot interfere our experiments because their amounts are less than 0.5% and their reactions with Ce^{4+} are negligible. The bromide impurity was calculated from the height of the injection peak (around 0.5% ~ 2.5% for different preparations).

We found that if the product stays longer (for more than 1 day) at room temperature or the desiccator used to dry the product is not close enough tartronic acid appears. Thus, we carried out kinetic measurements for each preparation, only those reducing Ce^{4+} with a rate constant of 0.1 $M^{-1}s^{-1}$ are to be used in our experiments. Moreover, bromomalonic acid can decompose slowly in aqueous solution giving tartronic acid, so we always use freshly prepared BrMA solution.

4.2 Purification of Tartronic Acid

Since the commercial available tartronic acid contains a large amount of impurities which may affect the kinetic measurements, the following procedure was carried out to purify it before use:

20 g of the solid was mixed with 200 mL of acetic acid ethylester at room temperature; the mixture was stirred with a magnetic stirrer for 4 hours, followed by filtration. The residue was washed three times with a small amount of ester and dried at room temperature in a vacuum desiccator overnight. We repeated the procedure several times.

4.3 Preparation of Hypobromous Acid

Hypobromous acid was prepared from sodium bromate in strong acidic medium according to the methods reported by Noszticzius et al.[17].

2 mL of a 1 M aqueous $NaBrO_3$ was added dropwise to a continuously stirred mixture of 3 mL of water and 5 mL of concentrated H_2SO_4 (96% W/W) at −10 °C. The mixture

was warmed up slowly to 40 °C, when the vigorous oxygen evolution ceased, the reaction mixture was diluted to 50 mL with distilled water. Br_2 was removed by bubbling nitrogen. The solution was analyzed by taking an UV-spectrum which is comparable to that reported in literature[29].

It should be mentioned that HOBr is an unstable compound slowly decomposing to bromine. Thus the yellowish-solution of HOBr was kept in a refrigerator and traces of bromine were removed by bubbling nitrogen through the solution before use. The concentration was calculated from the absorbance using the extinction coefficient $\varepsilon = 90\ M^{-1}cm^{-1}$ at 263 nm[23].

Chapter 5

Summary

The Belousov-Zhabotinsky reaction is a class of oscillatory, metal-ion-catalyzed oxidations of organic compounds by bromate ion. The malonic acid-bromate-cerium reaction is the most thoroughly studied reaction[62], its mechanism was elucidated by Györgyi, Turányi, and Field[13] in 1990 (referred as GTF model) by collecting 80 possible reactions. However, this powerful model failed to predict any oscillation in the cerium catalyzed BZ system starting with BrMA.

Later on Gao and Försterling explained their observations in a BZ system with ruthenium as a catalyst and bromomalonic acid as an organic substrate[22] (referred as GF model). But this model does not work in an analogous system with cerium as the catalyst. For this reason we reinvestigated the cerium catalyzed BZ system.

We first focus on the inorganic subset. The set of inorganic reactions is mainly that reported by Field and Försterling[21]. Modifications were made in reactions R_4, R_5, the mechanism of the disproportionation of bromous acid[19].

$Br^- + HOBr + H^+$	$\rightleftharpoons$	$Br_2 + H_2O$	R_1
$Br^- + HBrO_2 + H^+$	$\rightleftharpoons$	$2\,HOBr$	R_2
$Br^- + BrO_3^- + 2\,H^+$	$\rightleftharpoons$	$HOBr + HBrO_2$	R_3
$HBrO_2 + H^+$	$\rightleftharpoons$	$H_2BrO_2^+$	R_{4a}
$HBrO_2 + H_2BrO_2^+$	$\rightleftharpoons$	$HOBr + BrO_3^- + 2\,H^+$	R_{4b}
$HBrO_2 + BrO_3^- + H^+$	$\rightleftharpoons$	$Br_2O_4 + H_2O$	R_{5a}
Br_2O_4	$\rightleftharpoons$	$2\,BrO_2^\bullet$	R_{5b}
$Ce^{3+} + BrO_2^\bullet + H^+$	$\rightleftharpoons$	$Ce^{4+} + HBrO_2$	R_6
$2\,BrO_3^- + 2\,H^+$	$\rightarrow$	$2HBrO_2 + 2\,O_2$	R_7

A new decomposition path of $BrO_2^{\bullet}$, R_{17}, was discovered in this work. The mechanism of this is

$BrOO^{\bullet}$	$\rightarrow$	$Br^{\bullet} + O_2$	R_{17a}
$Br^{\bullet} + Br^{\bullet}$	$\rightarrow$	Br_2	R_{17b}
$Br^{\bullet} + BrOO^{\bullet}$	$\rightarrow$	$Br_2 + O_2$	R_{17c}
$BrO_2^{\bullet}$	$\rightarrow$	$\frac{1}{2} Br_2 + O_2$	R_{17}

Although this dissociation reaction proceeds too slow to be important for the kinetics of the oscillatory reaction, it verifies the result of quantum mechanical calculations[35, 36] that the mesomeric configuration of bromine dioxide, $BrOO^{\bullet}$, is more stable than $OBrO^{\bullet}$, thus providing a base for understanding the decomposition mechanism of the organic radical- $BrO_2^{\bullet}$ recombination products.

The most recent values of the rate constants for reactions R_1~R_7 are used, small corrections on k_2 and k_{-6} are applied. A decisive change was made on rate constant k_3, the reaction of bromide with bromate. So far it was believed from direct measurements that k_3 is 1.2 $M^{-1}s^{-1}$ at 20 °C. However, these experiments were carried out with initial concentrations of bromide much higher than the typical range in a BZ system. We reinvestigated this reaction using initial concentration of bromide c_0 down to 2×10^{-6} M. Surprisingly we found that k_3 depends on c_0, slowing down from k_3 = 1.4 $M^{1}s^{-1}$ at c_0 = 2×10^{-4} M to k_3 = 0.5 $M^{-1}s^{-1}$ at c_0 = 2×10^{-6} M. That means R_3 is not an elementary reaction, but follows a complex kinetics.

Using the results obtained in this work for k_3 two severe discrepancies found in earlier kinetic research could be resolved. First, the lower k_3 can quantitatively account for the induction time in the bromide inhibited autocatalytic Ce^{3+}-bromate reaction (k_3 = 1.2 $M^{-1}s^{-1}$ gives a value too low by a factor of 2). Second, the lower k_3 can quantitatively account for the rate of disappearance of bromine in the presence of acidic bromate (k_3 = 1.2 $M^{-1}s^{-1}$ leads to a decay of bromine too fast by a factor of 3).

We measured the overall autocatalytic reaction at different initial concentrations of bromate or bromide. The model calculation involving R_1~R_7 and R_{17} and the revised set of rate constants are in excellent agreement with the experiments.

We investigated the oxidation of bromomabnic acid, mesoxalic acid and oxalic acid by Ce^{4+}.

$$BrMA + Ce^{4+} \rightleftharpoons Ce^{3+} + BrMA^{\bullet} + H^{+} \qquad R_8$$

$$2\,BrMA^{\bullet} \rightarrow Br^{-} + BrEETRA + CO_2 \qquad R_9$$

$$OA + Ce^{4+} \rightarrow Ce^{3+} + CO_2 + COOH^{\bullet} + H^{+} \qquad R_{18}$$

$$COOH^{\bullet} + Ce^{4+} \rightarrow Ce^{3+} + CO_2 + H^{+} \qquad R_{19}$$

$$MOA + Ce^{4+} \rightarrow Ce^{3+} + OA + COOH^{\bullet} + H^{+} \qquad R_{20}$$

Some interesting facts are that oxygen can suppress R_8, in contrast to the reaction of malonic acid with Ce^{4+}; the mesoxalic acid (MOA), which has been treated as an end product in the GF model, can be rapidly oxidized by Ce^{4+} leading to carboxyl radicals and oxalic acid. k_{20} (7×10^3 $M^{-1}s^{-1}$) is the highest rate constant found for reactions of Ce^{4+} with organic intermediates, therefore it cannot be omitted in the BZ reaction; the oxidation of oxalic acid by Ce^{4+} is also rather fast ($k_{18} = 28$ $M^{-1}s^{-1}$).

A key reaction is reaction R_{21}:

$$COOH^{\bullet} + BrMA \rightarrow Br^{-} + MA^{\bullet} + CO_2 + H^{+} \qquad R_{21}$$

We could verify this reaction by oxidizing a mixture of oxalic acid and bromomalonic acid by Ce^{4+}. All the expected reaction products could be detected by HPLC.

Another important reaction is the generation of $HBrO_2$ by tartronic acid and bromate. It was verified by following $BrO_2^{\bullet}$ as an intermediate.

$$TA + BrO_3^{-} + H^{+} \rightarrow MOA + HBrO_2 \qquad R_{22}$$

In the presence of bromine and hypobromous acid, bromomalonic acid, tartronic acid and malonic acid, are brominated through the enolized pathway[45]:

$$BrMA \rightleftharpoons BrMAE \qquad R_{11}$$

$$BrMAE + Br_2 \rightarrow Br_2MA + Br^{-} \qquad R_{12}$$

$$BrMAE + HOBr \rightarrow Br_2MA + H_2O \qquad R_{13}$$

TA	$\rightleftharpoons$	TAEnol	R_{40}
TAEnol + Br_2	$\rightarrow$	BrTA + Br^- + H^+	R_{41}
TAEnol + HOBr	$\rightarrow$	BrTA + H_2O	R_{42}
MA	$\rightleftharpoons$	MAEnol	R_{44}
MAEnol + Br_2	$\rightarrow$	BrMA + Br^- + H^+	R_{45}
MAEnol + HOBr	$\rightarrow$	BrMA + H_2O	R_{46}

Radicals in the system disappear in a recombination path. The recombination products BrMA-TTA, TTA-TTA and MA-BrMA are assumed to decompose via an intramolecular hydrogen abstraction and decarboxylation mechanism, because –Br or –OH are strongly eletronegative substituents; BrMA-BrO_2, TTA-BrO_2 and MA-BrO_2 are assumed to undergo hydrolysis or oxygen transfer reactions.

$BrMA^\bullet$ + $BrO_2^\bullet$	$\rightarrow$	$BrMABrO_2$	R_{14}
$BrMABrO_2$ + H_2O	$\rightarrow$	BrTA + $HBrO_2$	R_{15}
$BrMABrO_2$	$\rightarrow$	Br^- + OA + HOBr + CO_2 + H^+	R_{16}
$COOH^\bullet$ + $BrMA^\bullet$	$\rightarrow$	BrMA + CO_2	R_{23}
$COOH^\bullet$ + $MA^\bullet$	$\rightarrow$	MA + CO_2	R_{24}
$COOH^\bullet$ + $BrO_2^\bullet$	$\rightarrow$	$HBrO_2$ + CO_2	R_{25}
2 $COOH^\bullet$	$\rightarrow$	OA	R_{26}
2 $MA^\bullet$	$\rightarrow$	ETA	R_{27}
$MA^\bullet$ + $BrO_2^\bullet$	$\rightarrow$	MA-BrO_2	R_{28}
$MA^\bullet$ + $BrMA^\bullet$	$\rightarrow$	EETA + Br^- + H^+	R_{29}
$MA^\bullet$ + BrO_3^- + H^+	$\rightarrow$	TA + $BrO_2^\bullet$	R_{30}
MA-BrO_2	$\rightarrow$	MOA + HOBr	R_{31}
MA-BrO_2	$\rightarrow$	TA + $HBrO_2$	R_{32}
TA + Ce^{4+}	$\rightleftharpoons$	$TA^\bullet$ + Ce^{3+} + H^+	R_{33}
2 $TA^\bullet$	$\rightarrow$	EEHTRA + CO_2 + H_2O	R_{34}
$TA^\bullet$ + $BrMA^\bullet$	$\rightarrow$	BrEETRA + CO_2 + H_2O	R_{35}
$TA^\bullet$ + $MA^\bullet$	$\rightarrow$	EETA + H_2O	R_{36}
$TA^\bullet$ + $COOH^\bullet$	$\rightarrow$	TA + CO_2	R_{37}

$$TA^{\bullet} + BrO_2^{\bullet} \rightarrow TA\text{-}BrO_2 \qquad R_{38}$$

$$TA\text{-}BrO_2 \rightarrow HBrO_2 + MOA \qquad R_{39}$$

$$MA + Ce^{4+} \rightleftharpoons MA^{\bullet} + Ce^{3+} + H^{+} \qquad R_{43}$$

Thus a new model including 46 elementary reactions was established for a BZ system with cerium as the catalyst and bromomalonic acid as the organic substrate. Two negative feedback loops are involved: the removal of $HBrO_2$ by bromide and the removal of $BrO_2^{\bullet}$ by organic radicals. With this model the observed oscillations in the Ce^{4+}- bromomalonic acid-bromate system are quantitatively reproduced.

Then, we applied this new model on systems starting with a mixture of BrMA and MA or pure MA. An important feature of this system is the appearance of the induction period. The length of the induction time increases with the content of MA. We have shown that the new model works also very well in these systems. Most important oscillatory features are well modeled, for example, the induction period.

The new model is also tested in the classic BZ system (MA-cerium-bromate) by comparing the CO_2 formation and the accumulation of oxalic acid, tartronic acid and bromomalonic acid. The model calculations agree well with the experiments. According to our model, mesoxalic acid and oxalic acid are the main sources of CO_2 in the classical BZ system.

Finally, we tested this model on BZ systems containing other catalysts: the ruthenium system which has been modeled by Gao and Försterling with a very simple model[24]; the ferroin system which has not yet been explained. Modifications were made by replacing reactions of Ce^{3+}/Ce^{4+} with those of Ru^{2+}/Ru^{3+} or Fe^{2+}/Fe^{3+}. For the ferroin system it is more complicated because Fe^{2+} can react with other oxybromine species:

$$Fe^{2+} + HBrO_2 + H^{+} \rightarrow Fe^{3+} + BrO^{\bullet} + H_2O$$

$$Fe^{2+} + BrO^{\bullet} + H^{+} \rightarrow Fe^{3+} + HOBr$$

$$2\,Fe^{2+} + Br_2 \rightleftharpoons 2Fe^{3+} + 2\,Br^{-}$$

$$2\,Fe^{2+} + 2\,HOBr + 2H^{+} \rightarrow Fe^{3+} + Br_2 + H_2O$$

$$Fe^{2+} + BrO_3^{-} + 2H^{+} \rightarrow Fe^{3+} + BrO_2^{\bullet}$$

It turns out that the new model can also reproduce the oscillations in ruthenium or ferroin catalyzed BZ system with BrMA as organic substrate.

Our results demonstrate that the GF model fails to predict oscillations in a cerium-bromomalonic acid BZ system because the negative feedback is underestimated and the consecutive reactions of mesoxalic acid are omitted.

Chapter 5

Zusammenfassung

Bei der Belousov-Zhabotinsky-Reaktion handelt es sich um die oszillatorisch ablaufende Oxidation organischer Substrate durch Bromationen, welche durch Metallionen katalysiert wird. Insbesondere die Malonsäure-Bromat-Cer-Reaktion ist intensiv untersucht worden[62]. Ein Mechanismus für diese Reaktion wurde 1990 durch Györgyi, Turányi, and Field[13] vorgeschlagen (GTF Modell); darin haben die Autoren 80 mögliche Reaktionen angenommen. Es zeigte sich aber, dass dieses umfangreiche Modell nicht in der Lage war, Oszillationen im Falle von Brommalonsäure als alleinigem Substrat vorauszusagen.

Später stellten Gao und Försterling ein Modell auf, mit dem die experimentellen Beobachtungen über ein BZ-System mit Ruthenium als Katalysator und Brommalonsäure als organischem Substrat gut beschrieben werden konnten[22] (GF-Modell). Dieses Modell war aber nicht dazu geeignet, die Oszillationen im analogen Cer-katalysierten System zu beschreiben. Deshalb wird in dieser Arbeit die Cer-katalysierte BZ-Reaktion erneut untersucht.

Zunächst betrachten wir die anorganischen Teilreaktionen. Zugrundegelegt wurde ein Satz von Reaktionen, wie er von Field und Försterling beschrieben wurde[21]. Modifiziert wurden die Reaktionen R_4 und R_5 Mechanismus der Disproportionierung von bromiger Säure [19]).

$$Br^- + HOBr + H^+ \rightleftharpoons Br_2 + H_2O \qquad R_1$$

$$Br^- + HBrO_2 + H^+ \rightleftharpoons 2\,HOBr \qquad R_2$$

$$Br^- + BrO_3^- + 2\,H^+ \rightleftharpoons HOBr + HBrO_2 \qquad R_3$$

$$HBrO_2 + H^+ \rightleftharpoons H_2BrO_2^+ \qquad R_{4a}$$

$$HBrO_2 + H_2BrO_2^+ \rightleftharpoons HOBr + BrO_3^- + 2\,H^+ \qquad R_{4b}$$

$$HBrO_2 + BrO_3^- + H^+ \rightleftharpoons Br_2O_4 + H_2O \qquad R_{5a}$$

$$Br_2O_4 \rightleftharpoons 2\,BrO_2^{\bullet} \qquad R_{5b}$$

$$Ce^{3+} + BrO_2^{\bullet} + H^+ \rightleftharpoons Ce^{4+} + HBrO_2 \qquad R_6$$

$$2\,BrO_3^- + 2\,H^+ \rightarrow 2HBrO_2 + 2\,O_2 \qquad R_7$$

In dieser Arbeit wurde ein neuer Reaktionsweg für die Zersetzung von $BrO_2^{\bullet}$, (Reaktion R_{17}) entdeckt. Der Mechanismus dieser Reaktion ist

$$BrOO^{\bullet} \rightarrow Br^{\bullet} + O_2 \qquad R_{17a}$$

$$Br^{\bullet} + Br^{\bullet} \rightarrow Br_2 \qquad R_{17b}$$

$$Br^{\bullet} + BrOO^{\bullet} \rightarrow Br_2 + O_2 \qquad R_{17c}$$

$$BrO_2^{\bullet} \rightarrow \tfrac{1}{2}Br_2 + O_2 \qquad R_{17}$$

Obwohl diese Reaktion zu langsam verläuft, um für die Kinetik der oszillierenden Reaktion wichtig zu sein, stellt sie doch eine experimentelle Bestätigung einer quantenmechanischen Voraussage[35, 36] über die Stabilität von Bromdioxid dar: die Konfiguration $BrOO^{\bullet}$ ist stabiler als die Konfiguration $OBrO^{\bullet}$; damit ergibt sich eine Grundlage für ein Verständnis des Zersetzungsmechanismus bei Verbindungen, die durch Rekombination aus einem organischen Radikal und $BrO_2^{\bullet}$ gebildet werden.

Für die Geschwindigkeitskonstanten der Reaktionen R_1~R_7 wurden die neuesten Werte verwendet, kleine Korrekturen wurden an k_2 and k_{-6} angebracht. Eine entscheidende Änderung betrifft die Geschwindigkeitskonstante k_3 (Reaktion von Bromid mit Bromat). Bisher legte man anhand von direkten Messungen den Wert $k_3 = 1.2\ M^{-1}s^{-1}$ bei 20 °C zugrunde. Diese Experimente wurden jedoch mit Anfangskonzentrationen an Bromid durchgeführt, die viel größer waren als die Konzentrationen, die typischerweise im BZ-System vorliegen. Wir haben diese Reaktion neu untersucht, und zwar bei kleinen Bromidkonzentrationen bis hinab zu $c_0 = 2\times10^{-6}$ M. Überraschenderweise fanden wir, dass k_3 von c_0 abhängt: von $k_3 = 1.4\ M^{-1}s^{-1}$ bei $c_0 = 2\times10^{-4}$ M verringert es sich auf $k_3 = 0.5\ M^{-1}s^{-1}$ bei $c_0 = 2\times10^{-6}$ M. Dies bedeutet, dass R_3 keinesfalls eine elementare Reaktion ist, sondern dass es sich um eine sehr komplexe Kinetik handelt.

Mit unserem neuen Wert für k_3 konnten zwei Diskrepanzen aufgeklärt werden, die in früheren Untersuchungen aufgetreten sind. Erstens kann unter Verwendung des kleineren Wertes von k_3 die Induktionszeit in der Bromid-inhibierten autokatalytischen Ce^{3+}-Bromat-Reaktion quantitativ wiedergegeben werden (der Wert $k_3 = 1.2\ M^{-1}s^{-1}$

führt zu einer Induktionszeit, die um den Faktor 2 zu klein ist). Zweitens kann damit die Geschwindigkeit der Reaktion von Brom mit Bromat quantitativ beschrieben werden (der Wert k_3 = 1.2 $M^{-1}s^{-1}$ führt zu einem Zerfallsgeschwindigkeit, die um den Faktor 3 zu groß ist).

Die autokatalytische Reaktion wurde für verschiedene Anfangskonzentrationen an Bromat und Bromid experimentell verfolgt. Die Modellrechnungen mit den Reaktionen R_1~R_7 and R_{17} und den revidierten Geschwindigkeitskonstanten sind in ausgezeichneter Übereinstimmung mit den Experimenten.

Wir haben die Oxidation von Brommalonsäure, Mesoxalsäure und Oxalsäure durch Ce^{4+} untersucht.

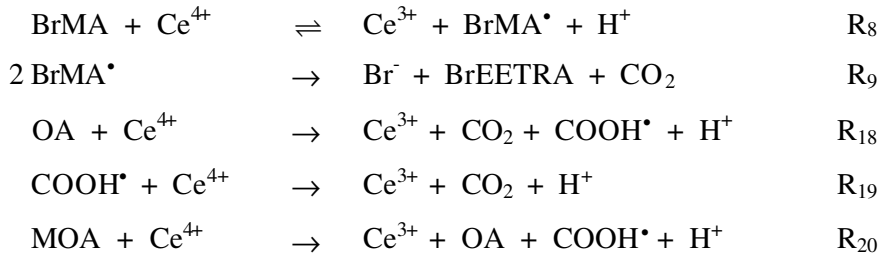

$BrMA + Ce^{4+}$	$\rightleftharpoons$	$Ce^{3+} + BrMA^{\bullet} + H^+$	R_8
$2\,BrMA^{\bullet}$	$\rightarrow$	$Br^- + BrEETRA + CO_2$	R_9
$OA + Ce^{4+}$	$\rightarrow$	$Ce^{3+} + CO_2 + COOH^{\bullet} + H^+$	R_{18}
$COOH^{\bullet} + Ce^{4+}$	$\rightarrow$	$Ce^{3+} + CO_2 + H^+$	R_{19}
$MOA + Ce^{4+}$	$\rightarrow$	$Ce^{3+} + OA + COOH^{\bullet} + H^+$	R_{20}

Es ist interessant, dass Sauerstoff R_8 verlangsamen kann, im Gegensatz zur Reaktion von Malonsäure mit Ce^{4+}; Mesoxalsäure (MOA), die im GFT-Modell als inertes Endprodukt betrachtet wird, kann durch Ce^{4+} sehr schnell zum Carboxylradikal und zur Oxalsäure oxidiert werden. k_{20} (7×10^3 $M^{-1}s^{-1}$) ist die größte Geschwindigkeitskonstante, die wir bei der Oxidation von Ce^{4+} mit organischen Säuren gefunden haben, deshalb darf diese Reaktion in einem Modell der BZ-Reaktion nicht weggelassen werden; die Oxidation von Oxalsäure durch Ce^{4+} läuft ebenfalls sehr schnell ab (k_{18} = 28 $M^{-1}s^{-1}$).

Eine Schlüsselrolle nimmt Reaktion R_{21}: ein:

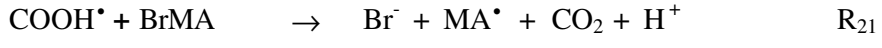

$COOH^{\bullet} + BrMA$	$\rightarrow$	$Br^- + MA^{\bullet} + CO_2 + H^+$	R_{21}

Wir konnten diese Reaktion verfolgen, indem wir eine Mischung von Oxalsäure und Brommalonsäure mit Ce^{4+} oxidierten. Alle erwarteten Reaktionsprodukte konnten im HPLC-Spektrum nachgewiesen werden.

Eine weitere wichtige Reaktion ist die Erzeugung von $HBrO_2$ aus Tartronsäure und Bromat. Dies Reaktion wurde verfolgt, indem das Zwischenprodukt $BrO_2^{\bullet}$ spektroskopisch gemessen wurde.

$$TA + BrO_3^- + H^+ \rightarrow MOA + HBrO_2 \qquad R_{22}$$

In der Gegenwart von Brom und hypobromiger Säure werden Brommalonsäure, Tartronsäure und Malonsäure auf dem Weg über die Enolformen bromiert[45]:

$$BrMA \rightleftharpoons BrMAE \qquad R_{11}$$
$$BrMAE + Br_2 \rightarrow Br_2MA + Br^- \qquad R_{12}$$
$$BrMAE + HOBr \rightarrow Br_2MA + H_2O \qquad R_{13}$$
$$TA \rightleftharpoons TAEnol \qquad R_{40}$$
$$TAEnol + Br_2 \rightarrow BrTA + Br^- + H^+ \qquad R_{41}$$
$$TAEnol + HOBr \rightarrow BrTA + H_2O \qquad R_{42}$$
$$MA \rightleftharpoons MAEnol \qquad R_{44}$$
$$MAEnol + Br_2 \rightarrow BrMA + Br^- + H^+ \qquad R_{45}$$
$$MAEnol + HOBr \rightarrow BrMA + H_2O \qquad R_{46}$$

In dem BZ-System verschwinden Radikale durch Rekombinationsreaktionen. Wir gehen davon aus, dass die Rekombinationsprodukte BrMA-TTA, TTA-TTA and MA-BrMA über intramoleculare Wasserstoff-Abstraktion and Decarboxylierung zerfallen, da –Br or –OH stark elektronegative Substituenten sind; wir nehmen weiter an, dass BrMA-BrO_2, TTA-BrO_2 and MA-BrO_2 über Hydrolyse oder Sauerstoff-Übertrageng reagieren.

$$BrMA^{\bullet} + BrO_2^{\bullet} \rightarrow BrMABrO_2 \qquad R_{14}$$
$$BrMABrO_2 + H_2O \rightarrow BrTA + HBrO_2 \qquad R_{15}$$
$$BrMABrO_2 \rightarrow Br^- + OA + HOBr + CO_2 + H^+ \qquad R_{16}$$

$COOH^{\bullet} + BrMA^{\bullet}$	$\rightarrow$	$BrMA + CO_2$	R_{23}
$COOH^{\bullet} + MA^{\bullet}$	$\rightarrow$	$MA + CO_2$	R_{24}
$COOH^{\bullet} + BrO_2^{\bullet}$	$\rightarrow$	$HBrO_2 + CO_2$	R_{25}
$2\ COOH^{\bullet}$	$\rightarrow$	OA	R_{26}
$2\ MA^{\bullet}$	$\rightarrow$	ETA	R_{27}
$MA^{\bullet} + BrO_2^{\bullet}$	$\rightarrow$	$MA\text{-}BrO_2$	R_{28}
$MA^{\bullet} + BrMA^{\bullet}$	$\rightarrow$	$EETA + Br^- + H^+$	R_{29}
$MA^{\bullet} + BrO_3^- + H^+$	$\rightarrow$	$TA + BrO_2^{\bullet}$	R_{30}
$MA\text{-}BrO_2$	$\rightarrow$	$MOA + HOBr$	R_{31}
$MA\text{-}BrO_2$	$\rightarrow$	$TA + HBrO_2$	R_{32}
$TA + Ce^{4+}$	$\rightleftharpoons$	$TA^{\bullet} + Ce^{3+} + H^+$	R_{33}
$2\ TA^{\bullet}$	$\rightarrow$	$EEHTRA + CO_2 + H_2O$	R_{34}
$TA^{\bullet} + BrMA^{\bullet}$	$\rightarrow$	$BrEETRA + CO_2 + H_2O$	R_{35}
$TA^{\bullet} + MA^{\bullet}$	$\rightarrow$	$EETA + H_2O$	R_{36}
$TA^{\bullet} + COOH^{\bullet}$	$\rightarrow$	$TA + CO_2$	R_{37}
$TA^{\bullet} + BrO_2^{\bullet}$	$\rightarrow$	$TA\text{-}BrO_2$	R_{38}
$TA\text{-}BrO_2$	$\rightarrow$	$HBrO_2 + MOA$	R_{39}
$MA + Ce^{4+}$	$\rightleftharpoons$	$MA^{\bullet} + Ce^{3+} + H^+$	R_{43}

Auf diese Weise erhalten wir ein neues Modell der BZ-Reaktion mit Cer als Katalysator und Brommalonsäure als organischem Substrat.. Zwei negative Rückkopplungsschleifen sind beteiligt: die Entfernung von $HBrO_2$ durch Bromid einerseits und die Entfernung von $BrO_2^{\bullet}$ durch organische Radikale andererseits. Mit diesem Modell können die beobachteten Oszillationen in dem Ce^{4+}- Bromomalonsäure-Bromate-System quantitative reproduziert werden.

Sodann haben wir dieses neue Modell auf eine Mischung von BrMA und MA sowie auf reine MA angewandt. In diesen Fällen erscheint eine Induktionsperiode vor dem Einsetzen der Oszillationen. Die Länge der Induktionsperiode steigt mit wachsendem Anteil an MA an. Wir zeigen, dass das Modell auch in diesen Fällen gut arbeitet. Die meisten wichtigen Eigenschaften, zum Beispiel die Induktionsperiode, werden gut wiedergegeben.

Das neue Modell wurde im Fall des klassischen BZ-Systems (MA, Cer, Bromat) weiterhin dadurch getestet, dass die Bildung von CO_2 , von Oxalsäure, Tratronsäure und von Brommalonsäure mit dem Experiment verglichen wurde. Die Modellrechnungen stimmen gut mit den Experimenten überein. Nach dem Modell sind die Intermediate Mesoxalsäure, und Oxalsäure die Hauptquellen für CO_2 im klassischen BZ-System.

Schließlich haben wir das Modell in Fällen getested, in denen andere Katalysatoren verwendet werden: das Ruthenium-System, das von Gao and Försterling mit einem sehr einfachen Modell simuliert wurde[24]; das Ferroin-System, bei dem eine gute Simulation bisher noch nicht gelungen ist. In unserem Modell wurden dazu Modifikationen eingeführt, in denen die spezifischen Reaktionen von Ce^{3+}/Ce^{4+} durch solche von Ru^{2+}/Ru^{3+} oder Fe^{2+}/Fe^{3+}ersetzt wurden. Das Ferroin-System is komplizierter, weil Fe^{2+} direkt mit anderen Oxybrom-Verbindungen reagieren kann:

$$Fe^{2+} + HBrO_2 + H^+ \rightarrow Fe^{3+} + BrO^{\bullet} + H_2O$$
$$Fe^{2+} + BrO^{\bullet} + H^+ \rightarrow Fe^{3+} + HOBr$$
$$2\,Fe^{2+} + Br_2 \rightleftharpoons 2Fe^{3+} + 2\,Br^-$$
$$2\,Fe^{2+} + 2\,HOBr + 2H^+ \rightarrow Fe^{3+} + Br_2 + H_2O$$
$$Fe^{2+} + BrO_3^- + 2H^+ \rightarrow Fe^{3+} + BrO_2^{\bullet}$$

Es zeigt sich, dass unser neues Modell auch die Oszillationen in diesen beiden Systemen (mit Brommalonsäure als Substrat) wiedergeben kann.

Unsere Resultate zeigen, daß das GF-Modell vor allem deshalb nicht zu Oszillationen im Cer-Brommalonsäure-System führt, weil die negative Rückkopplungsschleife unterschätzt wird und außerdem die Folgereaktionen von Mesoxalsäure nicht berücksichtigt werden.

References

[1] Belousov, B. P.; Sbornik Referatov po Radiatsionni Meditsine, Medgiz, Moscow, p. 145.

[2] Belousov, B. P. Khim. Zhizn, 1982, 7, 65.

[3] Lefever, R.; Nicolis, G.; Prigogine, I. *J. Chem. Phys.* 1967, 47, 1045.

[4] Field, R. J.; Körös, E.; Noyes, R. M. *J. Am. Chem. Soc.* 1972, 94,8649

[5] Field, R. J. and Noyes, R. M. *J. Chem. Phys.* 1974, 60,1877.

[6] Försterling, H. D. and Noszticzius, Z. *J. Phys. Chem.* 1989, 93, 2740.

[7] Edelson, D.; Field, R. J.; Noyes, R. M. *Int. J. Chem. Kinet.* 1975, 7, 417.

[8] Blanddamer, M. J.; Roberts, D. L. *J. C. S. Faraday I,* 1977, 73, 1056.

[9] Edelson, D.; Noyes, R. M.; Field, R. J. *Int. J. Chem. Kinet.* 1979, 11, 155.

[10] Noszticzius, Z. *J. Am. Chem. Soc.* 1979, 101, 3660.

[11] Brusa, M. A.; Perissinotti, L. J. and Colussi, A. J. *J. Phys. Chem.* 1985. 89, 1572.

[12] Försterling, H. D. and Noszticzius, Z. *J. Phys. Chem.* 1989, 93, 2740.

[13] Györgyi, L.; Turányi, T. and Field, R. J. *J. Phys. Chem.* 1990, 94, 7162.

[14] Försterling, H. D.; Stuk, L. *J. Chem. Phys*. 1991, 95, 7320.

[15] Försterling, H. D.; Stuk, L. *J. Chem. Phys*. 1992, 96, 3067.

[16] Försterling, H. D.; Stuk, L.; Barr, A.; McCormick, W. D. *J. Chem. Phys*. 1993, 97, 2623.

[17] Noszticzius, Z.; Noszticzius, E.; Schelly, Z. A. *J. Am. Chem.Soc.* 1982, 104, 6194.

[18] Noszticzius, Z.; Noszticzius, E.; Schelly, Z. A. *J. phys. Chem.* 1983, 87, 510.

[19] Försterling, H. D.; Varga, M. *J. Phys. Chem*. 1993, 97, 7932.

[20] Szalai, I.; Oslonovitch, J.; Försterling, H. D. *J. Phys. Chem*. 2000, 104, 1495.

[21] Field, R. J.; Försterling, H. D. *J. phys. Chem.* 1986, 90,5400.

[22] Gao, Y. Ph. D. Thesis, 1994, Philipps-Universität-Marburg/Lahn, FRG.

[23] Försterling, H. D.; Murányi, S.; Schreiber, H. *Z. Naturforschg*. 1989, 44a, 555

[24] Gao, Y. and Försterling, H. D. *J. Phys. Chem*. 1995, 99, 8638.

[25] Försterling, H. D.; Lamberz, H. J.; Schreiber, H. *Z. Naturforschg*. 1985, 40a, 368.

[26] Eigen , M.; Kustin, K. *J. Am. Chem. Soc.* 1962, 84,1355.

[27] Robertson, E. B. and Dunford, H. B. *J. Am. Chem. Soc.* 1964, 86,5080.

[28] Lamberz, H. J. Ph. D. Thesis, 1982, Philipps-Universität-Marburg/Lahn, FRG.

[29] Kshirsagar, G. and Field, R. J. *J. Phys. Chem.* 1988,92,7074.

[30] Kuhnert, L.; Krug, H. J.; Pohlmann, L. *J. phys. Chem.* 1985, 89,2022.

[31] Försterling, H. D.; Schreiber, H.; Zittlau,W. *Z. Naturforsch.* 1978, *33a,1552.*

[32] Försterling, H. D.; Lamberz, H. J.; Schreiber,H. *Acta Chim. Acad. Sci. Hung* . 1982, 110.

[33] Försterling, H. D.,; Lamberz, H.; Schreiber, H. *Z. Naturforsch.* 1978, *33a,329.*

[34] Försterling, H. D.; Lamberz, H. J.; Schreiber, H. *Z. Naturforsch.* 1980*,* 35a,1354.

[35] Blake, J. A.; Browne, R. J.; Burns, G. *J. Chem. Phys.* 1970, 53, 3320.

[36] Pacios, L. F. and Gómez, P. C. *J. Phys. Chem. A ,* 1997, 101, 1767.

[37] Barat, F.; Gilles, L.; Hickel, B.; Sutton, J. *J. Chem. Soc.* 1969, 1485 D.

[38] Bray, W. C. and Liebhafsky, H. A. *J. Am. Chem. Soc.,* 1935. 57, 51.

[39] Skrabal, A. and Weberitsch, S. R. *Monatsh.Chem.,* 1915, 36, 211.

[40] Lamberz, H. J. Ph. D. Thesis, 1982, Philipps-Universität-Marburg/Lahn, FRG.

[41] Ganapathlsubramanlan, N.; Noyes, R. M. *J. Phys. Chem.* 1982, 86, 3217.

[42] Gao, Y.; Försterling, H. D. *J. Phys. Chem*. 1994, 98, 8377.

[43] Oslonovitch, J.; Försterling, H. D. *J. Phys. Chem*. *A*. 1998, 102, 922.

[44] Jwo, J. J. and Noyes, R. M. *J. Am. Chem. Soc.,* 1975. 97, 5422.

[45] Sirimungkala, A. and Försterling, H. D. *J. Phys. Chem.* 1999, 103, 1038.

[46] Hegedüs, L.; Försterling, H. D.; Kókai, E.; Pelle, K.; Taba, G.; Wittmann, M. and Noszticzius, Z. *Phys. Chem*. *Chem*. *Phys.,* 2000, 2, 4023.

[47] Kansal, B. D.; Nepal Singh, *J. Indian Chem. Soc*. 1978, LV, 304-307.

[48] Barkin, S.; Bixon, M.; Noyes, R. M. and Bar-eli *K. Int. J. Chem. Kin*. 1977, XI, 841.

[49] Treind, L. and Ruoff, P. *J. Phys. Chem*. 1997, 101, 4606.

[50] Natarajan, R. and Venkatasubrananian, N. *Tetrahedron.* 1974, 30, 2785.

[51] Försterling, H. D.; Lamberz, H. J.; Schreiber, H., *Z. Naturforsch.* 1983, 38a, 483.

[52] Oslonovitch, J. Ph. D. Thesis, 1997, Philipps-Universität-Marburg/Lahn, FRG.

[53] Försterling, H. D.; Murányi, S.; Noszticzius, Z. *J. Phys. Chem*. 1990, 94, 2915.

[54] Brusa, M. A.; Perissinotti, L. J.; Colussi, A. J. *J. Phys. Chem*. 1985, 89, 1572.

[55] Sirimungkala, A. and Försterling, H. D. *J. Phys. Chem.* 1996, 100, 3051.

[56] Wang, W. F.; Schuchmann, M. N.; Schuchmann, H. P. and C. von Sonntag, Chemistry, 2001, 7, 791.

[57] Försterling, H. D.; Idstein, H. ; Pachl, R.; Schreiber, H. *Z. Naturforschg*. 1984, 39a, 993.

[58] Noszticzius, Z. *J. phys. Chem.* 1977, 81, 185.

[59] Murányi, S.; Försterling, H. D. *Z. Naturforschg*. 1990, 45a, 135.

[60] Nagygyöry, Sz.; Wittmann, M.; Pintér, Sz.; Visegrády, A.; Dancsó, A.; Thuy, Nguyen Bich; Noszticzius, Z.; Hegedüs, L. and Försterling, H. D. *J. Phys. Chem*. A 1999, 103, 4885.

[61] Chou, Y. C.; Lin, H. P. ; Sun, S. S. and Jwo, J. J. *J. Phys. Chem.* 1993, 97, 8450.

[62] Field, R. J.; Burger, M. Eds.; *Oscillations and Traveling Waves in Chemical system*; Wiley-Interscience: New York, 1985.